

2011

Elucidating the Role of Spy1A during c-Myc Induced Mammary Tumor Development

Evangelia Kirou
University of Windsor

Follow this and additional works at: <https://scholar.uwindsor.ca/etd>

Recommended Citation

Kirou, Evangelia, "Elucidating the Role of Spy1A during c-Myc Induced Mammary Tumor Development" (2011). *Electronic Theses and Dissertations*. 290.
<https://scholar.uwindsor.ca/etd/290>

This online database contains the full-text of PhD dissertations and Masters' theses of University of Windsor students from 1954 forward. These documents are made available for personal study and research purposes only, in accordance with the Canadian Copyright Act and the Creative Commons license—CC BY-NC-ND (Attribution, Non-Commercial, No Derivative Works). Under this license, works must always be attributed to the copyright holder (original author), cannot be used for any commercial purposes, and may not be altered. Any other use would require the permission of the copyright holder. Students may inquire about withdrawing their dissertation and/or thesis from this database. For additional inquiries, please contact the repository administrator via email (scholarship@uwindsor.ca) or by telephone at 519-253-3000ext. 3208.

ELUCIDATING THE ROLE OF SPY1A DURING C-MYC INDUCED MAMMARY
TUMOR DEVELOPMENT

by
Evangelia Kirou

A Thesis
Submitted to the Faculty of Graduate Studies
through the Department of Biological Sciences
in Partial Fulfillment of the Requirements for
the Degree of M.Sc. Biological Sciences at the
University of Windsor

Windsor, Ontario, Canada
2009
© 2009 Evangelia Kirou

ELUCIDATING THE ROLE OF SPY1A DURING C-MYC INDUCED MAMMARY
TUMOR DEVELOPMENT

by

Evangelia Kirou

APPROVED BY:

Dr. Panayiotis O. Vacratsis
Biochemistry

Dr. Andrew Swan
Biological Sciences

Dr. Lisa A. Porter, Advisor
Biological Sciences

Dr. Dennis Higgs, Chair of Defense

December 16, 2009

Author's Declaration of Originality

I hereby certify that I am the sole author of this thesis and that no part of this thesis has been published or submitted for publication.

I certify that, to the best of my knowledge, my thesis does not infringe upon anyone's copyright nor violate any proprietary rights and that any ideas, techniques, quotations, or any other material from the work of other people included in my thesis, published or otherwise, are fully acknowledged in accordance with the standard referencing practices. Furthermore, to the extent that I have included copyrighted material that surpasses the bounds of fair dealing within the meaning of the Canada Copyright Act, I certify that I have obtained a written permission from the copyright owner(s) to include such material(s) in my thesis and have included copies of such copyright clearances to my appendix.

I declare that this is a true copy of my thesis, including any final revisions, as approved by my thesis committee and the Graduate Studies office, and that this thesis has not been submitted for a higher degree to any other University or Institution.

Abstract

Speedy (Spy1A) is a novel cell cycle gene whose product binds to cyclin-dependent kinase-2 (CDK2) and activates its kinase activity to promote cell cycle progression through a cyclin independent mechanism. Spy1A is expressed naturally at high levels in the proliferating mammary gland, and aberrant overexpression of Spy1A results in precocious mammary development and eventually tumorigenesis *in vivo*. Induction of the mammary oncogene c-Myc upregulates Spy1A and I further demonstrate that Spy1A protein levels are elevated in mammary tissue and breast tumors derived from MMTV-Myc transgenic mice. Spy1A knockdown in F5A1-2 cell lines led to downregulation of cyclin-dependent kinase inhibitors (CKI) p21 and p27, a 23% reduction in proliferation rate, and a shift in cellular phenotype to a spindle-like/fibroblastic morphology. Together, findings support that Spy1A plays a functional role in mammary-related c-Myc signal transduction, and acts downstream of ER α , c-Myc, and the MAPK cascade to regulate proliferation, mammary development, and carcinogenesis.

Dedication

I would like to dedicate this text to the following individuals:

All who have suffered or died in the name of cancer, with particular reference to E. Liambra. May you forever rest in peace, and may a cure be found someday to save others from your ultimate fate.

Also, to my family. The phrase 'thank-you' does not nearly suffice to describe the gratitude I feel for receiving the unconditional love and support you have given me throughout this entire process.

Parents, you always speak of how faith can move mountains; your faith in me transcends beyond a million mountains, and for that I am forever grateful to you.

Acknowledgements

I extend my sincere and unfaltering gratitude to Dr. L.A. Porter for her continued guidance and supervision throughout this entire process; additionally, numerous thank-you's to Drs. A. Swan and P. Vacratsis for valuable input and time extension in writing. Many thanks to Dr. T. Seagroves for providing a series of MMTV-Myc, PyT, and Lac2 protein lysates, Dr. C. Shermanko for providing the HC11 cell line, and Mrs. G. Aili, Mr. M. Al Sorkhy, Ms. J. Carnevale, Ms. J. Caron, Mr. M. Crozier, Mr. G. Davis, Mr. M. Dezfulian, Ms. R-M. Ferraiuolo, Ms. B. Fifield, Ms. A. Golipour, Ms. M. Hanna, Ms. E. Jalili, Mrs. D. Lubanska, Mrs. A. Malysa, Ms. D. Myers, Ms. J. Ritchie, Mr. R. Shapiro, Mr. D. Shih, and Ms. J. Tubman for technical assistance. I extend my heartfelt gratitude to Dr. E. Fidalgo da Silva and Mrs. J. Maimaiti for valuable input; also, many thanks to Mrs. J. Maimaiti for lentiviral production and assistance with lentiviral transduction. Sincere thanks to Mrs. J. Sylvester for use of fluorescence microscopy equipment and training. This study is supported by operating funds from a partnership between the Canadian Institutes of Health Research (CIHR) and the Canadian Breast Cancer Research Alliance (CBCRA) (#151092), in addition to student funding through the Ontario Graduate Scholarship Program and Intra-University Scholarships/Travel Funds. L.A.P. gratefully acknowledges support from the CIHR New Investigator Program.

Table of Contents

<i>Author's Declaration of Originality</i>	<i>iii</i>
<i>Abstract</i>	<i>iv</i>
<i>Dedication</i>	<i>v</i>
<i>Acknowledgements</i>	<i>vi</i>
<i>Statement of Originality</i>	<i>vii</i>
<i>List of Figures</i>	<i>x</i>
<i>List of Abbreviations</i>	<i>xii</i>
<i>Introduction</i>	<i>1</i>
I. Mammary Gland Ultrastructure is Optimized for Stromal-Epithelial Crosstalk During Development	<i>1</i>
II. Continuous Cellular Turnover Features Throughout Post-natal Mammopoiesis...	<i>2</i>
III. Conserved Developmental Programs Regulate Mammary Remodelling in a Time-dependent Fashion	<i>3</i>
IV. The Tumor Promoting Role of ER α and its Connection to Antiestrogen Resistance	<i>6</i>
V. Hyperstimulation of MAPK Signaling During Mammary Tumorigenesis.....	<i>7</i>
VI. Aberrant Regulation of c-Myc Activity Encourages Formation of Aggressive Mammary Carcinomas.....	<i>9</i>
VII. Molecular Mechanisms Underlying Cell Cycle Control Prevent Uncontrollable Cell Proliferation	<i>10</i>
VIII. Intact Nuclear Function of Spy1A Regulates Cell Cycle Progression Through G ₁ /S Phase	<i>11</i>
IX. Spy1A Promotes Mammary Tumorigenesis in Various Cell Culture and Animal Models	<i>12</i>
<i>Materials and Methods</i>	<i>20</i>
I. Vector DNA Constructs	<i>20</i>
II. Site-directed Mutagenesis (SDM).....	<i>20</i>
III. Reverse Transcriptase-Polymerase Chain Reaction (RT-PCR).....	<i>26</i>
IV. Cell Lines and Culture Conditions	<i>27</i>
V. Assays for Transient Transfection and Stable Cell Line Production.....	<i>28</i>
VI. Quantification of Cell Proliferation (Trypan Blue Exclusion)	<i>30</i>
VII. Morphological Analysis and Quantification	<i>30</i>

VIII. Estradiol (E2) and MAPK Inhibition Treatments in MCF7 Cells	31
IX. Antibodies.....	32
X. Protein Lysis and Immunoblotting Assays	32
XI. Mammary Fat Pad Transplants.....	33
XII. Whole Mount Analysis	34
XIII. Transgenic MMTV-Myc Mouse Colony Propagation and Genotyping	34
<i>Results</i>	38
I. Creation of a Transgenic MMTV-Spy1A Mouse Model for In vivo Analysis of Spy1A Overexpression	38
II. Spy1A Elevation in c-Myc Overexpressing Mammary Tumors and Primary Tumor Cell Lines.....	41
III. RNAi-Mediated Spy1A Knockdown in F5A1-2 Cell Lines Reduces Cell Proliferation and Alters c-Myc Levels In vitro.....	46
IV. Transient Spy1A Knockdown May Alter Cellular Morphology In vitro	49
V. Estrogen Signaling Upregulates Spy1A mRNA and Protein Expression in MCF7 Cells	57
VI. MAPK Mediates the Ability of Estrogen to Induce Spy1A Expression in MCF7 Cells	60
VII. Disrupted MAPK Signaling in the HC11 Cell System Results in Reproducible Spy1A Downregulation	66
VIII. ER α -negative F5A1-2 Mammary Tumor Cells Harbour Intrinsic Defenses Against MAPK Inactivation	66
IX. Establishing a Tumor Baseline for F5A1-2 Cells in Cleared No. 4 Mammary Glands of FVB Females.....	72
X. Transient RNAi-Mediated Inhibition of Spy1A Slightly Reduces F5A1-2 Tumor Growth Rate In vivo	77
XI. Transient Spy1A Knockdown in F5A1-2 Cells Potentiates the Development of Ductal Outgrowths In vivo	80
XII. Transient Abrogation of Spy1A Signaling Downregulates c-Myc and MAPK Protein Expression In vivo.....	83
XIII. Stable Spy1A Knockdown In Late Passage F5A1-2 Cells Confirms Reduction of c-Myc and MAPK Protein Levels In vivo.....	89
XIV. Stable Spy1A Knockdown Encourages In vivo Ductal Formation in Late Passage F5A1-2 Tumor Cells	91

<i>Discussion</i>	96
I. Spy1A May Alter Cellular Distribution of p27 and Downregulate its Protein Expression in MMTV-Myc Overexpressing Tumors and Related F5A1-2 Cell Lines.	97
II. Late Passage F5A1-2 Tumor Cells May Acquire Additional Mutations and/or Genetic Lesions During Long-Term Cell Culture	99
III. Tamoxifen Resistance Is Thought to Arise from Constitutive c-Myc Overexpression and p21 Downregulation in Response to Persistent E2 Stimulation	99
IV. ER α Induction of Spy1A mRNA and Protein Expression May Be Mediated Preferentially Through the MAPK Cascade	101
V. MAPK and c-Myc Cross-talk May Not Affect Spy1A Protein Expression During c-Myc Induced Mammary Tumorigenesis.....	101
VI. Spy1A May Mediate the Development of Tamoxifen Resistance in Human BCs That Initially Respond to Antiestrogens	102
VII. Transient Spy1A Downregulation May Participate in Early Stages of EMT in Murine and Human BCs Overexpressing Deregulated c-Myc	104
VIII. F5A1-2 Cell Lines and Associated Tumor Tissue May Alter Tumorigenic Signaling and Tumor Phenotype in Response to Spy1A Knockdown	106
IX. Transient and Stable Spy1A Knockdown Reduces Cell Proliferation Rate in F5A1-2 Cells and Partially Restores Ductal Epithelial Branching In vivo	107
X. Caveats Associated with Mammary Fat Pad Transplantation, Whole Mount Analysis, and Utilization of pLB to Knockdown Spy1A In vivo	109
XI. Assessing the Role of Spy1A in Initiating Mammary Tumor Formation is Now Feasible Due to Creation of the First MMTV-Spy1A Transgenic Murine Model .	110
XII. Concluding Remarks and Future Directions	111
<i>References</i>	113
<i>Appendix</i>	122
<i>Vita Auctoris</i>	140

List of Figures

<i>Figure 1. Conserved developmental programs regulate mammary gland remodeling in a time-dependent fashion</i>	4
<i>Figure 2. The putative promoter sequence of Spy1A</i>	14
<i>Figure 3. Proposed signaling mechanism thought to activate Spy1A expression during mammary gland development and tumorigenesis</i>	17
<i>Figure 4. Vector map of pLB</i>	21
<i>Figure 5. Sequence and location of each Spy1A shRNA construct</i>	23
<i>Figure 6. Transgenic MMTV-Myc mouse colony propagation and genotyping</i>	36
<i>Figure 7. The coding sequence of the human Spy1A gene is targeted for mutation using SDM</i>	39
<i>Figure 8. Construction of the first MMTV-SV40-Spy1A transgenic mouse model</i>	42
<i>Figure 9. The endogenous expression profile of Spy1A protein in c-Myc overexpressing mammary tumors</i>	44
<i>Figure 10. MMTV-Myc primary tumor cell lines continue to express elevated levels of Spy1A protein</i>	47
<i>Figure 11. Transient Spy1A knockdown affects cell proliferation rate and c-Myc protein levels in vitro</i>	50
<i>Figure 12. Stable F5A1-2 cell lines exhibit differential signaling upon lentiviral-mediated Spy1A knockdown</i>	52
<i>Figure 13. Stable F5A1-2 primary tumor cell lines</i>	54
<i>Figure 14. F5A1-2 tumor cell phenotype partially acquires spindle-like morphology upon abrogation of Spy1A signaling</i>	58
<i>Figure 15. Treatment with estradiol (E2) induces Spy1A mRNA and protein expression in MCF7 cells</i>	61
<i>Figure 16. Estradiol (E2) requires intact MAPK activation to induce Spy1A protein expression in the MCF7 cell system</i>	64
<i>Figure 17. Inhibition of MAPK activity downregulates Spy1A protein levels in the immortalized HC11 cell system</i>	67
<i>Figure 18. ERα protein expression is absent in F5A1-2 cell lines</i>	70
<i>Figure 19. F5A1-2 primary tumor cell lines overexpressing c-Myc are resilient to chemical-mediated MAPK inhibition</i>	73
<i>Figure 20. Primary tumor cell lines overexpressing c-Myc are resilient to chemical-mediated MAPK inhibition</i>	75

<i>Figure 21. Tumor baseline for F5A1-2 cells.....</i>	<i>78</i>
<i>Figure 22. Transient Spy1A knockdown reduces F5A1-2 tumor growth rate in vivo.....</i>	<i>81</i>
<i>Figure 23. Transient Spy1A knockdown in F5A1-2 cells promotes ductal outgrowth development and ductal bifurcation in vivo</i>	<i>84</i>
<i>Figure 24. Transient abrogation of Spy1A signaling downregulates c-Myc expression in vivo</i>	<i>87</i>
<i>Figure 25. Stable Spy1A inhibition in late passage F5A1-2 cell lines induces MAPK Pathway and c-Myc downregulation and results in increased ductal morphogenesis in vivo</i>	<i>92</i>

List of Abbreviations

<i>BC</i>	<i>breast cancer</i>
<i>E2</i>	<i>17β-estradiol</i>
<i>TEB</i>	<i>terminal end bud</i>
<i>TED</i>	<i>terminal end ducts</i>
<i>ERK</i>	<i>extracellular signal-regulated kinase</i>
<i>ER</i>	<i>estrogen receptor</i>
<i>SERM</i>	<i>selective estrogen receptor modulator</i>
<i>TAM</i>	<i>tamoxifen</i>
<i>ERE</i>	<i>estrogen response element</i>
<i>CDK</i>	<i>cyclin-dependent kinase</i>
<i>MMTV-LTR</i>	<i>mouse mammary tumor virus-long terminal repeat</i>
<i>CKI</i>	<i>cyclin dependent kinase inhibitor</i>
<i>p21</i>	<i>CIP1</i>
<i>p27</i>	<i>KIP1</i>
<i>p57</i>	<i>KIP2</i>
<i>Re</i>	<i>restriction checkpoint</i>
<i>RINGO</i>	<i>Rapid Inducer of G₂/M progression in Oocytes</i>
<i>X-Spy1</i>	<i>Xenopus Spy1</i>
<i>Spy1A</i>	<i>Spy1/RINGO A</i>
<i>MEF</i>	<i>mouse embryonic fibroblast</i>
<i>shRNA</i>	<i>short hairpin RNA</i>
<i>GFP</i>	<i>green fluorescent protein</i>
<i>SDM</i>	<i>site-directed mutagenesis</i>
<i>RT-PCR</i>	<i>reverse transcriptase-polymerase chain reaction</i>
<i>PAGE</i>	<i>polyacrylamide gel electrophoresis</i>
<i>CS</i>	<i>calf serum</i>
<i>EGF</i>	<i>epidermal growth factor</i>
<i>PEI</i>	<i>polyethylenimine</i>
<i>P</i>	<i>passage</i>
<i>MOI</i>	<i>multiplicity of infection</i>

<i>TU</i>	<i>transducing units</i>
<i>E2</i>	<i>estradiol</i>
<i>DMSO</i>	<i>dimethyl sulfoxide</i>
<i>CK18</i>	<i>cytokeratin 18</i>
<i>CK19</i>	<i>cytokeratin 19</i>
<i>TBST</i>	<i>0.5% Tween-20/TBS</i>
<i>PyT</i>	<i>polyoma middle T</i>
<i>RNAi</i>	<i>RNA interference</i>
<i>r</i>	<i>correlation coefficient</i>
<i>NES</i>	<i>normalized enrichment score</i>
<i>kD</i>	<i>kilo Dalton</i>
<i>R</i>	<i>right gland</i>
<i>L</i>	<i>left gland</i>
<i>EMT</i>	<i>epithelial to mesenchymal transition</i>
<i>SV</i>	<i>simian virus</i>

Introduction

Amid all cancers known to afflict the Canadian population, breast cancer (BC) is documented as the “second leading cause of cancer mortality” among females to date.¹ Despite vast research and clinical efforts to reduce mortality rates in BC patients, 22 700 Canadian women are predicted to develop the disease in 2009 alone.¹ Current knowledge of the molecular signatures and biochemical pathways that govern BC initiation and progression is far from comprehensive and requires further expansion in order to identify putative biomarkers that undoubtedly predict the correct therapeutic course of action to take with each patient. Due to the heterogeneous nature of cell types which cooperate to form a functional post-natal mammary gland,² the various clinical forms of BC that may arise are currently distinguished based on prognostic criteria such as histological phenotype, steroid and growth factor receptor status, and tumor ability to metastasize to neighbouring lymph nodes.³ In order to fully understand the various molecular mechanisms underpinning the evolution of mammary tumorigenesis, post-pubertal mammary gland development is often looked upon to highlight critical signaling pathways that possess the inherent capacity to mutate and/or become deregulated in BC.⁴

I. Mammary Gland Ultrastructure is Optimized for Stromal-Epithelial Crosstalk During Development.

Defined as an exocrine organ,⁵ the mammary gland is essentially comprised of stromal and epithelial tissue compartments⁶ that intimately collaborate during embryonic and adult mammopoiesis, especially during ductal tree formation.⁷ Throughout ductal morphogenesis at pubertal onset,⁸ cells of epithelial origin are organized into mammary ductal outgrowths that primarily invade into the surrounding stromal fat pad and continue to branch outwards into functional alveolar subunits.⁶ In turn, alveolar epithelia are populated by luminal secretory cell types that are capable of producing milk upon hormonal stimulation. Additionally, alveoli are enclosed by basal myoepithelial networks that are contractile in nature and aid in milk secretion.⁶ In stark contrast, mammary stromal mesenchyme⁷ is predominantly assembled from adipocytes, and is more sparsely populated by fibroblasts, haematopoietic-derived cell types, nutrient-rich blood vessels, and neurons.⁶ The extracellular matrix (ECM) reinforces structural support of the stroma,

and consists of laminin, fibronectin, collagen, and proteoglycans, in addition to other proteins.⁷

II. Continuous Cellular Turnover Features Throughout Post-natal Mammapoiesis.

Prenatal mammary embryogenesis denotes a period of robust developmental activity directed under molecular⁹ and epigenetic mechanisms (chromatin remodelling)¹⁰ that, in turn, cooperate to induce mammary bud formation¹¹ and rudimentary ductal precursor establishment.^{8,10} Shortly after birth, post-natal maturity begins with a brief episode of developmental quiescence that eventually halts upon re-initiation of ductal morphogenesis in response to ovarian-produced steroidal hormones delivered to a pubescent mammary gland.^{8-9,11} More explicitly, pubertal onset is marked by increased ovarian follicular activity and responds to elevated production of 17 β -estradiol (E2).¹²⁻¹³ In turn, endocrine transport of ovarian estrogen to an immature mammary gland potentiates mammary ductal elongation and outgrowth by inducing the mitogenic action of both epithelial and stromal compartments.^{12,14-15} The establishment of a functional ductal tree commences with ductal outgrowth and terminal end bud (TEB) formation during early pubertal stages.^{6,16} Located within the leading edge of extending ducts, TEBs are defined as highly proliferative club-shaped units that serve a two-fold purpose: (a) invasion of the surrounding connective tissue to promote ductal elongation,^{6,16} and (b) production of ductal side branches upon TEB cleaving.¹⁶ TEBs transition into non-dividing terminal end ducts (TEDs) and alveolar precursor structures upon complete filling of the mammary fat pad with mature ductal networks during late puberty.¹⁷

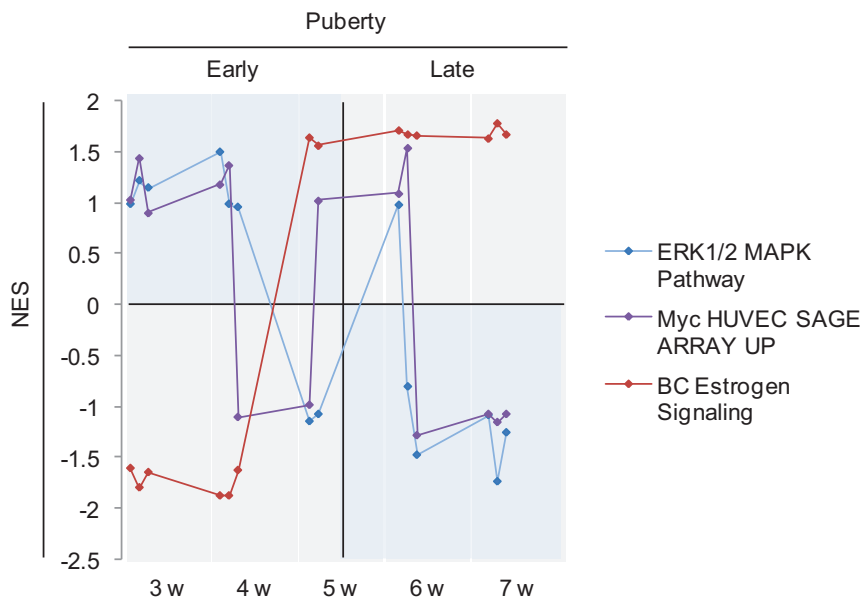
Once maturity is established, the adult virgin mammary organ retains the ability to cycle through four developmental stages: virgin, pregnancy, lactation, followed by involution and reversion to a virgin-like state.⁶ During early pregnancy-induced lobulo-alveolar development,¹¹ elevated expression of prolactin, placental lactogens, and progesterone⁶ results in escalated rates of luminal epithelial proliferation, and promotes functional differentiation of alveolar precursor cells into specialized structures proficient in milk release.⁶ Parturition-induced lactogenesis functions to nourish neonates⁸ through alveolar milk production and secretion of colostrum into enlarged luminal ducts.⁶ Neonate

weaning initiates extensive luminal alveolar cell death (apoptosis) and epithelial remodelling during involution, a process lasting for several days to allow for reinstatement of the mammary gland to a virgin-like appearance.^{6,16}

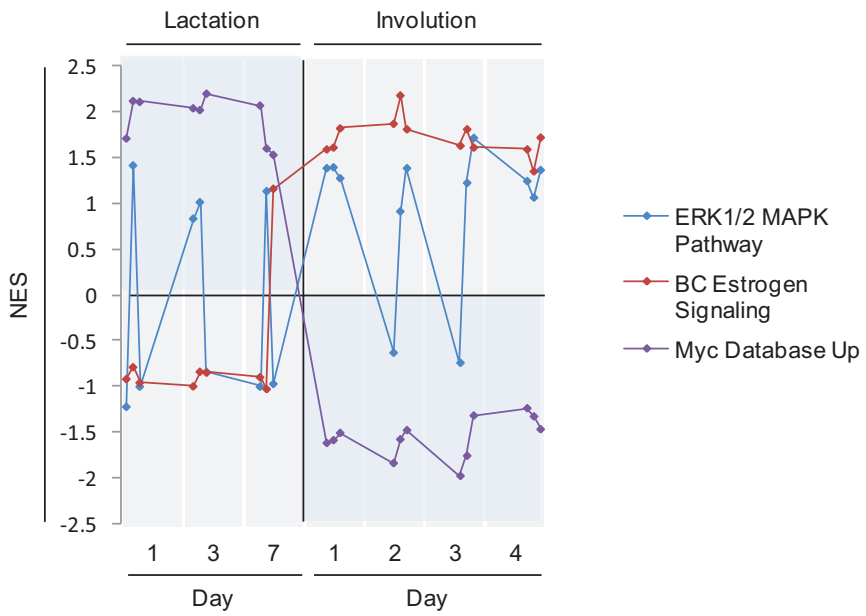
III. Conserved Developmental Programs Regulate Mammary Remodelling in a Time-dependent Fashion.

Throughout post-natal mammary development, rapid transitioning through cell growth, proliferation, apoptosis, and terminal differentiation is tightly coordinated under temporal activation of gene networks at discrete developmental time points.^{4,6} Molecular studies utilizing high through-put analysis and gene expression profiling of mouse mammary glands isolated at various stages of development have revealed three critical regulators of adult mammapoiesis: estrogen, extracellular signal-regulated kinases (ERK) 1 and 2, and c-Myc, the protein product of the *c-myc* gene.¹⁸⁻²¹ Simultaneous increase of ERK1/2 and c-Myc is prevalent throughout the third, sixth, and seventh weeks of murine pubertal development, whereas estrogen-regulated signaling is downregulated during third and fourth weeks of early puberty, followed by subsequent upregulation during week 5, and downregulation during weeks 6-7 (Fig.1a).²⁰ Throughout the final weeks of late puberty, elevated ERK1/2 and c-Myc expression (Fig.1a) precede pubertal completion.²⁰ In a separate report, Golipour and Myers et al. (2008) demonstrated that fully developed adult virgin mammary glands express significant levels of Spy1/RINGO (Spy1) A protein and mRNA, thereby correlating to periods of robust cell proliferation (Fig.1c).²² Pregnancy inception further stimulated Spy1A expression, which peaked at pregnancy day 6 and steadily declined during late pregnancy and lactation events (Fig.1c).²² In addition, c-Myc activity is predominant throughout all periods of lactation and involution, and its pattern of expression opposes that of estrogen-regulated signaling (Fig.1b).²⁰ ERK1/2 expression, on the other hand, continually fluctuates between active and inactive states during lactation and involution (Fig.1b).²⁰ Conclusively, involution is characterized by a potent increase in Spy1A activation (Fig.1c), a period of gland restoration marked by intensive apoptotic events.²²

A



B



C

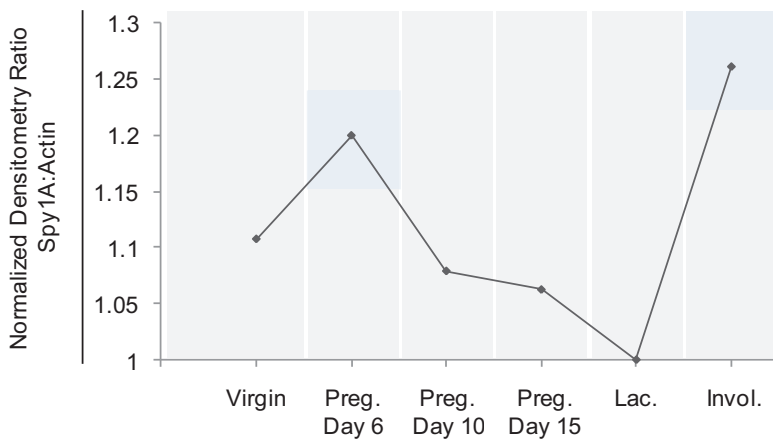


Figure 1. Conserved developmental programs regulate mammary gland remodeling in a time-dependent fashion. (a) As previously reported by Andrechek et al. (2008), normalized enrichment scores (NES) derived from Gene Set Enrichment Analysis were identified during weeks 3-7 of pubescence for each of the following data sets, and represent relative levels of gene expression at each week of pubertal development: ERK1/2 MAPK pathway (blue line); Myc HUVEC SAGE ARRAY UP (purple line); and BC estrogen signaling (red line).²⁰ Quadrants highlighted in blue indicate gene upregulation based on NES values reported for each developmental stage.²⁰ (b) NES values reported by Andrechek et al. (2008) were reported for days 1, 3, and 7 of lactation, and during days 1-4 of involution for the following data sets: ERK1/2 MAPK pathway (blue line); BC estrogen signaling (red line); and Myc Database Up (purple line).²⁰ Quadrants highlighted in blue indicate gene upregulation based on NES values reported for each developmental stage.²⁰ (c) As previously demonstrated by Golipour and Myers et al. (2008), the normalized densitometry ratio of Spy1A:Actin protein expression is depicted for virgin; pregnancy days 6, 10, and 15; lactation; and involution stages of mammary development, and represent relative levels of protein expression at each developmental stage.²²

IV. The Tumor Promoting Role of ER α and its Connection to Antiestrogen Resistance.

A master hormonal regulator of diverse cellular processes, the steroidal action of estrogen specializes in mediating cellular proliferation and mammary development via estrogen receptor (ER) activation.¹²⁻¹³ Classified under the nuclear receptor super family, the estrogen receptor exists as two isoforms, namely ER α and ER β , both of which function as global transcription factors.^{12,23} The differential expression of ER α and ER β is apparent in various tissues.¹² In wild type murine mammary glands, for instance, ER α predominantly localizes to luminal epithelial cell populations and is virtually absent in the surrounding myoepithelium,²³ whereas ER β localizes to both compartments.¹² Estrogen receptor isoforms also differ in function when coexpressed in ductal cells of the mammary epithelium, such that ER β represses ER α -stimulated proliferation and is thought to promote differentiation instead.¹²

Approximately 75% of diagnosed mammary neoplasias probe positive for estrogen receptor status²³ and are treated initially with antiestrogens,²⁴ aromatase antagonists such as letrozole,²⁵ and more commonly, selective estrogen receptor modulator (SERMs) such as tamoxifen (TAM).^{12,24} Thirty percent of aggressive ER α -positive tumors²³ eventually circumvent the growth inhibitory action of ER-targeted therapies^{23-24,26} and prompt chemotherapeutic agents like tamoxifen to delineate into proliferative stimulants of cancer cells.²⁵ Termed antiestrogen or tamoxifen resistance, this process often correlates clinically with a significant decrease in patient outcome.²³ The complex nature of estrogen signaling and its pervasive regulation over an extensive array of cellular mechanisms during normal mammary gland development and tumorigenic onset further complicates our understanding of how tamoxifen resistance may initially arise.²⁷ Although the full scope of estrogenic action has yet to be defined, several studies have predicted a role for estrogen-dependent mechanisms in the development of tamoxifen resistance.²⁷ For instance, the ERK1/2 pathway has been shown to trigger expression of intermediary target genes known to be implicated in tumor invasion, and is markedly elevated during mammary tumor progression.¹⁵ ERK1/2 functions to potentiate ER transcriptional activity via direct phosphorylation and activation of ER, and may alter ER localization, leading to an overall increase in mitogenesis and cell survival.¹⁵ Furthermore, elevation of ERK

levels in estrogen-expressing mammary tumors typically reduces patient outcome and contributes significantly to tamoxifen resistance.¹⁵ Conversely, mitogen-activated protein kinase (MAPK) activation of ERK isoforms may result in the phosphorylation and activation of ER coactivators instead of associating directly with ER.¹⁵

Analogous to MAPK, c-Myc – a nuclear transcription factor whose intracellular activity is contingent upon c-Myc dimerization with binding partner Max – functions as a direct downstream transcriptional target of ER α , and is traditionally defined as a central mediator of estrogen signaling.²⁷ Also, the c-Myc promoter harbours an estrogen response element (ERE), a DNA binding region deemed to be essential for ER α association with the c-Myc transcript.²⁷ Consequently, ER α induces c-Myc expression 15 minutes post-E2 exposure.²⁷ Furthermore, ER α and c-Myc are classified as potent mitogenic stimulants proficient in stimulating irrepressible BC tumor proliferation, and c-Myc activation is further required by ER α to promote cell cycle transitioning through G₁/S phase.²⁷ In this way, c-Myc potentiates cellular endpoints similar to those induced by ER α .²⁷ Upon transcriptional activation, c-Myc regulates a plethora of target genes, including cyclin E/CDK (cyclin-dependent kinase) 2 complexes through a mechanism that involves suppression of cell cycle inhibitor (CIP1) p21.²⁷ Moreover, in response to long-term E2 withdrawal, c-Myc gene levels increase.⁹ C-Myc has further been documented to partially re-initiate cell proliferation in MCF7 BC cell lines pre-treated with antiestrogens, and therefore potentiates cell cycle progression even in the continued presence of estrogen inhibitors.⁹ Based on these data, a central role has been implied for c-Myc in the development of antiestrogen resistance.²⁸

V. Hyperstimulation of MAPK Signaling During Mammary Tumorigenesis.

The MAPK family comprises a broad group of signal effectors able to respond to numerous receptor-bound ligands under differential cellular conditions.²⁹ Four distinct MAPK networks have been identified to date, and include ERK1/2, c-Jun-amino-terminal kinase, p38, and ERK5.²⁹ Under stringent molecular control, MAPK cascades are best known for their rapid ability to transduce extracellular growth factor, hormonal, and stress stimuli into physiological outputs such as cardiovascular development; differentiation;

mesoderm formation; cell cycle initiation; and cellular proliferation.²⁹⁻³⁰ Upregulation of MAPK signaling has also been implicated in tumor formation and migration.²⁹⁻³⁰ Additionally, select mammary epithelial cell systems have illustrated the importance of Raf/MEK/ERK activation during Ras-mediated metastatic progression,³¹ and increased Ras expression and activity is often identified in clinical cases of cancer.³² Consistent with the notion that ERK activity stimulates cell entry into G₁ following G₀ arrest,³⁰ human mammary tumor cell lines that no longer respond to estrogen contain elevated levels of ERK1/2.¹² More importantly, the ERK/MAPK pathway counteracts tamoxifen-mediated inhibition of the cell cycle, and favours evolution of tamoxifen resistance.³³

Canonical ERK1/2 signaling is induced upon receptor-mediated recognition of extracellular ligands, and leads to immediate activation of Grb2, a membrane-localized adaptor molecule known to tether itself to the guanine nucleotide exchange factor SOS.³⁰ Together, Grb2 and SOS indirectly promote MAPK signal transduction through Ras, a small molecule tumor promoter with intrinsic GTP binding capacity.^{30,34} Consequent stimulation of MAPK results in the feed-forward activation of cytoplasmic and nuclear target genes notorious for their pro-mitogenic effects.³⁰

MAPK activity is contingent upon tyrosine and serine/threonine phosphorylation.³⁰ Raf-1, a serine and threonine kinase, is recruited to the plasma membrane upon direct association with the N-terminus of Ras³⁰ and is positively regulated by phosphorylation.³⁵ In turn, Raf-1 activates three MEK isoforms (MEK1a, MEK1b, MEK2), a group of highly conserved serine/threonine kinases that require only serine phosphorylation to function.³⁰ In an effort to amplify the MAPK signal, the MEK family phosphorylates two downstream substrates ERK1 and ERK2 on select threonine and tyrosine residues.³⁰ In turn, kinase activation of ERK1/2 mediates its movement into the nucleus, and stimulates ERK1/2 to phosphorylate target substrates on serine and threonine residues commonly flanked by proline.³⁰ Direct targets include the promoter of transcription factors such as c-Myc,^{29-30,36-40} and ERKs are further capable of signaling back to upstream MAPK members (SOS, Raf-1, MEK).³⁰ ERK2 interacts with and hyperphosphorylates Raf-1 on five key residues bordered by proline in order to prevent association of Raf-1 with Ras, and to cripple Raf-1 activity.³⁵ Moreover, ERK2 phosphorylation of Raf-1 relies on upstream MEK activity in order to deactivate its substrate, and represents a negative

feedback loop utilized by MAPK cascades to temporally regulate Ras and cellular responses to mitogens.³⁵ Negative MAPK regulation is featured also in primary fibroblasts and chronic myeloid leukemia cells, where Ras uncharacteristically inhibits cell growth through Raf-1/MEK/ERK activation of the tumor suppressor p21.³⁴ C-Myc is able to restore cell proliferation upon suppression of Ras activity, and thus functions here to inhibit MAPK signaling.³⁴

VI. Aberrant Regulation of c-Myc Activity Encourages Formation of Aggressive Mammary Carcinomas.

C-myc – a potent oncogene, phosphoprotein, and transcription factor – governs a plethora of cellular events⁴¹⁻⁴² including proliferation, development, and apoptosis.^{4,43} Common to both humans and mice, the *c-myc* gene comprises three exons altogether, although protein synthesis is mainly directed through transcription of second and third exons.⁴² The protein product c-Myc is predicted to possess a molecular weight of 49 kDa (439 aa), however antibody detection identifies various c-Myc isoforms that range from 62 to 67 kDa in size.⁴² Biochemical studies of COS-7 cells transfected with numerous mutated c-Myc constructs have uncovered a partial role of amino acid regions 106-143, 320-368, and 370-412 for Myc subcellular localization.⁴² More importantly, regions 105-143 and 321-439 must remain intact for c-Myc to function properly.⁴² C-Myc is predominantly localized to the nuclear component of cells where it retains a relatively short half life of approximately 15-30 minutes,⁴² consistent with its classification as an immediate early gene.⁴⁴ Nuclear translocation typically results in transcriptional activation of Myc-responsive target genes through functional binding of c-Myc and its dimerization partner Max to canonical palindromic DNA motifs/E-boxes (CACGTG).⁴⁵ Alternatively, interaction between c-Myc and DNA may occur through recognition of different promoter response elements.⁴⁵

As a direct consequence of abnormal oncogenic activity in the tumor microenvironment, mammary-derived neoplasias are continually credited for their elusive ability to circumvent regulatory mechanisms that otherwise direct tissue homeostasis and the maintenance of developmental programs.^{4,42} C-Myc gene amplification has been described in 5-15% of all human BC cases, and strongly correlates with reduced patient

survival and aggressive tumor phenotypes.⁴ Identified in a broad spectrum of human tumors, the key mechanisms of c-Myc-induced tumorigenesis include abnormal c-Myc expression and activity, and its chromosomal translocation.⁴⁵ Transgenic murine models engineered to overexpress mammary c-Myc under the promoter control of the mouse mammary tumor virus long-terminal repeat (MMTV-LTR) consistently give rise to invasive mammary adenocarcinomas and demonstrate further anomalies in adult mammapoiesis.⁴ Furthermore, approximately 50% of virgin females give rise to stochastic mammary adenocarcinomas within a 7-14 month period following birth, in addition to 100% of females that have undergone two or more pregnancies.⁴⁶⁻⁴⁷ Development of the transgenic MMTV-Myc mouse model was previously described by Sinn, et al. (1987).^{46,48} Transgenic mice target constitutive overexpression of human c-Myc to mammary epithelial cells under MMTV-LTR promoter control.⁴⁶ Virgin mice particularly fall victim to deregulations in lobuloalveolar development in the mammary gland.⁴ Aberrations in c-Myc-overexpressing mammary glands encompass the premature withdrawal from postpartum lactation due to enhanced epithelial differentiation, and activate pregnancy-induced lactation precociously, which is then followed by the cessation of milk synthesis and untimely onset of gland remodelling during involution.⁴ Therefore, disrupted lactation in MMTV-Myc mothers causes subsequent neonatal death as early as 24 hours post-delivery.⁴

VII. Molecular Mechanisms Underlying Cell Cycle Control Prevent Uncontrollable Cell Proliferation.

The cell division cycle is regulated by a series of CDKs whose alternating expression levels and association with cyclins are fundamental to the progression of cell cycle events.^{18,49} Cyclin synthesis and degradation is paramount for the temporal regulation of CDKs and their ability to interact with and phosphorylate target substrates during key cell cycle phases: cyclin D/CDK4 and cyclin D/CDK6 at G₁; cyclin E/CDK2 at G₁/S; cyclin A/CDK1 at S/G₂; and lastly, cyclin B/CDK1 at G₂/M.⁵⁰ CDKs are controlled post-transcriptionally through various means: several examples include direct/indirect partnership with a repertoire of nuclear co-regulators, localization, proteolysis, as well as cyclin-mediated phosphorylation.¹⁸ CDK molecular structure reveals three critical

phosphorylation sites, two of which are inhibitory to CDK function, and one that positively directs CDK activity in the absence of inhibitory cyclin dependent kinase inhibitors (CKIs).¹⁸ Furthermore, interaction between CDKs and CKIs results in cell cycle arrest⁵¹ at G₁/S and G₂M checkpoints,⁵² and ultimately alerts cells to correct aberrations in DNA content and integrity prior to mitosis.⁵² CKIs are classified into two main subtypes, namely the CIP/KIP and INK4 families.⁵¹ The first group negatively mediates the transition through G₁/S and is comprised of p21, KIP1 (p27), and KIP2 (p57) proteins, whereas the INK4 group directly targets CDK4 and CDK6 to thwart complex formation with cyclin D.⁵¹

Endogenous activation of nuclear p27 contributes to cell cycle arrest at G₁ by directly binding to and inhibiting cyclin E/CDK2.³² Subsequent exposure to mitogens relieves p27 repression of cyclin E/CDK2 and stimulates cell movement through G₁/S by suppressing p27 function.³² Likewise, mitogen-dependent trimerization of p27/cyclin D/CDK4 limits the amount of unbound p27 substrate available to negatively associate with cyclin E/CDK2.⁵³ During G₁/S transitioning, ubiquitin-mediated proteolysis, cytoplasmic relocalization, and phosphorylation of p27 also remove its inhibitory action on cyclin E/CDK2 activity, and consequently promote the onset of DNA replicative events.^{32,53} Prior to S-phase entry, successful passage through the restriction (Re) checkpoint and its regulatory pathways⁴⁹ permits cells to deviate from the cell stimulatory effects of G₁-acting mitogens.⁵⁴ In this way, entry through Re ensures the success of cellular DNA replication⁴⁹ and allows for cell division to proceed through mitosis⁵⁵ uninterrupted, in the absence of apoptotic and DNA damaging stimuli.⁵⁶ Clinical relevance of p27 downregulation ultimately correlates with reduced patient survival, favours escape from estrogen-related signaling, and contributes to mammary tumorigenesis in breast cancer cell lines.³²

VIII. Intact Nuclear Function of SpylA Regulates Cell Cycle Progression Through G₁/S Phase.

Spy1/RINGO (Rapid Inducer of G₂/M progression in Oocytes) was first discovered to be an activator of G₂/M and a potent enhancer of oocyte maturation in *Xenopus* (X-Spy1).^{18-19,50,57} SpylA, the human homologue, shares 40% homology with X-Spy1.⁴⁹

Spy1A is classified as a novel cell cycle gene whose product binds to CDK2 and activates its kinase activity to induce cell cycle progression through a cyclin-independent mechanism,⁴⁹ and to promote cell movement into DNA synthesis.⁵⁸ Pinpointed to the nucleus,¹⁹ upregulation of Spy1A inevitably stimulates the precocious entry of cells into S-phase by shortening G₁, and thereby amplifies rates of cell proliferation.^{18,53} Moreover, somatic cell culture has revealed an ability for Spy1A to rescue mammalian cells from the deleterious effects of DNA damage.¹⁹ In contrast, *in vitro* studies have demonstrated that transient RNA interference (RNAi) knockdown of Spy1A results in cell cycle arrest at G₁/S phase as evidenced by declining cell populations undergoing G₂/M transition.¹⁸⁻¹⁹ Furthermore, all Spy1 forms contain a conserved 140-aa Speedy/RINGO box required and sufficient for CDK association and stimulation.¹⁸⁻¹⁹ Unique only to Spy1A, the CDK-binding domain is flanked by a C-terminal CDK activating domain, as well as an N-terminal domain whose function is mostly unknown but is thought to mediate Spy1A protein expression.¹⁸⁻¹⁹

In addition to Spy1A, which has two transcript variants – A1 and A2, Cheng et al. (2005) previously classified three distinct Spy1 homologues in mammals: Spy1B, C, and D.¹⁸ Other homologues have been identified since then, including Spy1E.¹⁹ Members of the Spy1 family may override select cell cycle regulatory mechanisms, and certainly respond with less intensity to CKI-mediated cell cycle effects.¹⁸ For instance, Cdk2/Spy1A complexes generally override p21-induced cell cycle arrest.⁵⁹ In a yeast two-hybrid screen conducted by Porter et al. (2003), direct binding of p27 to Spy1A was identified and confirmed *in vitro/in vivo*.⁵³ The direct interplay between Spy1A and p27 is contingent upon p27 residues 43-128, and endogenous p27 expression leads to elevated Spy1A/CDK2 association, thus demonstrating the ability of Spy1A to overrule p27-mediated inhibition of cyclin E/CDK2 during G₁/S.^{19,53,60} Shortly thereafter, McAndrew et al. (2007) established that CDK2 requires Spy1A to phosphorylate p27 (T187), thereby encouraging degradation of p27.⁶⁰

IX. Spy1A Promotes Mammary Tumorigenesis in Various Cell Culture and Animal Models.

Presence of Spy1A has been reported in both mouse and human tissues, although amino acid composition varies substantially between inter-species homologues.¹⁹ Spy1A is ubiquitously distributed throughout numerous cell and tissue types, and greatest levels occur in testicular organs and other tissues of meiotic origin.¹⁸⁻¹⁹ Recently, the Spy1A isoform was shown to be expressed naturally at high levels in the proliferating mammary gland, where it was found to predominantly localize to luminal epithelial cells, and exhibited decreased expression in myoepithelial and adipose tissue as evidenced by immunostaining (*Mus musculus*).²² When aberrantly overexpressed, Spy1A activity resulted in precocious development and eventually mammary tumorigenesis *in vivo*.²² In addition, Spy1A mRNA and protein levels were shown to increase substantially following induction of c-Myc using a Myc-ERTM mouse embryonic fibroblast (MEF) inducible cell system.²² Upregulation of Spy1A transpired in the absence of *de novo* protein synthesis, suggesting that c-Myc may act directly to trans-activate Spy1A expression.²²

The Spy1A promoter remains to be elucidated, although progress towards its determination is currently underway. Phylogenetic footprinting is defined as a bioinformatics method utilized to unearth the transcriptional co-regulators of a given gene by piecing together the necessary basal and modular response elements required for transcription initiation.⁶¹⁻⁶² Among other procedures, this approach often utilizes computational alignment in order to compare a promoter sequence of interest to comprehensive databases that house consensus DNA binding motifs recognized by transcription factors.⁶¹⁻⁶² Previously, the putative promoter sequence of Spy1A was subjected to phylogenetic footprinting, and as a result, we have uncovered prospective nuclear factors that participate in regulating Spy1A transcription depending on context-specific ligand activation (summarized in Fig.2). Of particular interest, both c-Myc and ER α response elements are found in close proximity to one another and hypothetically localize to the Spy1A promoter. *Taken together, these data support the hypothesis that Spy1A functions downstream of the c-Myc signalling pathway to regulate c-Myc effects on cell proliferation, mammary gland development, and mammary tumorigenesis.*

Signaling cascades are often initiated by activation of one or more receptors through ligand binding interactions. Within a mammary gland paradigm, we propose a pathway

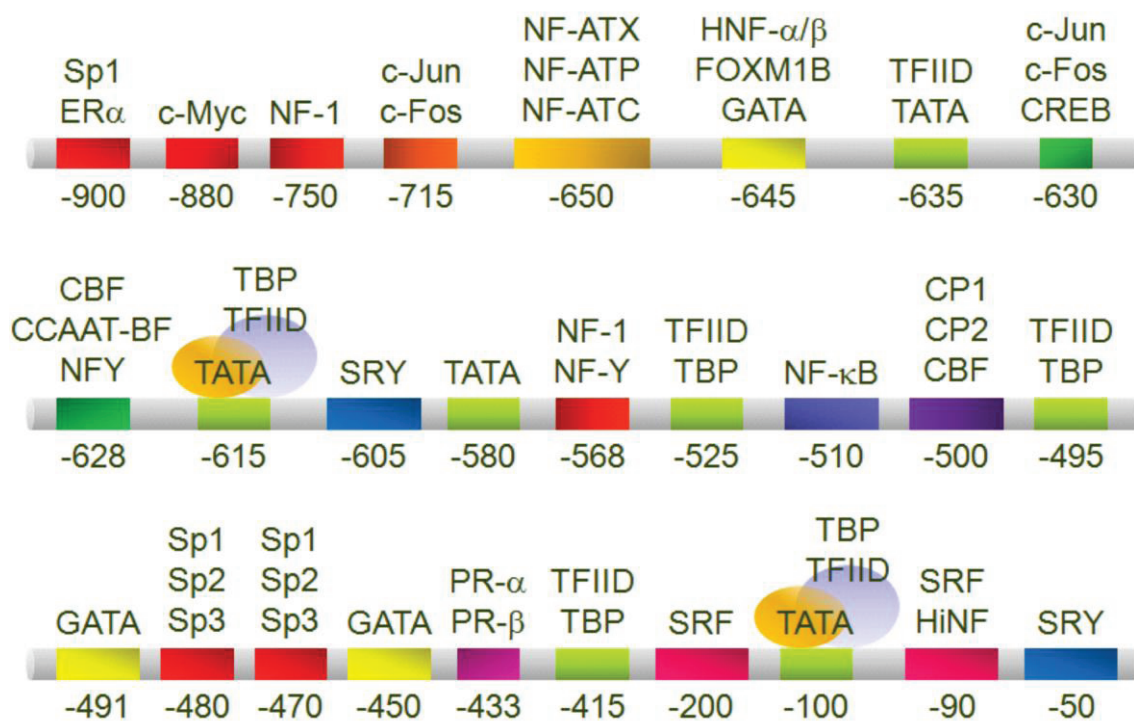


Figure 2. The putative promoter sequence of *Spy1A*. The predicted promoter sequence of *Spy1A* was aligned to various online databases that house consensus DNA binding motifs most frequently recognized by transcription factors (phylogenetic footprinting method). In reference to the transcription initiation start site (at position 0), the nucleotide position of each transcription factor response element is reported below each transcription factor. Two independent TATA boxes are illustrated at positions -615 and -100. ER α and c-Myc response elements are located in close proximity to one another.

that is kick started by estrogen binding to ER α . Estrogen receptor activation stimulates the MAPK pathway via Ras, and subsequently activates c-Myc. Following nuclear migration, c-Myc is thought to have two potential cellular outcomes. First, c-Myc may bind directly to a response element on Spy1A (particularly within the putative promoter region). Second, c-Myc has been shown to transiently activate CDK2 directly, and thus may have an indirect effect on Spy1A expression and regulation, both during development and carcinogenesis. Therefore, it is thought that c-Myc mediates the promotion or initiation of mammary gland oncogenesis in part through Spy1A (Fig.3).

The purpose of this study was two-fold: (a) first, I sought to determine the essentiality of Spy1A for mammary gland development, and further aimed to elucidate the degree to which Spy1A mediates c-Myc induced tumorigenesis; (b) second, I sought to determine the effects of constitutively active Spy1A on early mammary gland developmental events.

Objective 1: To determine the essentiality of Spy1A for post-natal mammary gland development, and to further clarify whether Spy1A mediates c-Myc induced tumorigenesis. To uncover the importance of Spy1A for post-natal mammapoiesis and c-Myc induced mammary oncogenesis, five novel short hairpin (sh) RNA constructs were designed against various regions of the mouse Spy1A homologue, and were subsequently utilized to assess the effects of Spy1A knockdown *in vitro* (cellular proliferation assays) and *in vivo* (mammary fat pad transplantation assays) in primary mammary tumor cell lines overexpressing c-Myc under control of the MMTV promoter.

Objective 2: To determine the effects of Spy1A overexpression on early mammary gland development. Evidence suggests that Spy1A accelerates mammary tumorigenesis and postnatal mammary development.²² Investigating the role played by Spy1A during embryonic formation of the mammary gland within the MMTV-SV (simian virus) 40-Spy1A transgenic murine model may shine light on these important observations.

Ultimately, this study aims to provide insight into key developmental and cell signaling events regulating formation of the mammary gland. Results from this work will contribute toward our greater understanding of the potential factors that may initiate and/or assist

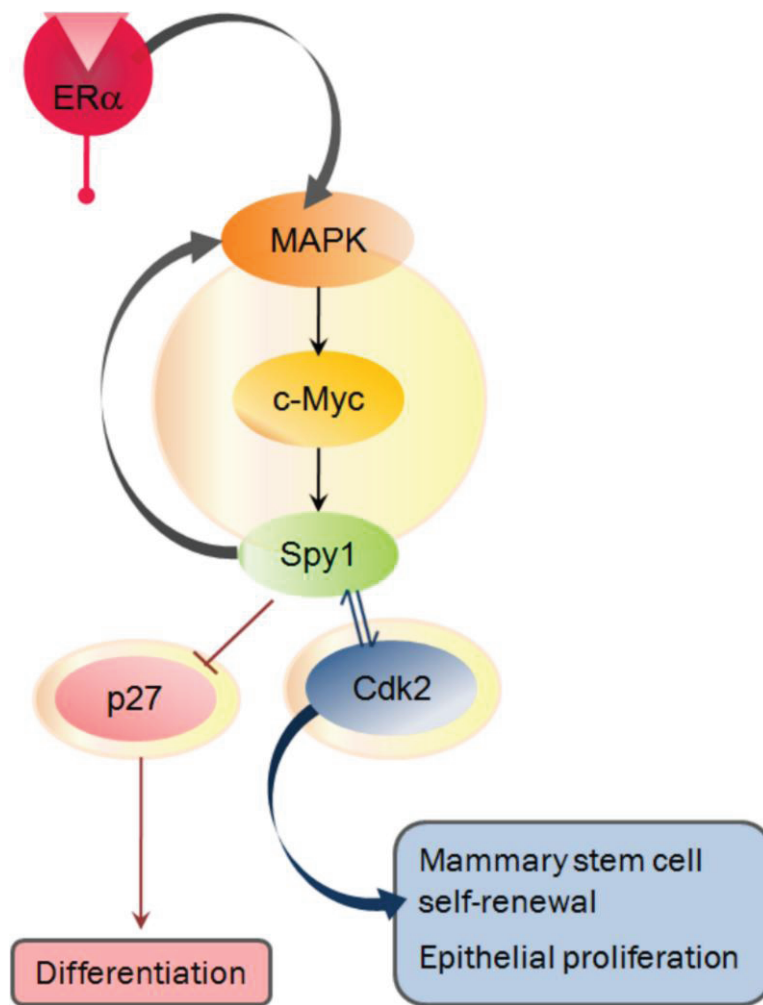


Figure 3. Proposed signaling mechanism thought to activate Spy1A expression during mammary gland development and tumorigenesis. In a mammary specific context, upon receiving mitogenic cues from estrogen, ER α is stimulated and further promotes MAPK pathway activation; in turn, the MAPK machinery is thought to induce c-Myc expression, followed by activation of Spy1A. Following nuclear migration, c-Myc is thought to have two potential cellular outcomes. First, c-Myc may bind directly to its response element on Spy1A (particularly within the putative promoter region). Second, c-Myc has been shown to transiently activate CDK2 directly, and thus may have an indirect effect on Spy1A expression and regulation, both during development and carcinogenesis. Therefore, it is thought that c-Myc mediates the promotion or initiation of mammary gland oncogenesis in part through Spy1A.

the progression of human breast cancer, in addition to de novo/acquired antiestrogen resistance. The mechanism(s) that ER α -positive mammary tumors utilize to develop resistance to antiestrogens has been partially evaluated, and constitutes a major clinical barrier in the successful treatment of BC patients currently. Our data further implicate the involvement of Spy1A during the acquisition of an antiestrogen resistant tumor phenotype, thereby potentiating cellular proliferation in the presence of antiestrogen treatments like tamoxifen. Although much work remains to be completed, results derived from this study suggest that Spy1A may be targeted therapeutically in order to effectively reduce the aggressiveness of ER α -positive mammary tumors that have undergone tamoxifen resistance.

Materials and Methods

I. Vector DNA Constructs.

pLB was purchased from Addgene (MA, USA). Flag-Spy1A-pLXSN plasmid construction was described previously by Porter et al. (2003).⁵³ The MMTV-SV40-TRPS-1 vector was provided as a kind gift from Dr. Gabriel E. DiMattia.

pLB represents a lentiviral vector that utilizes the mouse U6 promoter to express short hairpin RNA (shRNA), and the cytomegalovirus promoter to express green fluorescent protein (GFP) in murine cell systems (Fig.4). GFP fluorescence served as a positive indicator for induction of RNAi. Conventional restriction enzymes HpaI (Cat. No. ER1031) and XhoI (Cat. No. ER0691) (Fermentas, Ontario, Canada) were utilized to linearize pLB. Available online as free software (<http://www.oligoengine.com>), the program OligoEngine Workstation 2 was utilized to design five novel shRNA constructs directed against unique regions of the mouse Spy1A homologue (NCBI_70891), in addition to a scrambled shRNA construct chosen for its inability to recognize and target Spy1A for RNAi-mediated degradation (Fig.5). Forward and reverse sequences listed in the 5' to 3' direction are provided in Fig.5 for scrambled and Spy1A shRNA constructs. Constructs flanked by HpaI and XhoI restriction sites were synthesized by Sigma-Genosys Canada (Sigma-Aldrich, Ontario, Canada). Note that only constructs three and four target the mouse Spy1A protein isoform within the Speedy/RINGO box (amino acids 66-206). Construct two was subsequently subcloned into pLB and designated shSpy1A. Similarly, the scrambled construct was subcloned into pLB and designated shCntl. Since shRNA constructs do not equally or effectively silence target gene activity, the selectivity of construct two for silencing Spy1A transcriptional activity may be confirmed in future experiments by cloning and utilizing all five Spy1A shRNA constructs designed to date.

II. Site-directed Mutagenesis (SDM).

SDM primers A424 and A425 were designed against Flag-Spy1A-pLXSN to flank the vector region containing a putative EcoRI site, and were synthesized by Sigma-Genosys (Sigma-Aldrich):

forward primer (A424):

5'-GCCAGAATTCGATTTATGCATGTTGTTTACTGAGC-3'

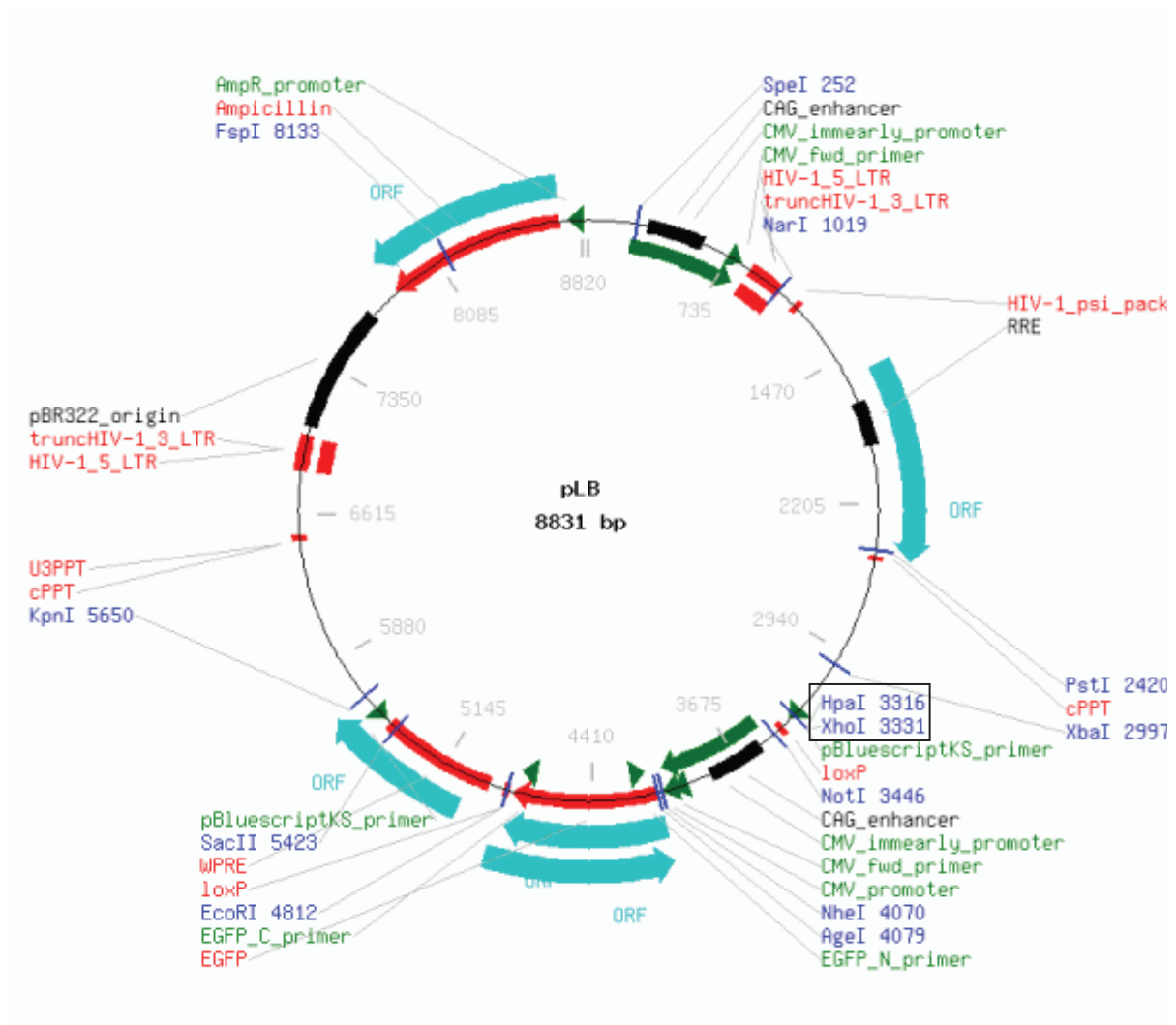
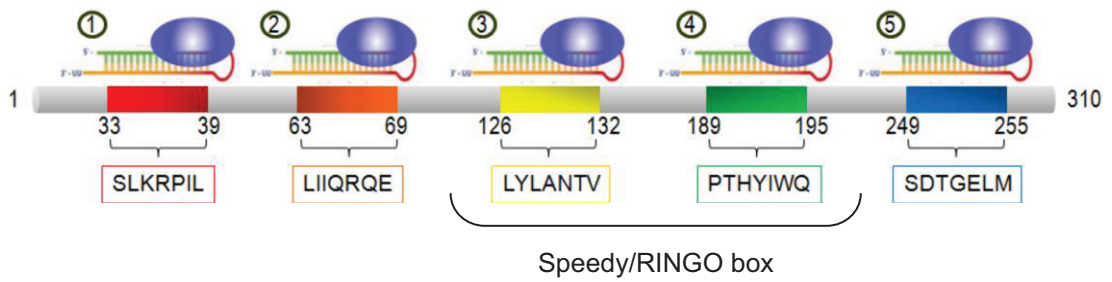


Figure 4. Vector map of pLB. The vector composition of pLB (Addgene) was obtained from the company website (<http://www.addgene.org>) and is illustrated here as a point of reference. Total size of the pLB vector backbone is estimated to be 8500 nucleotides. Each shRNA construct was subcloned into pLB through insertion at the HpaI (3316 bp) and XhoI (3331) restriction sites (black box). GFP expression is directed separately from shRNA expression, and is mediated through CMV promoter control, whereas shRNA expression is mediated through the mouse U6 promoter.



Mouse Specific shRNA Constructs

①	Top Strand	5'-GTCTGAAACGTCTATTCTTCAAGAGAAGAATAGGACGTTTCAGACG-3'
	Bottom Strand	5'-GATCCGTCGAAACGTCCTATTCCTCTTGAAGAATAGGACGTTTCAGACCG-3'
②	Top Strand	5'-GAATCATACAGCGCCAGGAATCAAGAGATTCCTGGCGCTGTATGATTG-3'
	Bottom Strand	5'-GATCCAATCATAACAGCGCCAGGAATCCTTGAATTCCTGGCGCTGTATGATTCCG-3'
③	Top Strand	5'-GTATCTGGCTAATACGGTTTTCAAGAGAAACCGTATTAGCCAGATACG-3'
	Bottom Strand	5'-GATCCGTATCTGGCTAATACGGTTCTCTTGAAACCGTATTAGCCAGATACCG-3'
④	Top Strand	5'-GCAACCCATTACATCTGGCATTCAAGAGATGCCAGATGTAATGGGTTGG-3'
	Bottom Strand	5'-GATCCAACCCATTACATCTGGCATCTTGAATGCCAGATGTAATGGGTTGCCG-3'
⑤	Top Strand	5'-GTGACACAGGAGAGCTAATTTCAAGAGAATTAGCTCTCCTGTGTACCG-3'
	Bottom Strand	5'-GATCCGTGACACAGGAGAGCTAATCTCTTGAAATTAGCTCTCCTGTGTACCG-3'

Scrambled Negative Control

	Top Strand	5'-AGTGTGCCTACATCTCTTCAAGAGAAGAGATGTAGGCACACTG-3'
	Bottom Strand	5'-GATCCAGTGTGCCTACATCTCTCTTGAAGAGATGTAGGCACACTCG-3'

Figure 5. Sequence and location of each *Spy1A* shRNA construct. (Top) Five novel shRNA constructs were designed to target the mouse *Spy1A* isoform at the indicated amino acid regions (1-5). A scrambled negative control was also designed to ensure that *Spy1A* knockdown was gene specific. Each shRNA sequence is flanked by *HpaI* and *XhoI* restriction sites to allow for direct subcloning into pLB (see Fig.5). Of the five *Spy1A* shRNA constructs designed, construct 2 has been subcloned into the pLB empty vector thus far. The degree to which shRNA constructs are expressed in a given cell population may be determined through GFP-fluorescence microscopy. Illustration of the highly conserved Speedy/RINGO box is provided on the *Spy1A* protein structure, and occupies amino acid positions 66 through 206. (Bottom) Forward (top strand) and reverse (bottom strand) sequences are listed for each *Spy1A* shRNA construct (5'-3'). Sense strands of each shRNA construct are highlighted in green; hairpin loop sequences are highlighted in red; antisense strands are highlighted in yellow. *HpaI* and *XhoI* restriction sites are highlighted in purple.

reverse primer (A425):

5'-GCTCAGTAAACAACATGCATAAAATCGAATTCTGGC-3'

SDM reactions contained the following components: Flag-Spy1A-pLXSN vector DNA (10-100 ng); 0.3 mM dNTP mix (Cat. No. DD0057, Biobasic Inc., Ontario, Canada); 1X pfx buffer and 1 µl pfx polymerase (Cat. No. 11708-013, Invitrogen, Canada); 1 mM MgSO₄; 1 µM each of A424 forward and A425 reverse primers; filter-sterilized nuclease free water up to 50.0 µl. Cycling conditions for SDM included (1) 2 minutes at 94°C, (2) 25 cycles of 94°C for 15 seconds, 55°C for 30 seconds, and 68°C for 5 seconds, and (3) 68°C for 10 minutes. DpnI digestion of SDM reaction products was performed for 2 h at 37°C as per manufacturer's instructions (Cat. No. ER1701, Fermentas, Burlington, Ontario, Canada). DpnI digested products were transformed utilizing TOP10 E.coli and plated onto 100 µg/ml Ampicillin plates. Plasmid DNA was extracted from select colonies utilizing the QIAprep Spin Miniprep Kit (Cat. No. 27104, Qiagen, Mississauga, Ontario, Canada), and was EcoRI digested for 20 minutes at 37°C (Cat. No. FD0274, Fermentas) as per manufacturer's instructions. Colonies that produced a 977 bp fragment upon EcoRI digestion were sent for sequencing (Robarts Sequencing Facility, London, Ontario, Canada) utilizing sequencing primers A210 and A211:

forward primer (A210):

5'-CCCTTGAACCTCCTCGTTTCGACC-3'

reverse primer (A211):

5'-GAGCCTGGGGACTTTCCACACCC-3'

Mutated to contain a second EcoRI site, Flag-Spy1A-pLXSN was EcoRI digested as per manufacturer's instructions (Cat. No. ER0271, Fermentas). Digestion products were electrophoresed at 100V for 1 h, and the resultant 977 bp fragment was gel extracted utilizing the EZ-10 Spin Column DNA Gel Extraction Kit (Cat. No. BS354, Biobasic Inc.). MMTV-SV40-TRPS1 was EcoRI digested for 1 h at 37°C, and incubated with calf intestinal alkaline phosphatase (Cat. No. EF0341, Fermentas) for 30 minutes at 37°C as per manufacturer's instructions. Reaction products were electrophoresed at 100V for 1 h, and the resultant 6.0 kb fragment was gel purified utilizing the EZ-10 Spin Column DNA Gel Extraction Kit. Vector ligation of gel extracts was performed as previously described,⁶³ utilizing T4 DNA ligase (Cat. No. EL0017, Fermentas) as per manufacturer's

instructions. Ligation products were transformed into TOP10 E. coli and plated onto 100 µg/ml Ampicillin plates. Vector DNA was purified from select transformants and sent for sequencing (Robarts Sequencing Facility) utilizing the following four primer sets:

<i>forward primer F1 (A252)</i>	5'-GTTTTATCTGTGCTTATGCC-3'
<i>reverse primer R1 (A253)</i>	5'-GCTCGTATGTTGTGTGGAA-3'
<i>forward primer F2 (A254)</i>	5'-AACCATCACCCCTAATCAAGT-3'
<i>reverse primer R2 (A255)</i>	5'-GTCGCCGCATACACTATT-3'
<i>forward primer F3 (A256)</i>	5'-TTATCCAGTCATACAGCAGG-3'
<i>reverse primer R3 (A257)</i>	5'-ACCCCTGCTGTATGACTGGA-3'
<i>forward primer F4 (A258)</i>	5'-GACCAGAATGTCCACCAGG-3'
<i>reverse primer R4 (A259)</i>	5'-GCCA CCTCTGACTTGAGCGT-3'.

Successful clones were designated as MMTV-SV40-Spy1A, 30 µg of vector DNA was subjected to XhoI (Cat. No. ER0691) and SpeI (Cat. No. ER1251) double digestion as per manufacturer's instructions (Fermentas), and was shipped to the London Transgenic and Gene Targeting Facility (London, Ontario, Canada) for blastocyst microinjection.

III. Reverse Transcriptase-Polymerase Chain Reaction (RT-PCR).

Total RNA was extracted from cell pellets utilizing the GenElute™ Mammalian Total RNA Miniprep Kit (Cat. No. RTN70-1KT, Sigma-Aldrich) or the RNeasy Plus Mini Kit (Cat. No. 74134, Qiagen) as per manufacturer's instructions. RNA concentration and quality were determined via spectrophotometric analysis utilizing the NanoDrop ND-1000 Spectrophotometer (Thermo Fisher Scientific, Wilmington, USA). As per manufacturer's instructions, SuperScript® II Reverse Transcriptase (Cat. No. 18064-014, Invitrogen) was utilized to convert up to 5 µg of total RNA to cDNA. Spectrophotometric analysis was utilized to determine the concentration and purity of resultant first-strand synthesis products. Human Spy1A and GAPDH forward and reverse primers were designed to recognize and amplify conserved exon-exon boundaries utilizing Primer Express 3.0 software:

<i>forward Spy1A primer (A091)</i>	5'-CCATGGGCTTTAGGGAAAAAC-3'
------------------------------------	-----------------------------

reverse Spy1A primer (A073) 5'-TGGCCATAACCTCCTCACAAC-3'
forward GAPDH primer (A087) 5'-GCACCGTCAAGGCTGAGAAC-3'
reverse GAPDH primer (A088) 5'-GGATCTCGCTCCTGGAAGATG-3'

Primers were synthesized by Sigma-Genosys (Sigma-Aldrich). PCR reactions included the following components: a 1:1 dilution of first-strand reaction product (500-1000 ng); 0.2 mM dNTP mix (Biobasic Inc.); 0.4 μ M each of forward and reverse primers; 1X PCR buffer (Qiagen); 2.5 units/ μ l HotStar Taq DNA polymerase (Qiagen); filter-sterilized nuclease free water up to 50 μ l. PCR cycling conditions included (1) denaturation at 94°C for 3 minutes, (2) annealing at 94°C for 1 minute, 55°C for 2 minutes, and 72°C for 1 minute ($N=25$ cycles), and (3) elongation at 72°C for 3 minutes. PCR products were separated on 8% polyacrylamide gel electrophoresis (PAGE) and imaged with GeneSnap software (SynGene) under UV fluorescence.

IV. Cell Lines and Culture Conditions.

MCF7 cells were routinely subcultured in RPMI media (Cat. No. R8758, Sigma-Aldrich) supplemented with 10% calf serum (CS, Cat. No. C8056, Sigma-Aldrich) and 30,000 units penicillin/30,000 μ g streptomycin solution (Cat. No. 15140-122, Invitrogen) and were maintained under normoxic conditions (5% CO₂) at 37°C. HC11 cells were provided as a kind gift by Dr. C. Shermanko, and were routinely subcultured in RPMI media supplemented with 10% calf serum, 30,000 units penicillin/30,000 μ g streptomycin solution, 10 ng/ml insulin, 10 ng/ml epidermal growth factor (EGF), and 1 mM L-glutamine, and were maintained under normoxic conditions (5% CO₂) at 37°C.

Isolation and routine subculture of MMTV-Myc tumor cell lines proceeded in the following manner. Mammary adenocarcinomas were freshly dissected from multiparous female F7 at 115 days (~16 wks). Similarly, virgin female F5A1 was derived from founder male F5 and developed aggressive mammary tumors that were subjected to fresh dissection 199 days (~28 wks) post-birth. Tumor tissue was directly placed in fresh, pre-weighed collagenase buffer (10 mM Hepes, 2.5% FBS, RPMI 1640 supplemented with L-glutamine) and subsequently weighed. In a sterile tissue culture hood, collagenase buffer and tumor tissue were poured together onto a 15 cm plate and chopped for 3 minutes,

using two 10-blade disposable scalpel blades bound together. Next, six razor blades were combined and utilized to break apart tumor tissue for an additional 10 minutes. At 5 ml/gram tissue, fresh collagenase buffer was added to the tumor homogenate and supplemented with a final concentration of 1 mg/ml Sigma Blend L collagenase (Cat. No. C8176, Sigma-Aldrich). Incubation of the tumor homogenate ensued for 1 h at 37°C during which the mixture was subjected to consistent shaking at 200 rpm. A second incubation period was initiated after addition of fresh 1mg/ml collagenase. The resultant mixture was pelleted at 1200 rpm in a refrigerated centrifuge for 10 minutes, followed by four 5 minute washes in collagenase buffer. All centrifugation spins were conducted at 1200 rpm. Primary growth media (1X) was utilized to resuspend a purified cell pellet to a final volume of 20 ml, and the resultant cell suspension was seeded onto four 10 cm plates followed by routine cell culture. Primary tumor cell lines were designated as F7-1 and F5A1-2, according to animal of origin and batch number. Cells were subcultured upon reaching 95% confluency. The subculture of cell lines required the removal of media, followed by 0.05% trypsinization (Cat. No. 25-052-CI, Mediatech, Inc., Manassas, VA, USA) for 2.5 minutes at 37°C. Trypsinized cells were resuspended in 10 ml of fresh primary growth media (1X) and centrifuged for 5 minutes at 800 rpm. Resultant cell pellets were resuspended in 1 ml of fresh media and plated in a 1:50 ratio, followed by incubation at 37°C under normoxic (5% CO₂) conditions. Preparation of primary growth media (1X) required assembly of the following constituents: 500 ml DMEM-F12 media (Cat. No. D6421, Sigma-Aldrich) supplemented with 1 mM L-glutamine (Cat. No. G7513, Sigma-Aldrich); 5µg/ml insulin (Cat. No. I-6634, Sigma-Aldrich); 1µg/ml hydrocortisone (Cat. No. H0888-5G, Sigma-Aldrich); 10 ng/ml human EGF (Cat. No. 13247-051, Invitrogen); 10% fetal bovine serum (Cat. No. F1051, Sigma-Aldrich); 5ng/ml cholera toxin (Cat. No. C8052, Sigma-Aldrich); 100µg/ml penicillin/streptomycin (Cat. No. 15140-122, Invitrogen); 50 µg/ml gentamycin (Cat.No. 15710-064, Invitrogen).

V. Assays for Transient Transfection and Stable Cell Line Production.

Twenty-four hours prior to transfection, cells were seeded at a 1:50 ratio on 10 cm plates in 7 ml of fully supplemented cell-specific media. As an alternative, cells may be

incubated in antibiotic/serum-free media in order to enhance DNA delivery, although this step is not required for successful transfection of F5A1-2 cells. Cells were transfected at 40-50% confluency utilizing polyethylenimine (PEI) transfection reagent (Cat. No. 408727, Sigma-Aldrich), prepared at a final concentration of 0.07 $\mu\text{g}/\mu\text{l}$ in 750 μl media for each plate of cells. A nonviral polycationic polymer, PEI, was utilized for its efficient ability to complex to and deliver vector DNA to mammalian cell lines.⁶⁴ Transfection assays were initially optimized for F5A1-2 primary cells by altering the PEI to DNA ratio and determining which concentration of GFP-tagged vector DNA (2 μg , 4 μg , 8 μg , 12 μg , 20 μg) yielded the highest transfection rates. A concentration of 12 μg resulted in the greatest transfection efficiency. Therefore, 12 μg of plasmid DNA were added to each PEI-media mixture and vortexed for 30 s, followed by incubation at room temperature for 5 minutes. PEI-DNA-media complexes were added directly to cells plated in 7 ml of fully supplemented media, gently rocked, and incubated at 37°C under normoxia (5% CO₂) overnight. Media removal ensued 18-24 h post-transfection followed by downstream analysis. Transfection efficiency was assessed under GFP fluorescence microscopy, and was estimated to range from 20-30% at best in F5A1-2 cell lines.

PEI transfection of Lenti-XTM 293 producer cell lines (Cat. No. 632180, Clontech, Mountain View, CA, USA) was conducted in a similar manner, and was utilized to introduce control or Spy1A-shRNA vectors to a series of pre-optimized packaging vectors that code for the necessary viral components required to form lentiviral particles upon transduction of mammalian cell lines. Following production of infectious lentivirus, control and Spy1A knockdown particles were each concentrated and titered as previously outlined in Welm et al. (2008),⁶⁵ proceeded by infection of F5A1-2 primary tumor cell lines with respective shCntl or shSpy1A filter-sterilized viral preparations. Briefly, 2x10⁵ F5A1-2 cells (passage P60) were plated per well (6-well plate) to determine the multiplicity of infection (MOI) value for late passage F5A1-2 primary cells. 50 μl , 100 μl , or 250 μl of infectious shCntl lentiviral particles were utilized to transduce F5A1-2 cells. Similarly, 50 μl , 150 μl , or 250 μl of infectious shSpy1A lentiviral particles were utilized to transduce F5A1-2 cells. ShCntl and shSpy1A lentiviral stocks utilized at 250 μl per well (6-well plate) yielded the highest transduction levels in F5A1-2 cells (~40%

infection efficiency). Successfully infected shCntl and shSpy1A cell lines were determined through GFP-fluorescence microscopy. Subsequent culturing of each stable cell line ensued for an additional three passages, followed by preparation of frozen-down stable cell line stocks (stored in liquid nitrogen). Stock shCntl lentiviral particles contained a viral titre of 4×10^6 transducing units (TU) per ml. Stock shSpy1A lentiviral particles contained a viral titre of 1×10^7 TU per ml. The MOI value for F5A1-2 primary tumor cell lines was estimated at 5. Future preparation of early passage F5A1-2 stable cell lines, 20 μ l of shCntl and 50 μ l of shSpy1A lentiviral particles may be administered per well in order to infect a starting number of 1.6×10^4 F5A1-2 cells per well (24-well plate). Lentiviral production and infection procedures have been separately described in further detail in the *Appendix* section.

VI. Quantification of Cell Proliferation (Trypan Blue Exclusion).

As described above, control or Spy1A knockdown-treated cell suspensions were prepared 18-24 h post-transfection, and vortexed for 30 s prior to cell counting. Equal parts of trypan blue (Cat. No. T8154, Sigma-Aldrich) and cell suspension were combined (1:1 ratio), and differences in live cell number in response to treatment were quantified with the assistance of a haemocytometer under Brightfield microscopy. In total, an average of the number of live cells counted in each of four quadrants was calculated and applied to the following formula, in order to determine the total cell number present in 1 ml of cell suspension:

$$\text{cells/ml} = (\text{Average Cell Number}) \times (2 \times 10^4 \text{ cells/ml})$$

All trials were completed in triplicate to impart statistical significance ($N=3$ replicates, $p=0.0395$, 1-tail distribution, unequal variance).

VII. Morphological Analysis and Quantification.

F5A1-2 cells that scored positive for GFP were quantified utilizing the 20X magnification objective, and each 10 cm plate was examined for changes in cellular phenotype. Five morphologic categories were derived based on the following features: (1) round, (2) projected round, (3) spindle-like, (4) star-like or undefined, and (5) triangular.

Total cell number was quantified for each category and averaged over a total of three trials ($N=3$). Subsequently, averaged cell numbers for each category were converted to percentages in order to universally compare morphological changes from plate to plate, and also to account for plate variance in total number of positively transfected cells. Student's *t*-test was utilized to determine whether percent differences in cell morphology were biologically significant. Results from quantification studies were verified by completing an additional three trials ($N=3$ replicates). The second set of replicates was conducted by screening a selected portion of each 10 cm plate held consistent between each treatment. Morphologic quantification and statistical analysis (Student's *t*-test) were carried out as described above.

VIII. Estradiol (E2) and MAPK Inhibition Treatments in MCF7 Cells.

Upon 80% confluency, MCF7 cells were incubated in 7 ml of phenol red-free RPMI media (Cat. No. 11835, Invitrogen) supplemented with dextran-coated charcoal (Cat. No. C6241, Sigma-Aldrich) stripped CS and 30,000 units penicillin/30,000 μ g streptomycin solution for 2-3 days prior to treatment in order to remove endogenous effects of local hormone and growth factor signaling. On the day of treatment, cells were incubated with either dimethyl sulfoxide (DMSO, Cat. No. D4540, Sigma-Aldrich) or 50 ng/ml E2 (Cat. No. E1024, Sigma-Aldrich) for 2, 4, or 24 h, followed by cell harvesting for RNA or protein extraction at respective time points. Similarly, in a second set of experiments, MCF7 cells were incubated in phenol-red free, fully supplemented RPMI media for 2-3 days. On the day of treatment, cells were incubated with either 10 μ M SB202474 (control) or 10 μ M U0126 (MEK1/2) inhibitors for 1 h, followed by treatment with 50 ng/ml E2 for 2 or 4 h, after which cell pellets were lysed for protein and analyzed through 10% SDS-PAGE. E2 was initially prepared at a concentration of 10 mg/ml and serially diluted into 0.1 mg/ml and 50 ng/ml working solutions. The latter concentration was utilized for E2 treatment. SB202474 (Cat. No. 444180) and U0126 (Cat. No. 662005-1MG) inhibitors were purchased from CalBiochem (San Diego, CA, USA), respectively and prepared as 10 mM stock solutions in DMSO.

IX. Antibodies.

Primary Antibodies: Rabbit polyclonal anti-Speedy/RINGO antibody (NB100-2521) was purchased from Novus Biologicals (Littleton, CO, USA). Rabbit anti-c-Myc antibody (C3956) was purchased from Sigma-Aldrich. Rabbit polyclonal anti-ER α (HC-20) (sc-543); rabbit polyclonal anti-ERK2 (C-14) (sc-154); goat polyclonal anti-p-ERK1/2 (Thr 202/Tyr 204) (sc-16982); rabbit polyclonal anti-p21 (C-19) (sc-397); goat polyclonal anti-Cytokeratin 19 (CK19, N-13) (sc-33119); mouse monoclonal anti-Cytokeratin 18 (CK18, C-04) (sc-51582) antibodies were purchased from Santa Cruz Biotechnology, Inc. (Santa Cruz, CA, USA). Phospho-p44/42 MAPK (Erk1/2) (Thr202/Tyr204) (D13.14.4E) XP™ Rabbit monoclonal antibody (#4370) was purchased from Cell Signaling (Danvers, MA, USA). Anti-p27^{kip-1} (Ab-2) Mouse monoclonal antibody (DCS72) (NA35) was purchased from CalBiochem. Mouse anti-Actin, Clone C4 (MAB1501R) was purchased from Millipore (Etobicoke, Ontario, Canada). Secondary Antibodies: Anti-Rabbit IgG (whole molecule)–Peroxidase antibody produced in goat (A0545) was purchased from Sigma-Aldrich. Secondary goat antibody (sc-2020) was purchased from Santa Cruz Biotechnology, Inc. Anti-Mouse IgG (Fab specific)–Peroxidase antibody produced in goat (A9917) was purchased from Sigma-Aldrich.

X. Protein Lysis and Immunoblotting Assays.

Homogenized tissue or cell pellets were re-suspended in appropriate volumes of protein extraction buffer and were subjected to cell lysis for 1 h at 4°C with occasional vortexing. Tissue protein extraction buffer comprised the following ingredients: 50 mM Tris-HCl (Cat. No. T5941-1KG, Sigma-Aldrich), pH 7.4; 1.0% Nonidet P40 (Cat. No. 5990-5, Caledon Laboratories LTD., Georgetown, Ontario, Canada); 0.25% sodium deoxycholate (Cat. No. BP349-100, FisherBiotech, Fair Lawn, NJ, USA); 1 mM EGTA (Cat. No. D0077, Biobasic Inc.), pH 8.0; 0.2% sodium dodecyl sulphate (Cat. No. L4509-1KG, Sigma-Aldrich); 150 mM low salt sodium chloride (Cat. No. S-2830-1KG, ACP Chemicals Inc., Montreal, Quebec, Canada); 1.5% Antifoam Y-30 Emulsion (Cat. No. A6457-100ML, Sigma-Aldrich); nuclease-free water to a final volume of 10 ml. Cell protein extraction buffer entailed the following ingredients: 0.1% Nonidet P40; 20 μ M

Tris (Cat. No. T-9235, ACP Chemicals Inc.), pH 7.5; 5 μ M EDTA (Cat. No. 3460-1, Caledon Laboratories LTD.); and 0.1 mM sodium chloride. 1 ml of protein extraction buffer was supplemented with the following protease inhibitors: 5 μ g/ml aprotinin (Cat. No. D0153-50MG, Biobasic Inc.); 5 μ g/ml leupeptin (Cat. No. 103476-89-7, Biobasic Inc.); 5 μ g/ml pepstatin A; 100 μ g/ml PMSF (Cat. No. 52332, EMD Chemicals Inc., USA). Cell lysates were centrifuged for 10 minutes at 4000 rpm to pellet cellular debris, and protein supernatants were collected into a separate tube. A second 100-200 μ l aliquot of each supernatant was prepared for protein quantification. The Bradford assay was utilized to create a standard curve of absorbance (595.0 nm) plotted against known BSA concentrations (0.3125 mg/ml, 0.625 mg/ml, 1.25 mg/ml, 2.5 mg/ml, and 5 mg/ml). Bradford reagent (B6916, Sigma-Aldrich) was added to 5 μ l of protein sample to a final volume of 1 ml, and measured for absorbance at 595.0 nm. Protein samples (300 μ g) were analyzed through 10% SDS-PAGE and membranes were blocked for 20 minutes in 1% BSA (Cat. No. D0024, Biobasic, Inc.) followed by overnight incubation in primary antibody (4°C). Primary antibodies were diluted in 1% BSA accordingly: 1:500 rabbit polyclonal anti-Spy1/RINGO; 1:1000 rabbit anti-c-Myc; 1:833 ER α ; 1:833 total ERK2; 1:833 phospho-ERK1/2 (Santa Cruz Biotechnology); 1:2000 phospho-ERK1/2 (Cell Signaling); 1:500 p21; 1:833 mouse p27; and 1:1000 actin. Membranes were washed three times for 2-3 minutes per wash in 0.5% Tween-20/TBS (TBST), followed by 1 h incubation in the corresponding secondary antibody prepared at a 1:5000 dilution. Membranes were washed three times for 2-3 minutes per wash in TBST, and imaged with AlphaEaseFC software under chemiluminescence (Alpha Innotech HD2 Gel Documentation System). Pierce* Enhanced Chemiluminescent Western Blotting Substrate (PI32106) was purchased from Thermo Fisher Scientific Co. (Ottawa, Ontario, Canada).

XI. Mammary Fat Pad Transplants.

Please see the *Appendix* section for the impending protocol. Briefly, No. 4 inguinal mammary glands were cauterized to prevent endogenous stem cell populations from colonizing the mammary fat pad, which in turn served as an environmental substrate to

support transplanted stable cells of either type. Left cleared fat pads were injected with control shRNA stable cells, whereas right cleared fat pads were injected with Spy1A shRNA stable cells, unless otherwise stated.

XII. Whole Mount Analysis.

Please see the *Appendix* section for the impending protocol.

XIII. Transgenic MMTV-Myc Mouse Colony Propagation and Genotyping.

Three established MMTV-Myc (01XG2) breeder pairs were obtained as founders of our colony from the repository of Mouse Models of Human Cancer Consortium (MMHCC, Frederick, MD, USA). Each breeder pair was comprised of a hemizygous male or female, as well as a wild type FVB partner of female or male origin, depending on hemizygous gender. Three wild type breeder pairs of FVB mice were also purchased from Charles River Laboratory (Wilmington, MA, USA) to prevent inbreeding within the transgenic colony. Utilizing the optimized MMHCC guidelines outlined in *Protocol 1: Allele: Tg(MMTV-Myc)3Led*, all founder pairs were tail clipped and genotyped (http://mouse.ncifcrf.gov/available_details.asp?ID=01XG2). Tail clips (0.5 cm) were processed utilizing the PureLink™ Genomic DNA Mini Kit (Cat. No. K1820-02, Invitrogen). Spectrophotometric analysis was utilized to determine the concentration of genomic DNA isolated from all tail clip samples. The following genotyping primers were utilized to amplify isolated genomic DNA:

forward primer (M022) 5'-CCCAAGGCTTAAGTAAGTTTTTGG-3'

reverse primer (M023) 5'-GGGCATAAGCACAGATAAAACACT-3'

Primers were synthesized by Sigma-Genosys Canada (Sigma-Aldrich). Polymerase chain reaction (PCR) thermo-cycling resulted in the production of an 825 bp amplicon. Each PCR reaction consisted of 100 ng of purified genomic DNA; 0.2 mM dNTP mix; 0.5 μM each of M022 and M023 primers; 1X PCR buffer; 2.0 mM MgCl₂; and 2.5 units/μl HotStar Taq DNA polymerase. PCR buffer, MgCl₂, and HotStar Taq DNA polymerase were purchased from Qiagen (Cat. No. 203205). A final reaction volume of 50 μl was obtained using filter-sterilized nuclease free water. PCR cycling conditions included (1)

denaturation at 94°C for 3 minutes, (2) annealing at 94°C for 1 minute, 65°C for 2 minutes, and 72°C for 1 minute ($N=35$ cycles), and (3) elongation at 72°C for 3 minutes. PCR products were analyzed through 4.25% polyacrylamide gel electrophoresis (PAGE), and imaged with GeneSnap software (SynGene) under UV fluorescence. Two transgenic females (F7, F8) and one transgenic male (F5) were identified (Fig.6a) and could successfully transmit the MMTV-Myc transgene to offspring (Fig.6b). F5 and F7 animals were ear tagged (Cat. No. 1005-1, National Band and Tag Co., Newport, KY, USA). Subsequent breeding of hemizygous females with wild type mating partners led to development of aggressive mammary adenocarcinomas, and resulted in female sacrifice and tissue harvesting. Hence, hemizygous male F5 was utilized to derive the MMTV-Myc transgenic mouse colony for the duration of experiments.

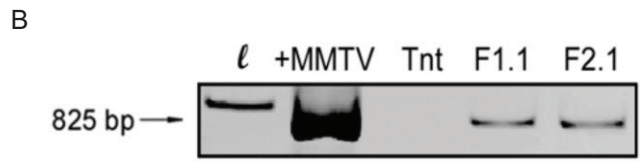
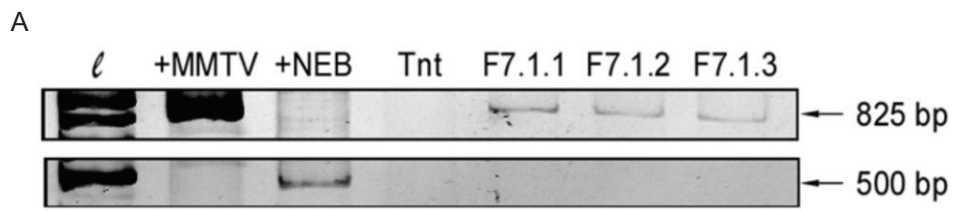


Figure 6. Transgenic MMTV-Myc mouse colony propagation and genotyping. Tail clip samples derived from **(a)** MMTV-Myc female F7, and **(b)** Generation 1 MMTV-Myc offspring F1.1 and F1.2, were subjected to genomic DNA extraction, followed by PCR detection of the MMTV-Myc transgene. **(a)** ℓ = molecular weight standard; +MMTV = a vector backbone known to contain the MMTV-LTR promoter served as a positive control for the successful detection of the 825 bp amplicon produced upon genotyping transgenic animals; +NEB = positive PCR control utilized to ensure that PCR conditions were in working order; Tnt = a negative primer control utilized to confirm the specificity of genotyping primers by excluding the transgene DNA template; F7.1.1 = 200 ng of F7 genomic (g) DNA template utilized during PCR; F7.1.2 = 100 ng of F7 gDNA template; F7.1.3 = 50 ng of F7 gDNA template. **(b)** ℓ = molecular weight standard; +MMTV = positive control that contains the transgene DNA template; Tnt = negative primer control; F1.1 = female offspring 1.1 probed positive for transgenic status; F2.1 = female offspring 2.1 also probed positive for transgene status.

Results

I. Creation of a Transgenic MMTV-Spy1A Mouse Model for In vivo Analysis of Spy1A Overexpression.

As previously described, Flag-Spy1A-pLXSN contains the complete coding sequence of the human Spy1A gene conjugated to a flag tag.⁵³ SDM was utilized to create a second EcoRI site positioned near the terminal region of the human Spy1A coding sequence (Fig.7) in Flag-Spy1A-pLXSN for efficient removal of the intrinsic poly-A tail. SDM primers A424 and A425 were designed to flank the vector region targeted for mutation. SDM reaction products were DpnI digested, and subsequently transformed utilizing TOP10 E.coli and plated onto 100 µg/ml Ampicillin plates. Select colonies were screened for EcoRI insertion and were identified upon detection of a 977 bp fragment following EcoRI digestion of isolated plasmid DNA from each colony (Fig.8a). Successful EcoRI insertion was confirmed through sequencing for two colonies in particular, Is.1 and IIs.3, utilizing A210 and A211 sequencing primers. Purified vector DNA from Colony IIs.3 was subjected to EcoRI digestion, and produced two fragments at 7.0 kb (vector backbone) and 1.0 kb (Spy1A gene insert). Digestion products were separated, and the appropriate 1.0 kb fragment was gel extracted and purified.

EcoRI digestion of 2 µg of MMTV-SV40-TRPS-1 vector DNA ensued, followed by the immediate removal of terminal phosphate groups from digested ends utilizing calf intestinal alkaline phosphatase. Phosphatase treatment was necessary in order to prevent the re-ligation of linearized vector DNA termini. Consequently, reaction products were separated, followed by gel purification of the resultant 6.0 kb fragment (MMTV-SV40 backbone). Ligation of the Spy1A gene insert into the MMTV-SV40 backbone was conducted, and ligation reactions were subsequently transformed utilizing TOP10 E. coli and plated onto 100 µg/ml Ampicillin plates. Select colonies were screened for EcoRI insertion and were identified upon detection of a 977 bp fragment following EcoRI digestion of isolated plasmid DNA from each colony (Fig.8b). Successful cloning of the Spy1A coding sequence into the MMTV-SV40 vector backbone was confirmed through sequencing. Sequencing primers A252, A253, A254, A255, A256, A257, and A258 were utilized in order to verify the intactness of all transgenic vector components.

GAATTCGCGGCCGCGTCGACCTGCGACGGAGCCTTGACCGCCGTTGCCCGGCCCTCTCCC
GCGCAGCCCCGGGCTTCCGCAGGAATATTGGGAAACCAAAATGAGGCACAATCAGATGTG
TTGTGAGACACCACCTACTGTCACTGTTTATGTAAAATCAGGGTCAAATAGATCACATCA
GCCTAAAAAGCCCATTACTCTGAAGCGTCCTATTTGTAAAGATAATTGGCAAGCATTTGA
AAAAAATACACATAATAACAACAAATCTAAACGCCCCAAAGGACCTTGTCTGGTTATACA
GCGTCAGGATATGACTGCTTTCTTTAAATTATTTGATGACGATTTAATTCAAGATTTCTT
GTGGATGGACTGCTGCTGTAAAATTGCAGACAAGTATCTTTTGGCTATGACCTTTGTTTA
TTTCAAGAGGGCTAAATTTACTATAAGTGAGCATAACCAGGATAAATTTCTTTATTGCTCT
GTATCTGGCTAATACAGTTGAAGAAGATGAAGAAGAAACCAAGTACGAAATTTTTCCATG
GGCTTTAGGGAAAAACTGGAGAAAATTGTTCCCTAATTTCTTAAAGTTAAGGGACCAGCT
CTGGGATAGAATTGACTATAGGGCTATTGTAAGCAGGCGATGTTGTGAGGAGTTATGGC
CATTGCACCAACCCATTATATCTGGCAAAGAGAACGTTCTGTTCATCACAGTGGAGCTGT
CAGAACTACAACAGAGATGAAGTTCAGCTGCCCCGGGGACCTAGTGCCACACCAGTAGA
TTGTTCACTCTGTGGTAAAAAAGAAGATATGTTAGACTGGGATTGCTTTCATCATCATC
TTTATCCAGTCATACAGCAGGGGTGACAGAAAAACATTCTCAGGACTCATACAACTCACT
GTCAATGGACATAATAGGTGATCCTTCTCAAGCTTATACTGGTTCTGAAGGTATGATATA
GTAATA

C

↑

TGCCAGAATTAAGATTTATGCATGTTGTTTACTGAGCTCTAGTCAGTCCTTTCTGGCGGGG
ATACATAATAATTTATATACTCCAACAATATGAGTTAAATTAATCTTGAAACTTTCTCCC
CTTTCAGTTACTTTTTTGTCTTGTGTCCATATTTGTTTTGTGGTGACCCACCTAAACAGAT
TTTTAATGTGACCTATGTTAAGTTGAAAATAATGCACCATAAGCCTCAGTATTTTAAGA
GCCTGAATCATTTTTTTTGAATGTTTATTTTATTTCAAAGGGTTTTCAAGAAGAAAAATAA
TTTACTTGTAATCTCAAAAAAAAAAAAAAAAAAAAAA

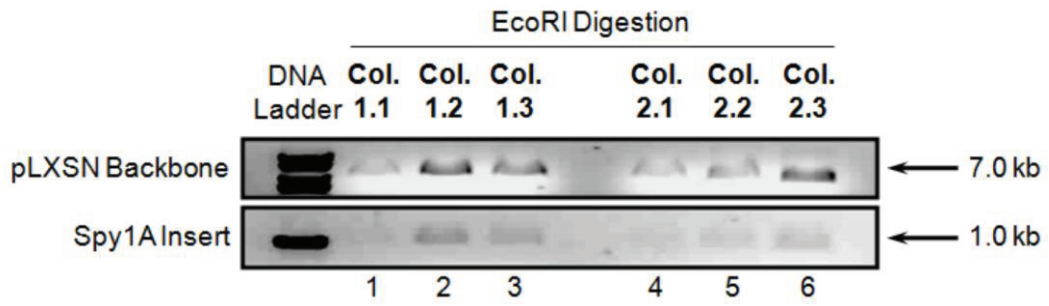
Figure 7. The coding sequence of the human Spy1A gene is targeted for mutation using SDM. SDM was utilized to create a second EcoRI site positioned near the terminal region of the human Spy1A coding sequence in flag-Spy1A-pLXSN for efficient removal of the intrinsic poly-A tail, since the MMTV-SV40-TRPS-1 vector already harbours a unique poly-A tail flanked by an SV-40 intron recommended for transgene expression. The flag-Spy1A-pLXSN vector contains a single EcoRI site at the beginning of the Spy1A coding sequence (highlighted in red, underlined). The mutated nucleotide falls within the second EcoRI insertion site and is highlighted in bold red to demonstrate the change (highlighted in red, underlined), thereby representing creation of a second EcoRI restriction site. The ATG start site is highlighted in blue (underlined).

The resultant transgenic vector was designated as MMTV-SV40-Spy1A and contains an untranslated portion of the Ha-*ras* gene, in addition to an SV40 polyadenylation site.⁶⁶ Bacterial sequences such as those found in vector backbones have been noted to inhibit successful incorporation of transgenic DNA into the mouse blastocyst genome. Thus, XhoI/SpeI double digestion of purified vector DNA (30 µg per tube) ensued, and resulted in the production of two fragments: 4.7 kb (MMTV-SV40-Spy1A transgene) and 2.9 kb (remaining backbone). Two vials of XhoI/SpeI digested transgenic DNA were made available for microinjection into mouse blastocysts for subsequent creation of the first MMTV-SV40-Spy1A transgenic mouse model known to date (Fig.8c). Transgene detection of a single copy of MMTV-SV40-Spy1A DNA was tested utilizing the PCR conditions outlined for M022 and M023 genotyping primers (Fig.8d).

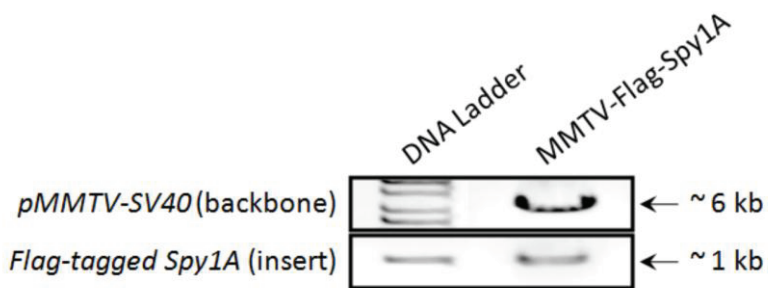
II. Spy1A Elevation in c-Myc Overexpressing Mammary Tumors and Primary Tumor Cell Lines.

The polyoma middle T (PyT) oncogene lies upstream of both the c-Src/PI3K/Akt and Shc/Ras/MAPK pathways,⁶⁷ whereas c-Myc is an established downstream target of MAPK signaling.⁶⁸ For this reason, mammary tumor tissue derived from either MMTV-Myc or MMTV-PyT transgenic mouse models (kindly provided by Dr. T. Seagroves) were utilized to determine the extent to which the endogenous expression profile of Spy1A varies in response to distinct tumorigenic hits in the mammary gland, particularly those associated with altered Raf/ERK kinase activity. Despite the involvement of MAPK signaling in both of these murine models, Spy1A elevation was unique only to c-Myc overexpressing mammary glands and tumor tissue (Fig.9) confirming Spy1A as a downstream target of c-Myc.²² Taken together, these data suggest that c-Myc induction of Spy1A may be mediated in part through Ras/Raf/ERK kinase signaling *in vivo*. Tissue localization in heterogeneous tumor samples is thought to account for the overall upregulation of p27 that occurs in concert with upregulated protein levels of Spy1A in MMTV-Myc mammary tissue (Fig.9), contrary to results obtained from *in vitro* Spy1A overexpression in myc-Spy1A inducible U2OS cells.⁶⁰ Actin was implemented as a loading control for all data derived through immunoblotting. Next, to determine whether

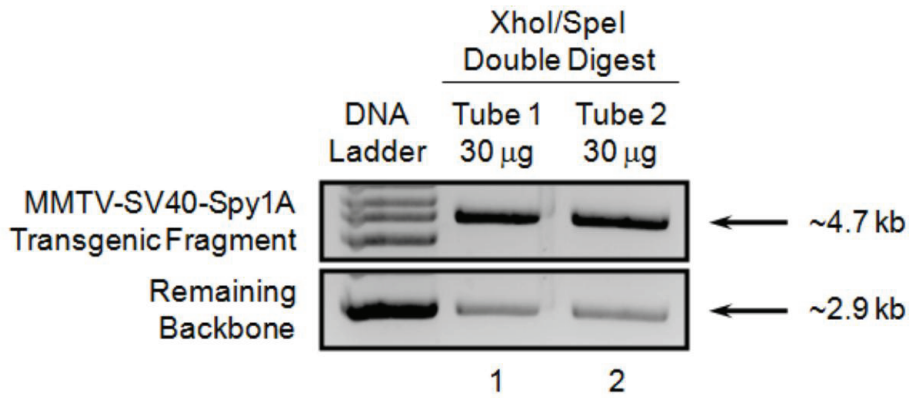
A



B



C



D

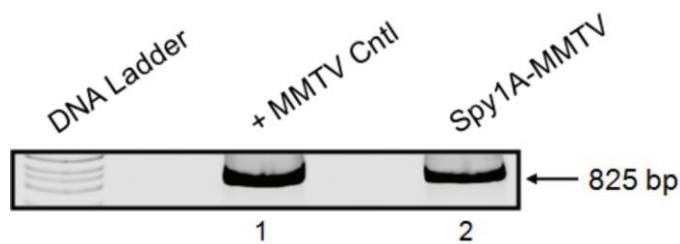


Figure 8. Construction of the first MMTV-SV40-Spy1A transgenic mouse model. (a) SDM-derived mutant Flag-Spy1A-pLXSN constructs were identified upon detection of a 977 bp fragment following EcoRI digestion of isolated plasmid DNA from each colony: colony 1.1 (lane 1); colony 1.2 (lane 2); colony 1.3 (lane 3); colony 2.1 (lane 4); colony 2.2 (lane 5); and colony 2.3 (lane 6). The pLXSN vector backbone was estimated at 7.0 kb, and the Spy1A insert was estimated at 1.0 kb (997 bp). (b) EcoRI digestion of the MMTV-SV40-Spy1A transgenic vector released the flag-Spy1A coding sequence from the remaining vector backbone. EcoRI digestion of the resultant transgene DNA produced a 977 bp fragment as expected, and confirmed successful cloning. The pMMTV-SV40 backbone was estimated at 6.0 kb, and the flag-tagged Spy1A insert was estimated at 1.0 kb (997 bp). (c) The MMTV-SV40-Spy1A vector was double digested with XhoI and SpeI to release the transgenic fragment from the remaining backbone. Digested vector DNA resulted in the production of two fragments: 4.7 kb (MMTV-SV40-Spy1A transgene) and 2.9 kb (remaining backbone). Two vials of XhoI/SpeI digested transgene DNA were prepared for microinjection (lanes 1 and 2). (d) A single copy of MMTV-SV40-Spy1A DNA can be detected utilizing PCR genotyping methods previously described in *Materials and Methods*. Transgene DNA was successfully detected using 8% PAGE, in order to verify the success of using the M022/M023 primer set for detection of the Spy1A transgene in tail clip samples. PCR amplification of MMTV-SV40-Spy1A vector DNA (lane 2) using M022/M023 primers produced an 825 bp amplicon, identical to the positive MMTV vector control (+ MMTV, lane 1) as expected.

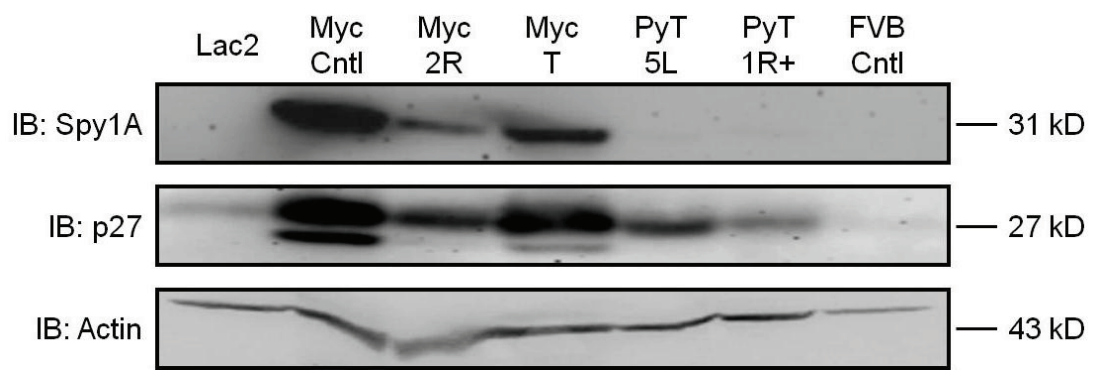


Figure 9. The endogenous expression profile of *Spy1A* protein in *c-Myc* overexpressing mammary tumors. Fourth inguinal mammary tissue and tumors were isolated from wild-type FVB, MMTV-Myc, and Polyoma Middle T Antigen (PyT) mouse models. Protein lysates were analyzed by 10% SDS-PAGE and probed with the indicated antibodies (sizes are included on the right in kilo Dalton (kD) units): non-transgenic control gland (Lac2); unaffected MMTV-Myc gland in transgenic animal (Myc Cntl); MMTV-Myc tumor in right gland (Myc 2R); MMTV-Myc tumor, gland not indicated (Myc T); PyMT 4154 tumor in left gland (PyT 5L); PyMT 4153 tumor in right gland (PyT 1R+); wild-type FVB gland (FVB Cntl). The blot depicted here is one representative of $N=2$ replicates.

Spy1A elevation in c-Myc overexpressing tumors can be maintained during primary tumor culture, the MMTV-Myc mouse model, well documented for its ability to form aggressive mammary adenocarcinomas,⁶⁹ was utilized to derive a previously uncharacterized tumor cell line engineered to overexpress c-Myc, henceforth referred to as F5A1-2. Fourth inguinal mammary glands were also extracted from wild-type FVB females, and utilized to determine whether c-Myc overexpression correlates with an increase in Spy1A expression in F5A1-2 cell lines. Thus, control glands represent a non-tumorigenic equivalent of signaling within the breast micro-environment. Additionally, upregulation of c-Myc protein in primary tumor cells was confirmed through immunoblotting, correlating with a persistent elevation in Spy1A, whereas p27 levels remained virtually undetectable in comparison to control mammary gland tissue ($N=3$ replicates, Fig.10).

III. RNAi-Mediated Spy1A Knockdown in F5A1-2 Cell Lines Reduces Cell Proliferation and Alters c-Myc Levels In vitro.

To determine the essentiality of Spy1A for c-Myc induced tumorigenesis, F5A1-2 cell lines were transiently transfected with either shCntl or shSpy1A recombinant pLB vectors. Twenty-four hours post-transfection, alterations in cell proliferative capacity were quantified through trypan blue exclusion, demonstrating a statistically significant decrease in cell number upon short-term abrogation of Spy1A (Fig.11a). Knockdown of Spy1A was confirmed at the protein level through immunoblotting and appeared to downregulate c-Myc at earlier cell passages (~P35) when normalized to Actin (Fig.11b). Thus, under *in vitro* conditions, Spy1A has been implicated here as a potential mediator of tumor cell proliferation in mammary cells governed by enhanced c-Myc signaling.

In order to partially clarify the mechanism utilized by c-Myc to maintain a tumorigenic state in the mammary gland when the proto-oncogene is overexpressed, a subset of primary tumor cultures were independently infected with either control or Spy1A shRNA lentiviral particles for 24 h prior to removal of viral-containing media. Hereafter, resultant stable F5A1-2 cell lines will be referred to as F5A1-2^{shCntl} and F5A1-2^{shSpy1A}, respectively. To allow for stable integration of each shRNA construct into the tumor cell genome, transduced cells were passaged three times (P3) and cell lines were subjected to

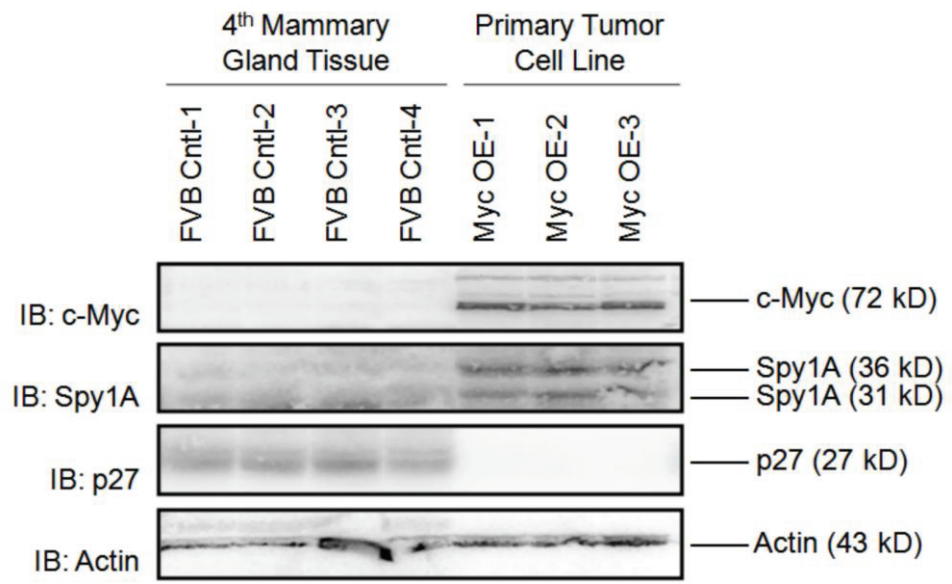


Figure 10. MMTV-Myc primary tumor cell lines continue to express elevated levels of *Spy1A* protein. F5A1-2 primary mammary tumor cell lines were derived from MMTV-Myc transgenic mice (Myc OE-1, 2, 3). No. 4 inguinal mammary glands were extracted from wild-type FVB mice (FVB Cntl-1, 2, 3, 4) as an internal reference. Protein extracts were analyzed through 10% SDS-PAGE and probed with the indicated antibodies (sizes are included on the right in kilo Dalton (kD) units). The blot depicted here shows all replicates ($N=4$) for control fourth mammary gland tissue, in addition to displaying all replicates ($N=3$) for F5A1-2 whole cell extracts.

immunoblotting in order to assess the efficacy of long-term Spy1A inhibition. In direct discordance with previous data (Fig.11b), immunoblotting revealed an upregulation of c-Myc protein levels upon genetic silencing of Spy1A, together with an increase in phospho-ERK1/2 expression (Fig.12a). Note that overall changes in MAPK expression were calculated through densitometry by normalizing phosphorylated levels of ERK1/2 to those of total ERK1/2, whose basal protein expression remained consistent throughout all treatments (Fig.12b). Next, stable F5A1-2 cell lines were cultured for an additional two passages in preparation for upcoming mammary fat pad transplants. Analysis of protein expression via immunoblotting indicated insignificant Spy1A knockdown for either cell set, as evidenced by a 2% decrease (lanes 1-2, Cell Set No.1) and a 0.5% increase (lanes 3-4, Cell Set No.2) in Spy1A protein expression, respectively (Fig.13a-b). Likewise, c-Myc, ERK1/2, p21, and p27 protein levels did not fluctuate significantly for either cell set when compared to control knockdown treatments (Fig.13a-b). Thus, late passage F5A1-2 cell lines appear to acquire resistance to RNAi-mediated Spy1A inhibition in response to long-term subculture. Note that densitometry values are considered to be preliminary at this stage of analysis due to inadequate statistical replication of data.

IV. Transient Spy1A Knockdown May Alter Cellular Morphology In vitro.

Upon RNAi-mediated attenuation of Spy1A activity in P33 F5A1-2 cells, subtle morphological changes in cellular phenotype were consistently detected in comparison to control knockdown treatments. To discern the underlying reason for these alterations in phenotypic state, F5A1-2 cell lines were subjected to transient shRNA transfection for 24 h and visualized through GFP-fluorescence microscopy. Morphological assessment of cell types could not be conducted under Brightfield microscopy, since transfection efficiencies never reached past 30%. A total of five morphological categories were chosen to represent the scope of phenotypic states available to each cell mass. These included round, projected round, spindle-like, undefined or star-like, and triangular (Fig.14). Only those cells successfully transfected and thus actively co-expressing GFP and either control or Spy1A shRNA were considered for the study. Green fluorescing cells were examined at a magnification of 20X and scored for their morphological appearance, followed by tallying the total number of cells that portrayed each phenotypic

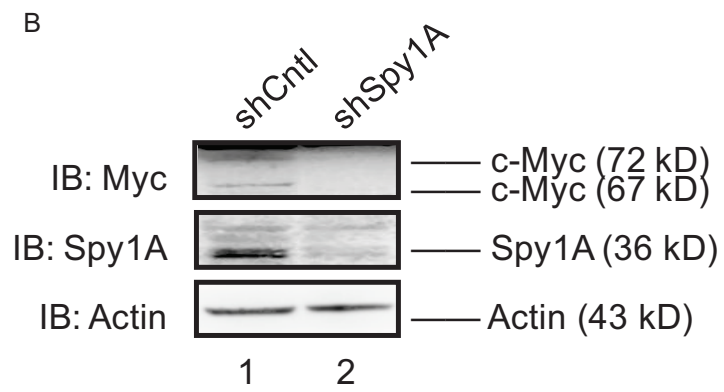
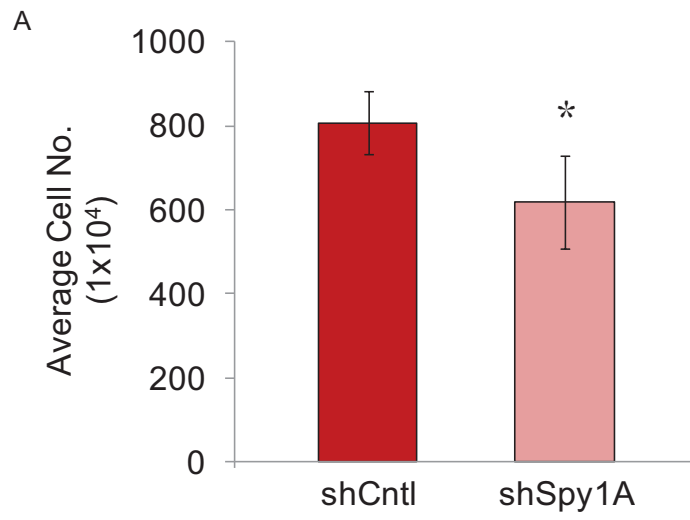


Figure 11. Transient *Spy1A* knockdown affects cell proliferation rate and *c-Myc* protein levels *in vitro*. (a) Late passage F5A1-2 cell lines (>P60) were transfected with GFP-tagged *Spy1A* shRNA (sh*Spy1A*) or scrambled shRNA (shCntl) recombinant constructs. Cells were counted 48-72 h post-transfection using trypan blue exclusion methods. Error bars indicate measurements of standard deviation calculated for $N=3$ separate trials. *Student's *t*-test was utilized to verify statistical significance where applicable ($p=0.0395$, 1-tail distribution, unequal variance). (b) Early passage F5A1-2 whole protein extracts (P33) were assessed through 10% SDS-PAGE, followed by immunoblotting for *c-Myc* (67kD); *Spy1A* (36 kD); and Actin (43 kD). Actin was implemented as a suitable loading control; protein data were normalized to total levels of Actin. The blot depicted here is one representative of $N=2$ replicates.

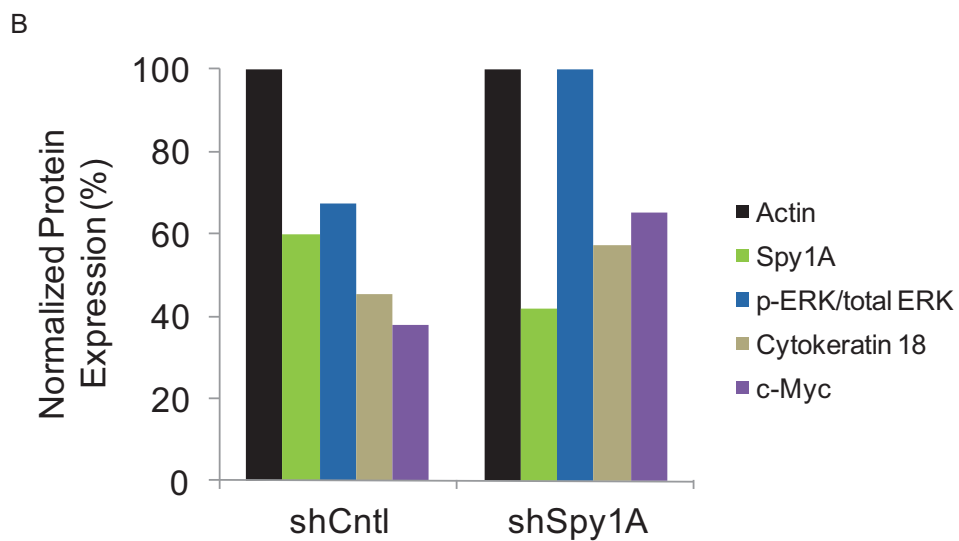
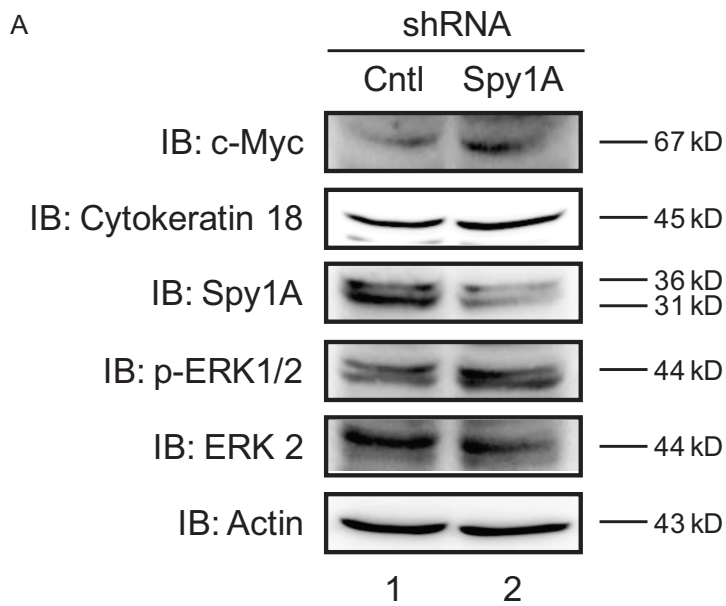
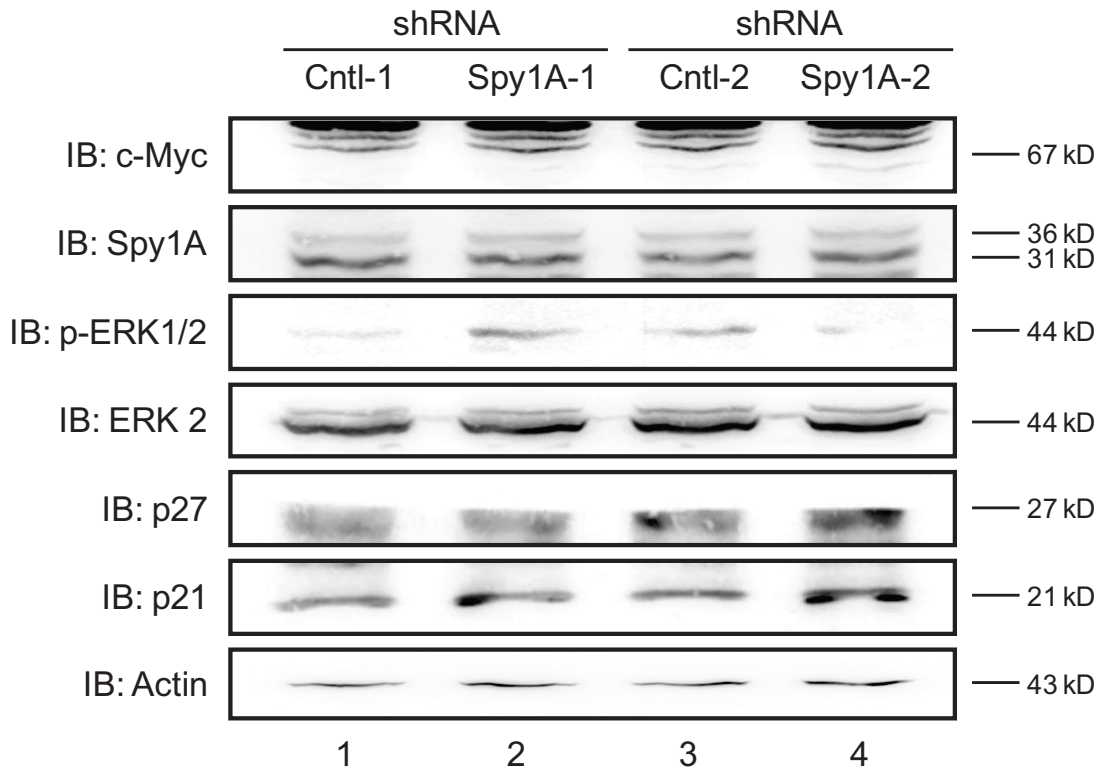
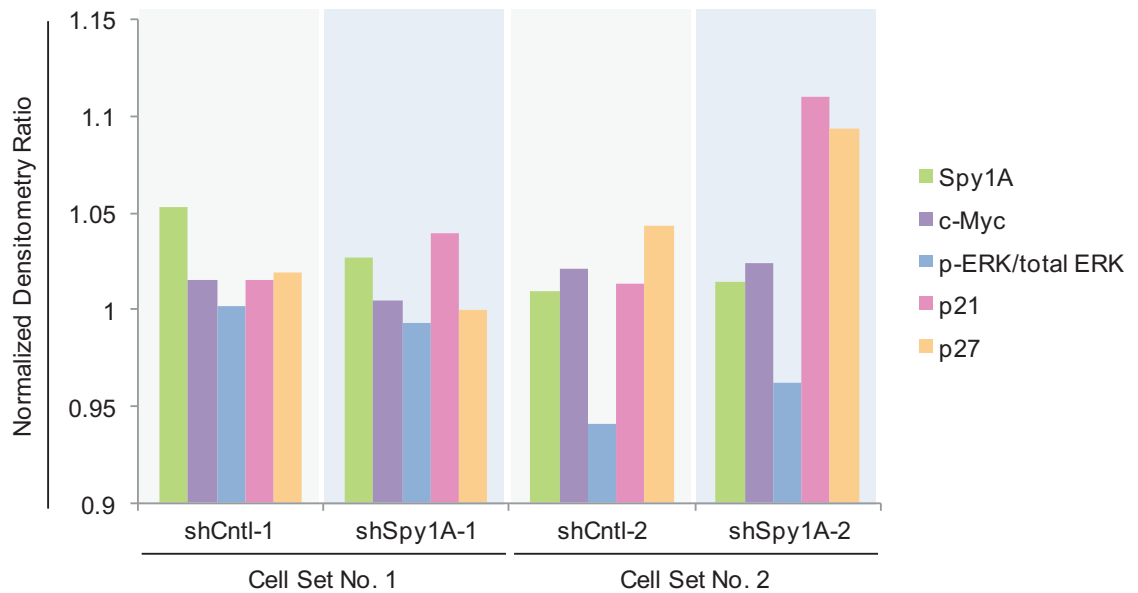


Figure 12. Stable F5A1-2 cell lines exhibit differential signaling upon lentiviral-mediated Spy1A knockdown. Primary cells cultured to passage 60 were stably infected with scrambled (shCntl) or Spy1A (shSpy1A) shRNA lentiviral particles for 72 h, after which stable knockdown cell lines were subcultured for an additional three passages (P3). **(a)** Protein lysates were extracted and subsequently analyzed through 10% SDS-PAGE, followed by immunoblotting with the indicated antibodies: c-Myc (67kD); CK18 (45 kD), a luminal epithelial cell marker; Spy1A (31 and 36 kD isoforms); phosphorylated ERK1/2 (p-ERK 1/2) (42 and 44 kD isoforms); total ERK2 (ERK 2) (44 kD); and Actin (43 kD), utilized as a reliable loading control. The blot depicted here is representative of $N=1$ replicate. **(b)** Densitometry was implemented in order to quantify pixel intensity for each protein band, and made use of Actin levels to normalize each data set. Resultant values were interpreted here as relative measures of protein expression for Actin (black); Spy1A (green); p-ERK/total ERK (blue); CK18 (tan); and c-Myc (purple).

A



B



C

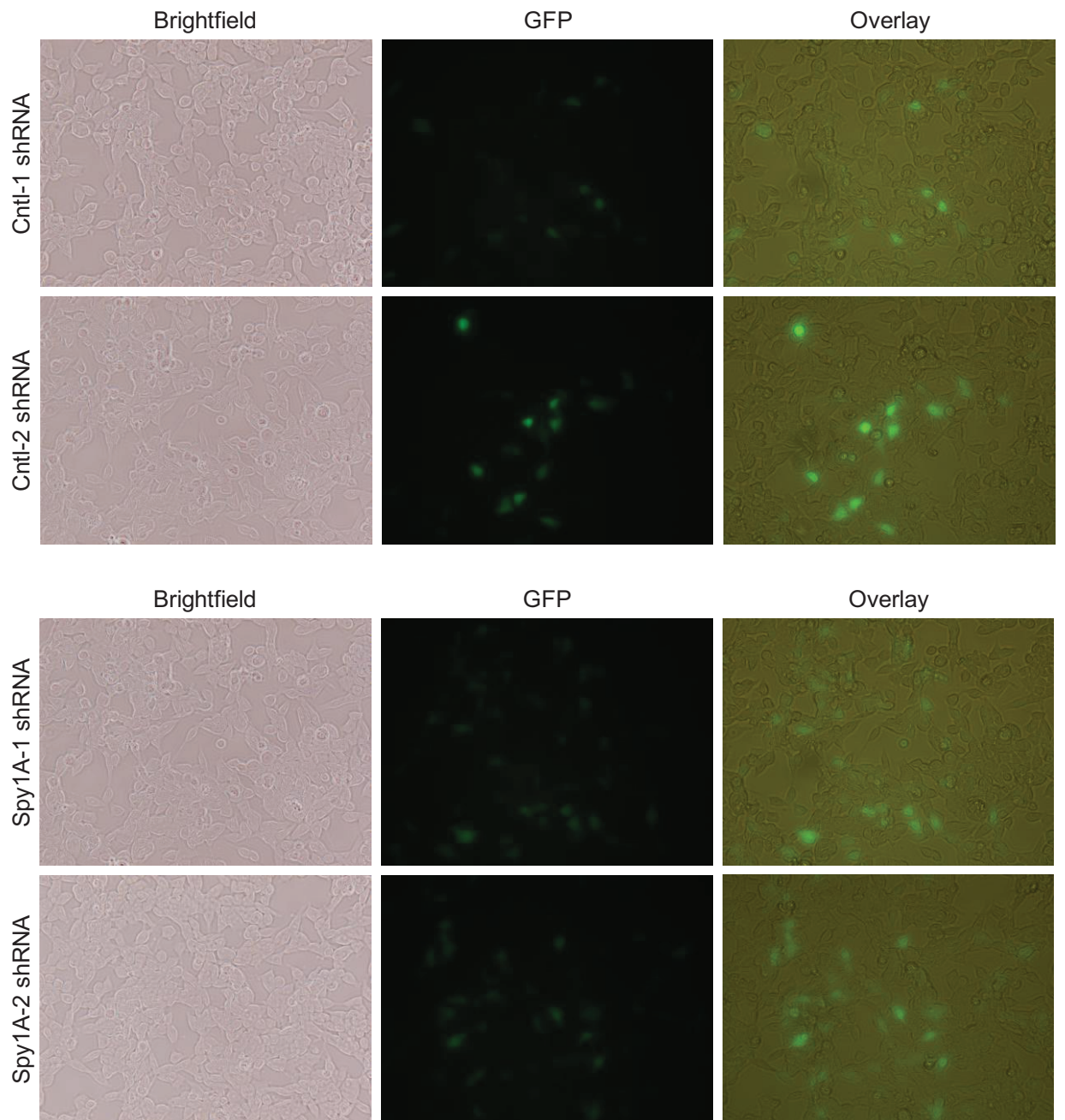


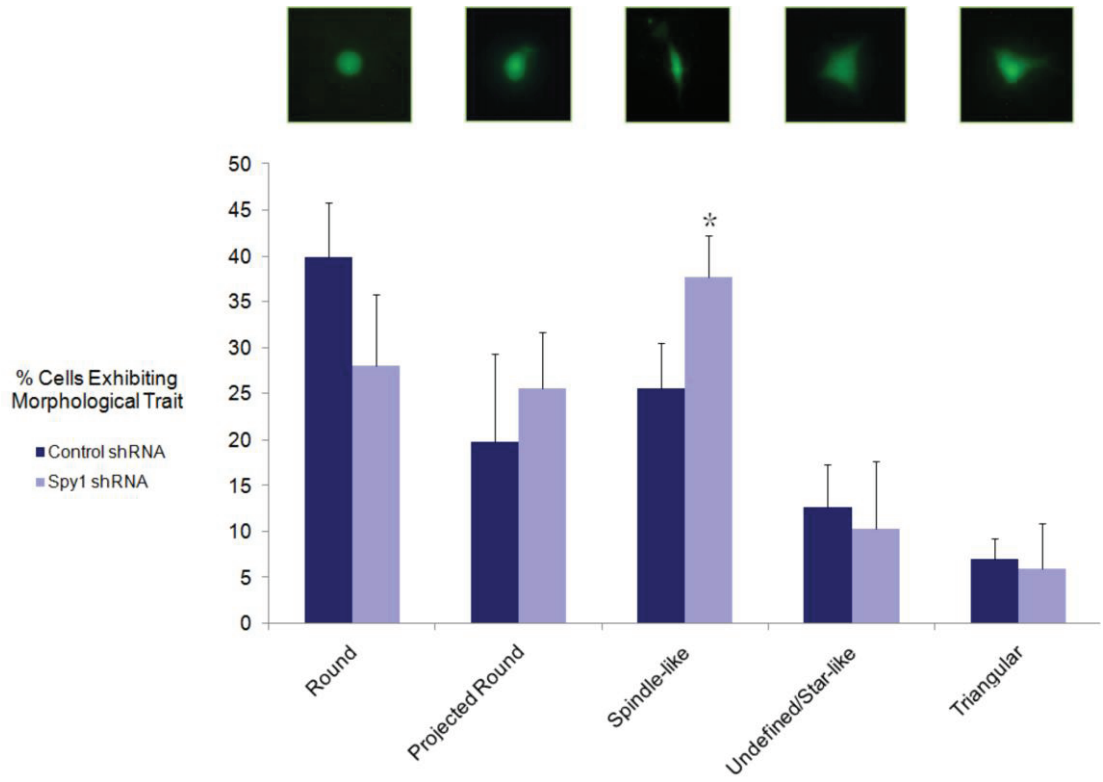
Figure 13. Stable F5A1-2 primary tumor cell lines. Stable scrambled (shCntl) and Spy1A (shSpy1A) knockdown cell lines were subcultured over a total of five passages (P5) to a confluency of 90-95%, immediately after lentiviral infection. **(a)** Protein lysates freshly isolated from P5 stable cell lines were analyzed through 10% SDS-PAGE, and immunoblotted with the indicated antibodies: c-Myc (67kD); Spy1A (31 and 36 kD isoforms); phosphorylated ERK1/2 (p-ERK 1/2) (44 kD isoform); total ERK1/2 (ERK 2) (42 and 44 kD isoforms); p27 (27 kD); p21 (21 kD); and Actin (43 kD), a loading control. The blot depicted here depicts $N=2$ replicates of each F5A1-2 stable cell line. Cell set No. 1 includes Cntl-1 (lane 1) and Spy1A-1 (lane 2) samples; cell set No. 2 includes Cntl-2 (lane 3) and Spy1A-2 (lane 4) samples. **(b)** Normalized densitometry ratios measuring pixel intensity of each protein band were graphed for cell sets No. 1 (shCntl-1, shSpy1A-1) and No. 2 (shCntl-2, shSpy1A-2): c-Myc (purple); Spy1A (green); p-ERK/total ERK (blue); p21 (fuschia); and p27 (orange). **(c)** Representative Brightfield (left panels) and GFP-fluorescence (middle panels) images were taken for shCntl and shSpy1A stable cell lines. An overlay of Brightfield and GFP-fluorescence images is also displayed (right panels), and provides an estimation of lentiviral infection efficiency.

state in a given 10 cm plate. Total cell counts for each morphological category were averaged against 3 replicates and converted to percentages based on total GFP-positive cell number (Fig.14a). Overall, the percentage of primary tumor cells exhibiting spindle-like morphology increased significantly upon Spy1A knockdown (Fig.14a), whereas remaining phenotypic categories did not exhibit variations that were considered to be statistically significant, as evidenced by probability values greater than 5% (statistical *p*-values not reported). It follows that an increase in the quantity of spindle-shaped F5A1-2 tumor cells should correlate significantly with reduced cell types that exhibited round/projected round morphology at the time of analysis. However, a *p*-value of 0.054 – although marginal in statistical significance – demonstrated that this does not hold true. Therefore, to further clarify whether morphological changes resulted from a true change in cellular phenotype, rather than as a by-product of increased space within the tissue culture dish, and also to determine whether phenotypic changes were attributed to altered cell signaling, the protein status of CK18, a structural marker traditionally utilized to detect mammary cells of epithelial lineage,⁷⁰ was assessed in mid passage (P33) F5A1-2 cells differentially treated with shCntl or shSpy1A RNAi. Protein isolation ensued 24 h after shRNA treatment, followed by 10% SDS-PAGE analysis and immunoblotting for Spy1A, Actin, and CK18 (Fig.14c). Protein expression was subsequently quantified through densitometric analysis for both Spy1A and CK18 (data normalized to Actin). Following transient suppression of Spy1A gene activity (48%), CK18 protein levels decreased significantly by 31%, supporting that F5A1-2 cells respond to Spy1A inhibition by reverting to a myoepithelial-like cell state, *in vitro*. Immunoblotting ensued for a second luminal epithelial marker, CK19 to confirm CK18 results. However, since CK19 protein expression was undetectable in both shCntl and shSpy1A treated cell lines (data not shown), acquisition of a myoepithelial cell fate remains to be verified.

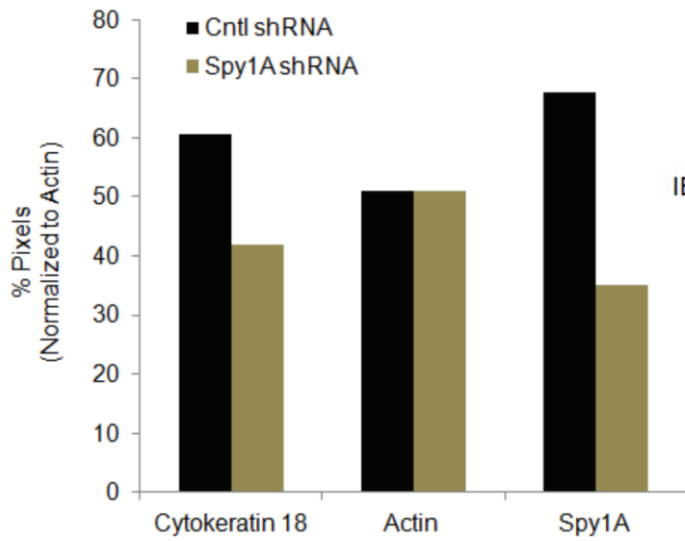
V. Estrogen Signaling Upregulates Spy1A mRNA and Protein Expression in MCF7 Cells.

ER α positive MCF7 cell lines are documented for their ability to respond to estradiol treatment with an increase in cell proliferative capacity.¹² For this reason, MCF7 cells were utilized to determine the effects of estrogen signaling on Spy1A mRNA and protein

A



B



C

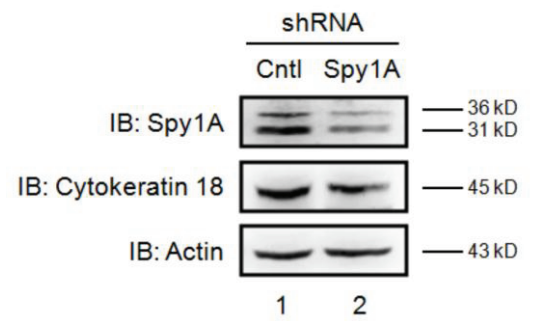


Figure 14. F5A1-2 tumor cell phenotype partially acquires spindle-like morphology upon abrogation of *Spy1A* signaling. F5A1-2 primary tumor cell lines were transfected with shCntl or shSpy1A recombinant pLB vectors. GFP-positive cells were counted under GFP fluorescence and were categorized into five morphological categories: round, projected round, spindle-like, undefined/star-like, and triangular. **(a)** Representative GFP-fluorescence images appear above each cell type. Error bars indicate measurements of standard deviation as calculated for three separate trials. *Student's *t*-test was utilized to verify statistical significance where applicable ($p=0.02$, Student's *t*-test, 1-tail distribution, unequal variance; $N=3$ replicates). **(b)** Densitometry was conducted for the protein blot indicated in (c) for CK18, Actin, and Spy1A. Black bars are indicative of percent pixel intensity for Cntl shRNA samples; tan bars are indicative of percent pixel intensity for Spy1A shRNA samples (data normalized to Actin). **(c)** P33 F5A1-3 cell lines were subjected to protein extraction, followed by 10% SDS-PAGE and immunoblotting for the following antibodies: Spy1A (31 kD); CK18 (45 kD), an epithelial marker of luminal cell fate; and Actin (43 kD), utilized as a loading control. The blot depicted here is representative of $N=1$ replicate.

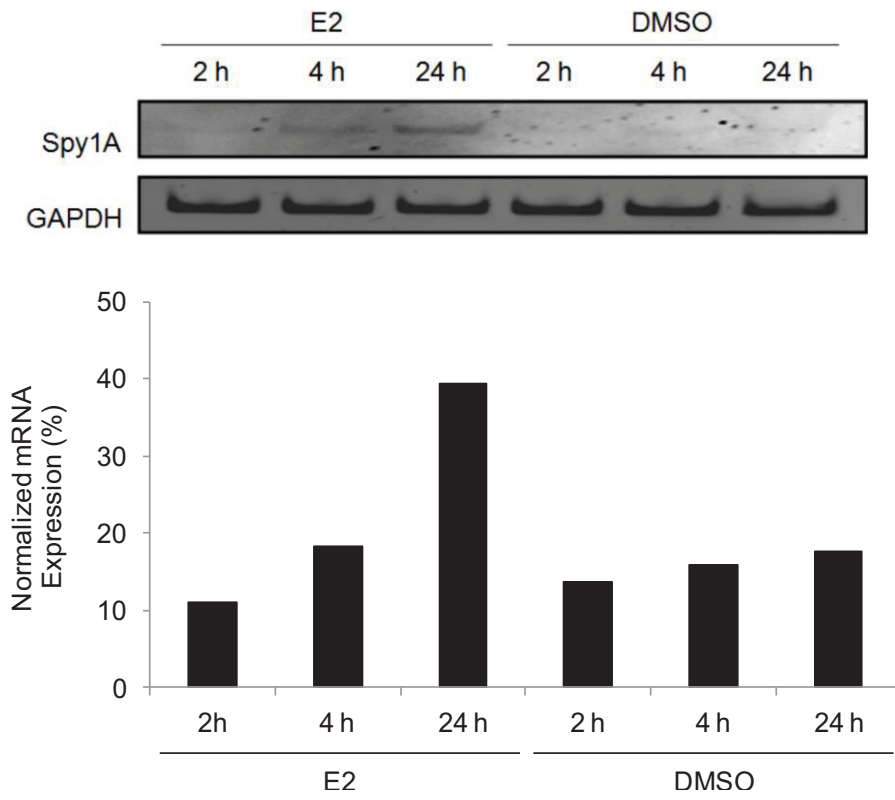
levels *in vitro*. The promiscuous behaviour of ER α and its ability to crosstalk and provide feedback to numerous signaling pathways during mammary development and tumorigenesis confounds the analysis of estrogen signaling alone.⁷¹ For this reason, media for estrogen receptor-positive MCF7 cells were charcoal-stripped of all endogenous hormone/growth factor signaling, and cells were treated for a period of 72 h or greater, prior to treatment with DMSO (vehicle control) or E2, a molecular derivative of estrogen. Administration of DMSO or E2 treatment for 2, 4, or 24 h preceded analysis through immunoblotting and RT-PCR. E2 increasingly stimulated Spy1A mRNA levels over a 24 h time period, and effects of estrogen on Spy1A transcription were most prominent at 24 h post-treatment (Fig.15a). Western blots confirmed the upregulation of Spy1A protein as early as 2 h post-treatment in response to E2 (Fig.15b), implicating Spy1A as a candidate downstream target for short-term estrogen signaling.

VI. MAPK Mediates the Ability of Estrogen to Induce Spy1A Expression in MCF7 Cells.

Beyond MAPK-mediated transcriptional activation of ER, recent reports have indicated a heightened ability for E2 to stimulate ERK1/2 activity five minutes post-administration in ER-positive cell types.¹⁵ In an effort to determine the underlying mechanism exploited by E2 to upregulate Spy1A in aberrantly proliferating mammary cells, we postulated that MAPK signaling plays a central role in E2-stimulated Spy1A expression. Although no study to date has evaluated the potential for MAPK members to directly elevate Spy1A, PD098059 inhibition of MEK1 activity produces *in vitro* downregulation of Spy1A in the immortalized HC11 cell system.²² Furthermore, Lenormand et al. (1999) previously established that Spy1A induction of *Xenopus* oocyte maturation is dependent upon intact MAPK signaling, and utilizing electromobility shift assays, demonstrated the capacity of exogenous Spy1A mRNA to trigger MAPK phosphorylation events in *Xenopus* oocytes as early as 2 h post-injection,⁷² suggesting the existence of a positive feedback loop between Spy1A and MAPK.

Therefore, in order to elucidate the degree to which E2 requires MAPK activation to induce Spy1A, I evaluated the ability of E2 to stimulate expression of Spy1A in MCF7 cell lines subjected to short-term treatment with control (SB202474) or MEK1/2 (U0126)

A



B

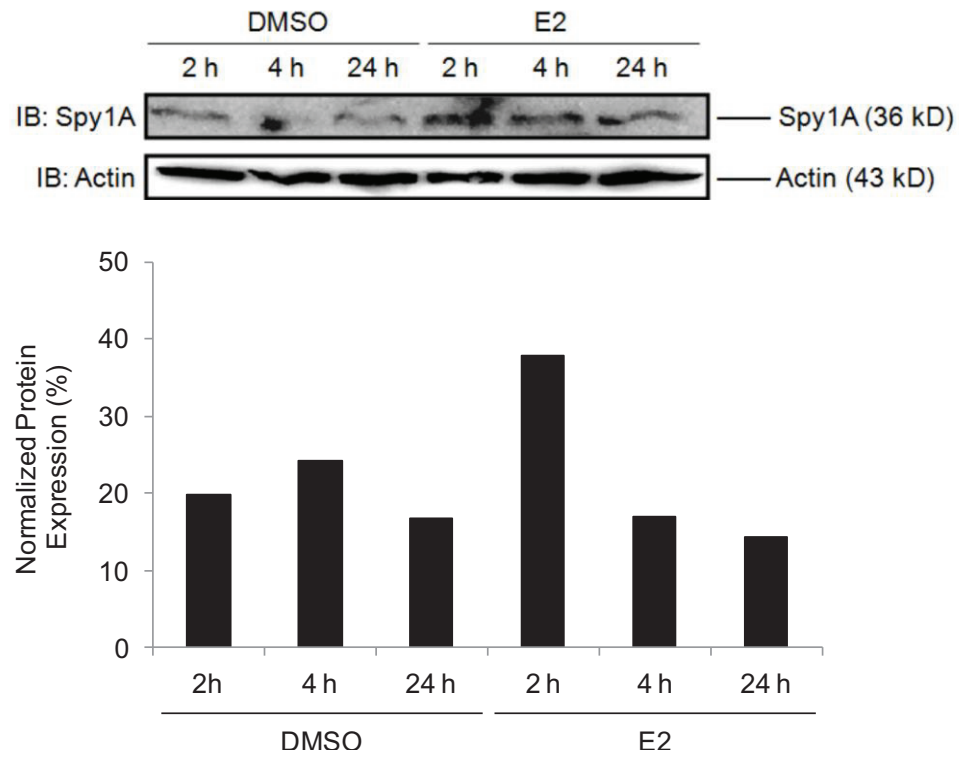
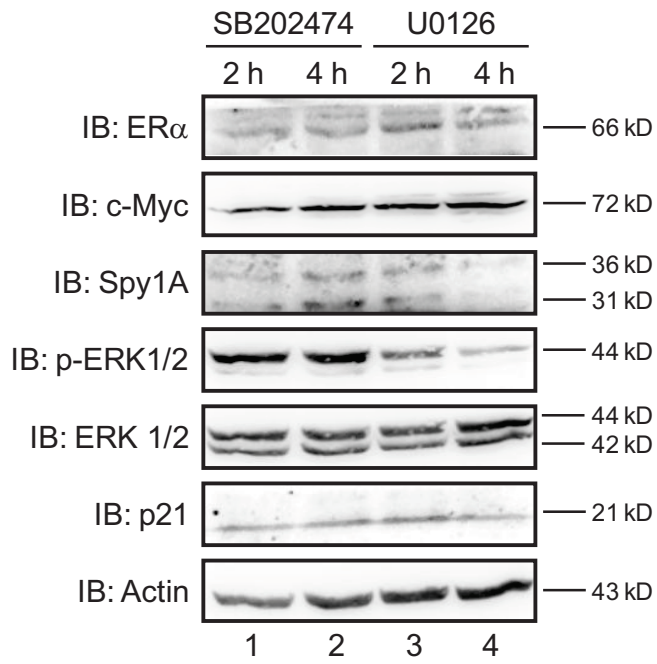


Figure 15. Treatment with estradiol (E2) induces *Spy1A* mRNA and protein expression in MCF7 cells. MCF7 cells were incubated in phenol red free media supplemented with charcoal-stripped serum prior to treatment with E2 or DMSO. **(a)** Total RNA and **(b)** protein were extracted from cells undergoing treatment for 2, 4, or 24 h. **(a)** RT-PCR was performed (n=25 cycles) utilizing *Spy1A* and GAPDH specific primers. The blot depicted here is representative of *N*=1 replicate. Densitometry values for each mRNA band were normalized to GAPDH and converted to normalized mRNA expression (%). 2 h, 4 h, and 24 h treatments (black bars). **(b)** Protein lysates were analyzed through 10% SDS-PAGE and probed with the indicated antibodies (sizes are included on the right in kilo Dalton (kD) units). The blot depicted here is one representative of *N*=2 replicates. Densitometry values for each protein band were normalized to Actin and converted to normalized protein expression (%). 2 h, 4 h, and 24 h treatments (black bars).

inhibitors. Following overnight incubation in phenol red free media containing charcoal-stripped serum, MCF7 cells were treated chemically for 1 h with SB202474 or U0126 inhibitors, followed by immediate administration of E2 for 2 h or 4 h. Isolation of protein ensued at respective time points, and protein lysates were analyzed through 10% SDS-PAGE for ER α , c-Myc, Spy1A, phosphorylated and total levels of ERK1/2, in addition to the CKIs p21 and p27 (Fig.16a). Actin was implemented as a loading control due to its stable expression in mammary cells.²² Note that SB202474 and U0126 inhibitors were not removed prior to treatment with E2, allowing control and MEK1/2 inhibition to continue respectively throughout the entire time course. In this way, a total of 3 h of U0126 treatment resulted in a 50% decrease in ERK1/2 protein expression as compared to 3 h of SB202474 control treatment (Fig.16b). Relative to 5 h of SB202474 control inhibition, MEK1/2 inhibition caused an 86% decline in ERK1/2 protein expression in response to 5 h of U0126 treatment, further demonstrating that the potency of MAPK knockdown increases over longer treatment periods (Fig.16b). Interestingly, 2 h and 4 h of E2 treatment following administration of MAPK inhibitory particles resulted in a respective decrease in total ER α levels by 20% and 27%, whose pattern of expression coordinated with the apparent decrease in p21 levels (16% and 35%, respectively) when compared to control inhibition (Fig.16b). Of key importance was a prominent decrease in Spy1A protein expression (43% and 91%, respectively) in response to 1 h of MAPK inhibition coupled to 2 h or 4 h of E2 stimulation when compared to control time points (Fig.16b). In contrast to previous reports,⁷³ MAPK inhibition resulted in a 24% increase in c-Myc protein levels as early as 2 h post-E2 stimulation relative to control treatment, whereas the 4 h time point did not invoke any significant changes in c-Myc expression (Fig.16b), as previously documented by Lobenhofer et al. (2000).⁷³ Taken together, these data demonstrate that *in vitro* disruption of MAPK signaling reduces Spy1A protein levels in ER α -positive, estrogen-responsive BC cell lines, depending on the length of time cell populations are subjected to inhibitory exposure. Furthermore, results depicted here imply that E2 requires functional MAPK signal transduction to effectively upregulate Spy1A protein expression within the MCF7 cell system, although results are strictly preliminary and require additional replication to verify changes in protein expression.

A



B

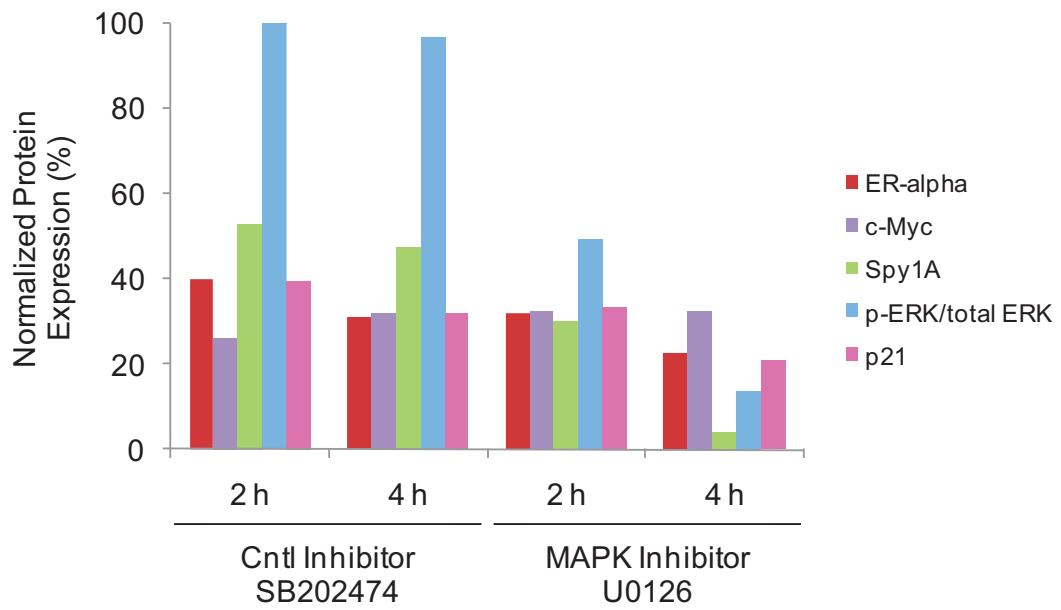


Figure 16. Estradiol (E2) requires intact MAPK activation to induce Spy1A protein expression in the MCF7 cell system. MCF7 cells were incubated in phenol red free media supplemented with charcoal-stripped serum prior to 1 h treatment with control (SB202474) or MAPK (U0126) inhibitors. Following 1 h incubation with each inhibitor, E2 treatment ensued for 2 h or 4 h. **(a)** Total protein was extracted from cells undergoing E2 treatment for 2 h or 4 h, followed by analysis through 10% SDS-PAGE. Protein lysates were immunolabelled with the following antibodies: ER α (66kD); c-Myc (72 kD); Spy1A (31 and 36 kD isoforms); phosphorylated ERK1/2 (p-ERK1/2) (42 and 44 kD isoforms); total ERK1/2 (42 and 44 kD isoforms); p21 (21 kD); and Actin (43 kD), the loading control. The protein blot depicted here is representative of *N*=1 replicate. **(b)** Densitometry values for each protein band were normalized to Actin and converted to normalized protein expression (%): ER α (red); c-Myc (purple); Spy1A (green); p-ERK/total ERK (blue); and p21 (fuschia).

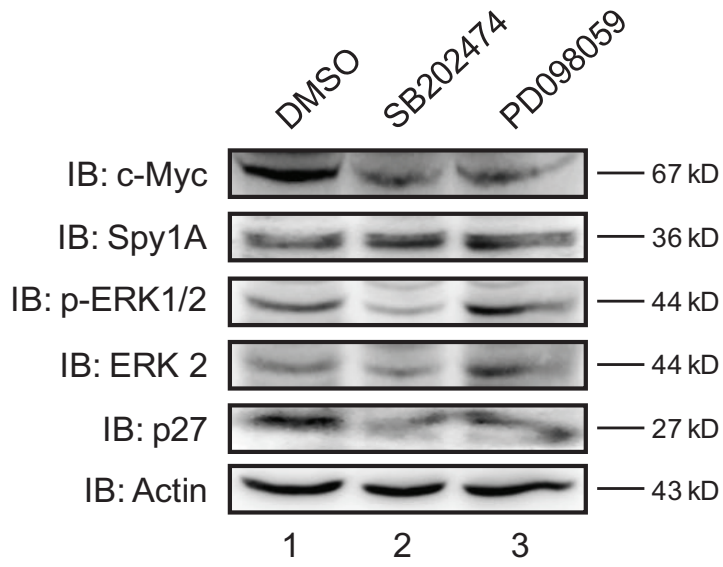
VII. Disrupted MAPK Signaling in the HC11 Cell System Results in Reproducible Spy1A Downregulation.

Since MAPK was shown to support Spy1A protein upregulation in an ER α -positive tumorigenic context (Fig.16a-b), I sought to further clarify the ability of MAPK signaling to precede Spy1A activation in a non-tumorigenic state. For this reason, the outcome of disrupted MAPK signaling on Spy1A expression was evaluated in the immortalized HC11 cell system, a p53 mutated mammary epithelial cell line that has been clonally derived from mid-pregnant BALB/c mammary epithelium.⁷⁴⁻⁷⁵ HC11 cells were exposed to 24 h treatment with either DMSO (vehicle control), 10 μ M SB202474 (control), or 10 μ M PD098059 (MEK1) inhibitors. Protein isolation ensued, followed by immunoblotting for c-Myc, Spy1A, total and phosphorylated ERK1/2 levels, and the CKI p27 (Fig.17a). Actin was utilized as a loading control, and was further employed during densitometric analysis in order to normalize protein expression data. Utilizing SB202474 treatment as a baseline for protein expression, PD098059 inhibition of MEK1 activity by as little as 2% resulted in a 13% reduction in c-Myc, a 3% reduction in Spy1A, and an overall 2% increase in p27 protein levels (Fig. 17b). Overall, HC11 cells demonstrated inadequate MAPK inhibition in response to PD098059 exposure, and did not undergo significant changes in c-Myc, Spy1A, or p27 protein expression. Note that results have not been verified at this stage of analysis ($N=1$ replicate) and require additional replication in order to verify changes in protein expression.

VIII. ER α -negative F5A1-2 Mammary Tumor Cells Harbour Intrinsic Defenses Against MAPK Inactivation.

Based on the importance of MAPK signaling for Spy1A stimulation in MCF7 cell lines subjected to long-term E2 exposure, MAPK was postulated to be indispensable for sustaining Spy1A upregulation in a c-Myc overexpressing tumor microenvironment. First, to resolve the extent to which F5A1-2 cells fall under ER α regulation, protein lysates isolated from F5A1-2 and MCF7 cell lines were subjected to 10% SDS-PAGE analysis and probed for ER α status. In relation to the naturally augmented protein levels of ER α pervasive in the MCF7 cell line, F5A1-2 cells were characterized accordingly as

A



B

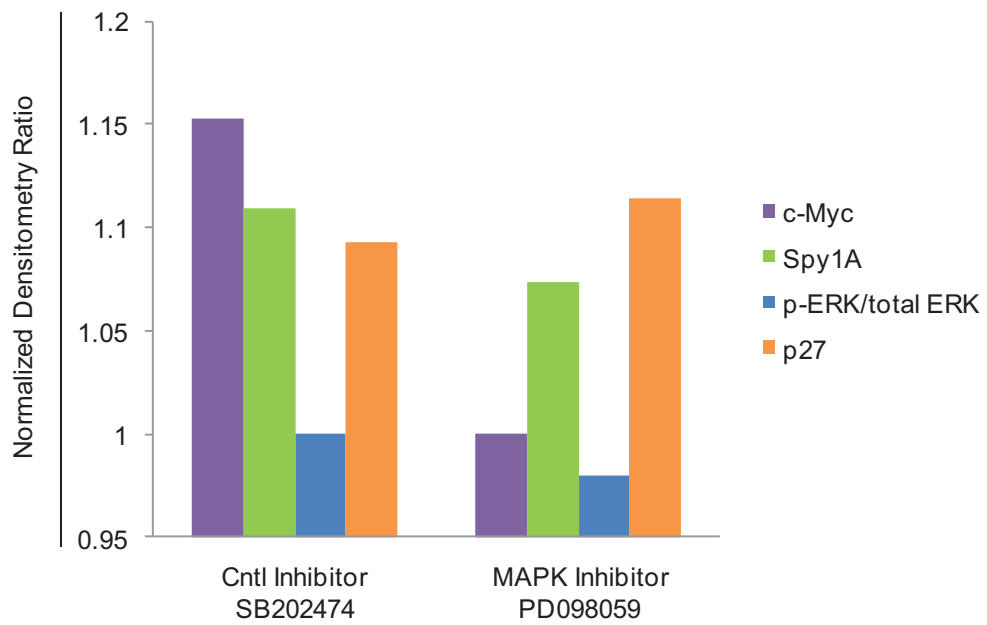


Figure 17. Inhibition of MAPK activity downregulates Spy1A protein levels in the immortalized HC11 cell system. HC11 cells were treated independently for 24 h with either DMSO, 10 μ M control inhibitor (SB202474), or 10 μ M MAPK inhibitor (PD098059), followed by protein extraction and lysate analysis through 10% SDS-PAGE. **(a)** Protein lysates were immunoblotted utilizing the indicated antibodies: c-Myc (67 kD); Spy1A (36 kD isoform); phosphorylated ERK1/2 (p-ERK1/2); total ERK 2 (ERK 2); p27; and Actin (43 kD), utilized as a loading control. The blot depicted here is representative of $N=1$ replicate. **(b)** Densitometry values for each protein band were normalized to Actin and converted to normalized densitometry ratios: c-Myc (purple); Spy1A (green); p-ERK/total ERK (blue); and p27 (orange).

ER α -negative (Fig.18). Thus, in a manner independent of ER α crosstalk, Myc-mediated upregulation of Spy1A is predicted to govern aberrant cell growth and irrepressible cell proliferation in those mammary adenocarcinomas derived from *de novo* overexpression of c-Myc.

Next, to determine the essentiality of MAPK for c-Myc induced stimulation of Spy1A in an ER α -negative context, F5A1-2 cells cultured beyond passage sixty were subjected to 24 h treatment with DMSO (vehicle control), 10 μ M SB202474, 10 μ M PD098059, or 20 μ M PD098059, according to PD098059 concentrations pre-optimized by Lobenhofer et al. (2000) in the MCF7 cell system.⁷³ Protein lysates were analyzed through 10% SDS-PAGE, followed by antibody-mediated detection of Spy1A, phosphorylated ERK1/2, and total ERK1/2 levels (Fig.19a, Fig.20a). As determined through densitometric analysis, the ratio of phosphorylated ERK1/2 to total ERK1/2 was utilized as a method of quantifying changes in MAPK protein expression (Fig.19b, Fig. 20b). Relative to SB202474 treatment, administration of PD098059 particles led to weak inactivation of MAPK by 21% at 10 μ M, and virtually no inactivation of MAPK (0.3%) at 20 μ M concentrations (Fig.20a-b). Thus, optimal ERK1/2 inhibition was achieved at 10 μ M. Downregulation of ERK1/2 by 21% corresponded to a 41% increase in Spy1A protein levels, in response to 10 μ M MAPK inhibition (Fig.20a-b). Similarly, negligible silencing of ERK1/2 (0.3%) produced a 5% increase in Spy1A protein expression, following 20 μ M MAPK inhibition (Fig.20b). Collectively, these results demonstrate the ability of late passage F5A1-2 cells to evade the inhibitory effects of PD098059 within an ER α -negative tumorigenic context. Results, however, are strictly preliminary at this stage of analysis.

To determine the consequence of both MEK1 and MEK2 suppression on Spy1A-associated signaling in F5A1-2 cell lines, SB202474 or U0126 inhibitor particles were utilized at 10 μ M to treat passage 33 cells over a 24 h treatment period, followed by protein extraction and lysate analysis through 10% SDS-PAGE. Immunoblotting was utilized to assess deviations in protein expression for c-Myc, Spy1A, phosphorylated ERK1/2, and total ERK1/2, in addition to the cell cycle inhibitors p27 and p21 (Fig.19a). Densitometric analysis was subsequently utilized to quantify relative changes in protein expression, as determined through the normalization of data to Actin, the resident loading

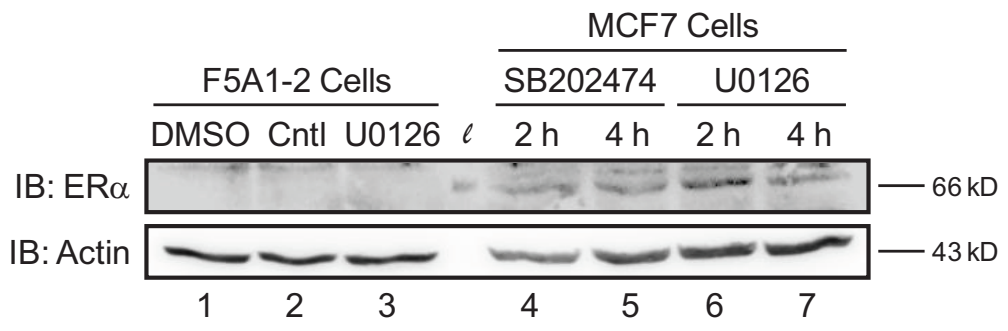


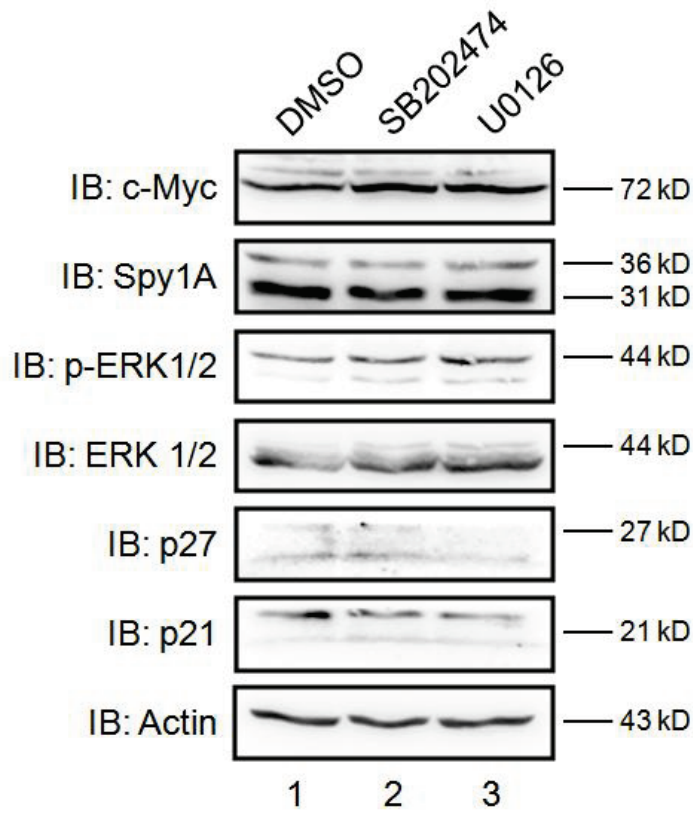
Figure 18. ER α protein expression is absent in F5A1-2 cell lines. Protein extracts isolated from mid passage F5A1-2 (P33) and MCF7 (P30) cell lines were subjected to 10% SDS-PAGE analysis and immunoblotted for ER α (66 kD) and Actin (43 kD), the loading control. The protein blot depicted here is representative of $N=1$ replicate. *Lanes 1-3:* Mid passage F5A1-2 cell lines (P33) were treated independently for 24 h with DMSO (vehicle control), 10 μ M control inhibitor (SB202474), or 10 μ M MEK1/2 inhibitor (U0126). ℓ = protein standard. *Lanes 4-7:* MCF7 cells were incubated in phenol red free media supplemented with charcoal-stripped serum prior to 1 h treatment with control (SB202474) or MAPK (U0126) inhibitors. Following 1 h incubation with each inhibitor, E2 treatment ensued for 2 h or 4 h.

control (Fig.19b). Whereas U0126 treatment (10 μ M) effectively reduced ERK1/2 protein expression in MCF7 cell cultures (Fig.16), F5A1-2 cells remained impervious to inhibitor effects, as evidenced by stable ERK1/2 expression across all treatments (Fig.19). Despite the inability of U0126 to inhibit MAPK signaling in F5A1-2 cells, Spy1A protein levels increased by 12% relative to control treatments, whereas c-Myc, p21, and p27 levels were largely unaffected (Fig.19b). Furthermore, the ability of PD098059 to reduce ERK1/2 protein expression was approximately 46-fold superior to that of U0126 when utilized at a final concentration of 10 μ M in F5A1-2 cell cultures. Conversely, analogous experiments conducted in MCF7 cells identified U0126 as a more potent inhibitor of MAPK signaling in comparison to PD098059.⁷³ Taken together, these data reveal an interesting property of F5A1-2 cell lines, i.e. their ability to circumvent MAPK inhibition when exposed to well characterized MEK inhibitors.

IX. Establishing a Tumor Baseline for F5A1-2 Cells in Cleared No. 4 Mammary Glands of FVB Females.

To determine whether FVB-derived F5A1-2 cell lines retained their potential to form tumors *in vivo*, the rate of F5A1-2 tumor development was established in 24-day old FVB females via mammary fat pad transplantation, coupled to subsequent monitoring of tumor growth. Mammary fat pad removal primed each No. 4 inguinal mammary gland for injection with (a) saline solution (left gland), or (b) F5A1-2 cell suspension (right gland) at a dosage of 1×10^6 cells per gland. Tumor nodules localized to the right-hand side first appeared 5 days post-surgery in all replicates tested, as detected through daily palpitation of recuperating No. 4 mammary glands. The absence of tumor formation on the left-hand side was confirmed through post-mortem dissection of each test subject. Representative autopsy images have been provided for test subject No.97, whose untimely death transpired 20 days post-surgery (Fig.21a). Serving as a general indicator for overall tumor size, calliper measurements of tumor height (depicted in Fig.21b) were reported for living test subjects on post-surgery days 5, 19-21, 24-26, 28, and 30-31 (Fig.21c). To determine the rate of F5A1-2 mediated tumor growth in transplanted FVB test subjects, linear regression analysis $\{y = (0.8 \text{ mm}/\text{day})(x) - 2.8 \text{ mm}\}$ for average tumor height (y) plotted

A



B

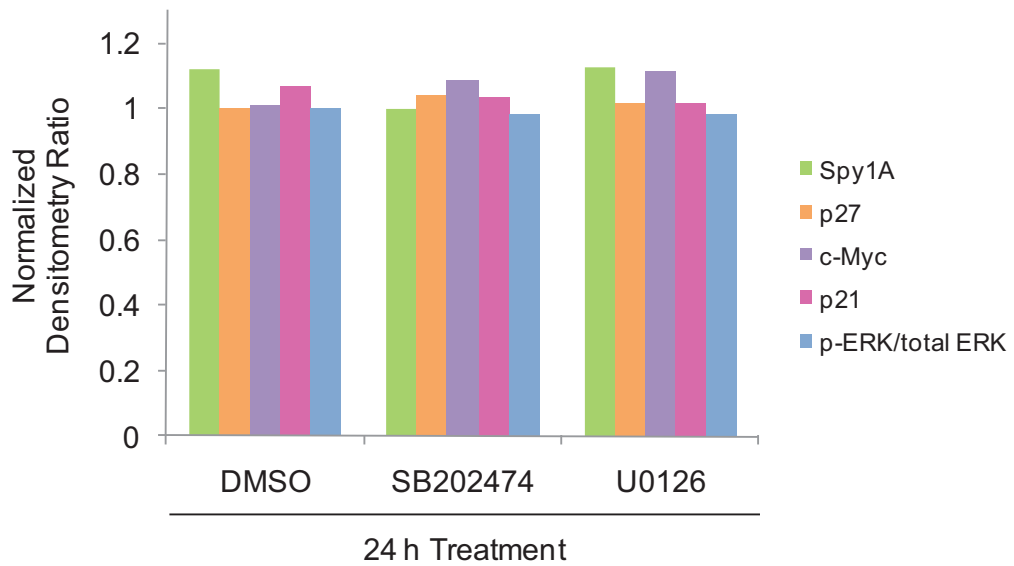
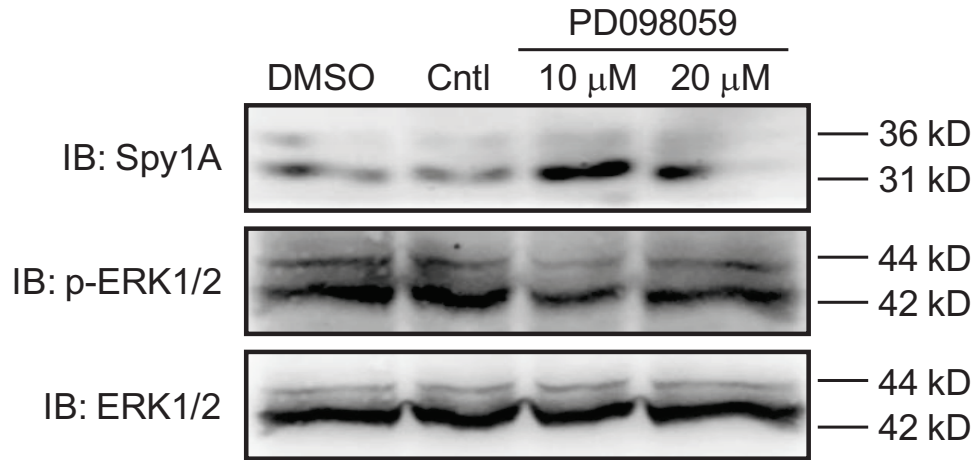


Figure 19. F5A1-2 primary tumor cell lines overexpressing c-Myc are resilient to chemical-mediated MAPK inhibition. Mid passage F5A1-2 cell lines (P33) were treated independently for 24 h with DMSO (vehicle control), 10 μ M control inhibitor (SB202474), or 10 μ M MEK1/2 inhibitor (U0126). Protein lysates were prepared after each treatment and analyzed through 10% SDS-PAGE, followed by immunoblotting. The protein blot depicted here is representative of $N=1$ replicate. **(a)** Protein lysates were immunolabelled with the following antibodies: c-Myc (72 kD); Spy1A (31 and 36 kD isoforms); phosphorylated ERK1/2 (p-ERK1/2) (42 and 44 kD isoforms); total ERK 1/2 (ERK 1/2) (42 and 44 kD isoforms); p27 (27 kD); p21 (21 kD); and Actin (43 kD), utilized as a loading control. **(b)** Densitometry values for each protein band were normalized to Actin and converted to normalized protein expression (%): Spy1A (green); p27 (orange); c-Myc (purple); p21 (fuschia); and p-ERK/total ERK (blue).

A



B

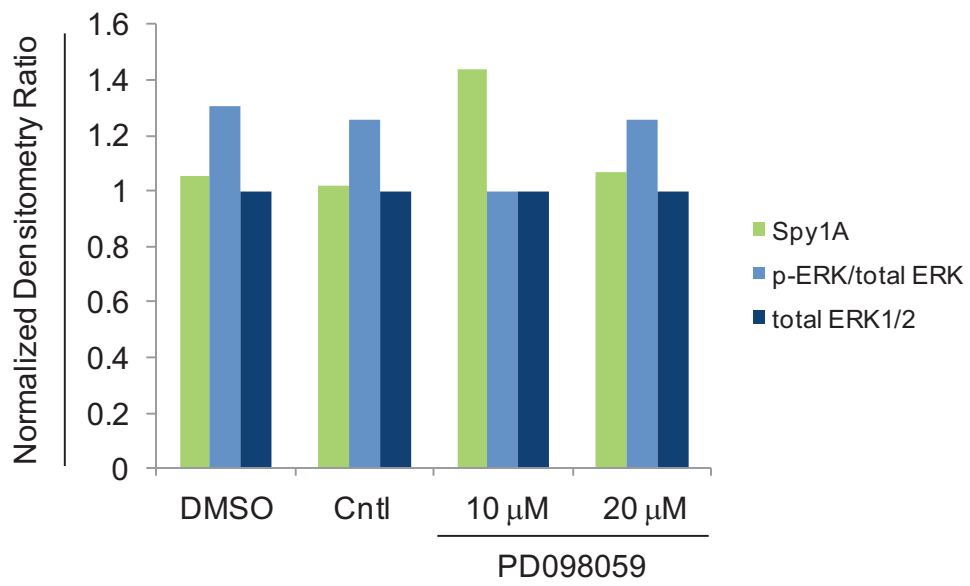


Figure 20. Primary tumor cell lines overexpressing c-Myc are resilient to chemical-mediated MAPK inhibition. Primary tumor cell lines cultured beyond passage 60 (~P60) were treated independently for 24 h with DMSO, 10 μ M control inhibitor (SB202474), 10 μ M MAPK inhibitor (PD098059), or 20 μ M PD098059. Protein lysates were prepared after each treatment and analyzed via 10% SDS-PAGE. The protein blot depicted here is representative of $N=1$ replicate. **(a)** Protein lysates were immunolabelled with the following antibodies: Spy1A (31 and 36 kD isoforms); phosphorylated ERK1/2 (p-ERK1/2) (42 and 44 kD isoforms); and total ERK 1/2 (ERK 1/2) (42 and 44 kD isoforms), utilized here as the loading control. **(b)** Densitometry values for each protein band were normalized to total ERK, and converted to normalized densitometry ratios: Spy1A (green); p-ERK/total ERK (light blue); and total ERK (dark blue).

against the number of days post-surgery (x) was subsequently conducted. Thus, tumor development progressed at an estimated rate of 0.8 mm per day. The linear relationship established between average tumor size and passage of time was significantly strong, as evidenced by a correlation coefficient (r) of 0.97 (Fig.21c). Only test subject No.99 survived to day 31 post-surgery, exhibiting a final tumor height that exceeded 25.0 mm in length (Fig.21b-c). Due to enlarged tumor growth, humane sacrifice was conducted. Note that all error bars displayed in Fig.21c represent standard error values that have been calculated separately for each time point.

X. Transient RNAi-Mediated Inhibition of Spy1A Slightly Reduces F5A1-2 Tumor Growth Rate In vivo.

To assess the essentiality of Spy1A for c-Myc induced tumor proliferation *in vivo*, F5A1-2 cells were transiently transfected for 24 h with either control or Spy1A shRNA vectors, followed by transplantation into the cleared fat pads of fourth inguinal mammary glands residing in 24-day old FVB females. Once again, mammary fat pad removal prepared each fourth gland for injection with (a) saline solution (left gland), or (b) control shRNA-treated F5A1-2 cell suspension (right gland) at a dosage of 1×10^6 cells per gland. A second set of transplants was conducted in parallel to the first via injection of (a) saline solution (left gland), or (b) Spy1A shRNA-treated F5A1-2 cell suspension (right gland) at a dosage of 1×10^6 cells per gland. Similar to the tumor baseline established for untreated F5A1-2 cells, tumor activity was initially observed ~7 days post-surgery and was restricted to the right-hand side in both control and Spy1A-shRNA treated animals, as determined through daily palpitation of each mammary gland. In addition to both shRNA transplant models described above, transplantation of one animal was conducted in the following manner to confirm the sterility of the saline solution, and to ensure proper clearing of the mammary fat pad: (a) un-cleared left gland, and (b) saline injected, cleared right gland (Fig.22a). Dissection of control (Fig.22b) and Spy1A (Fig.22c) shRNA-treated animals ensued at various time points, and at first glance, did not display significant variances in gross tumor size between treatments. Consequently, calliper measurements of tumor height were utilized as indicators of overall tumor size for both transplantation sets, and were reported for living test subjects on post-surgery days 23-24,

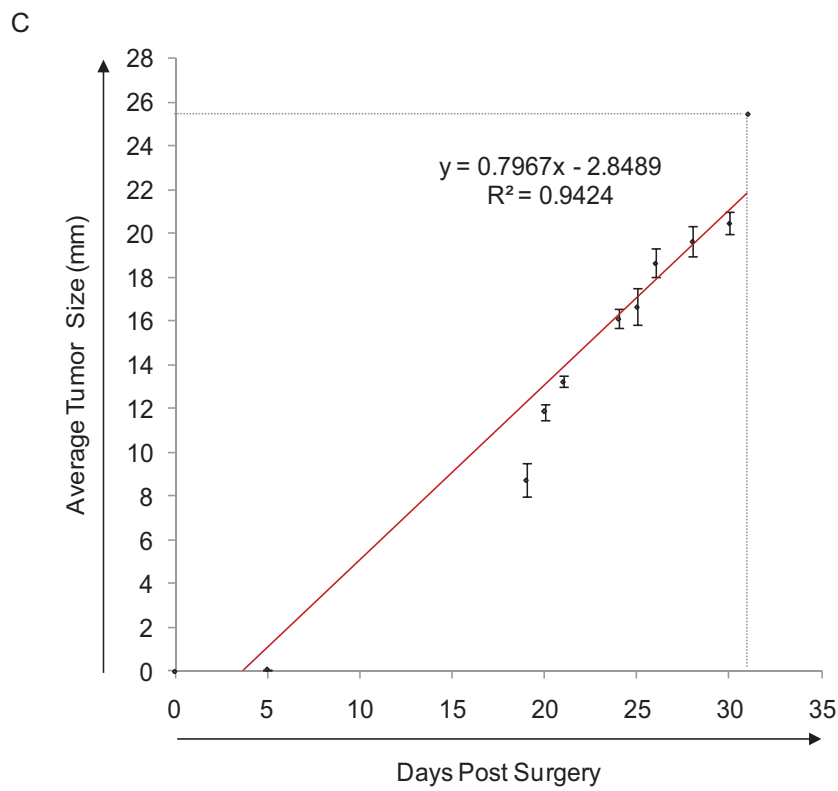
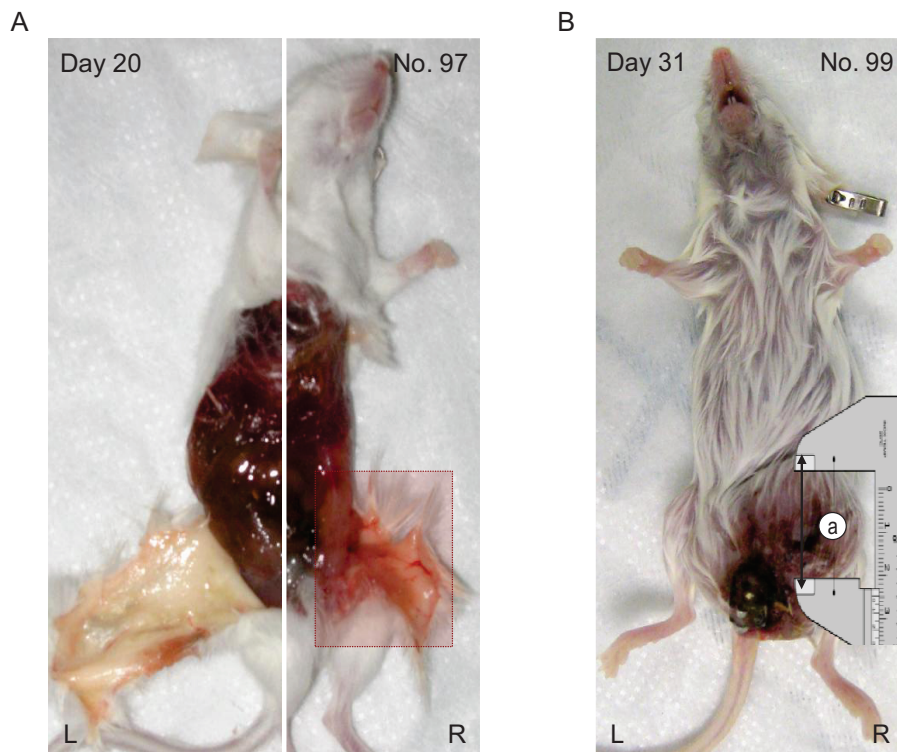


Figure 21. Tumor baseline for F5A1-2 cells. Cleared No. 4 inguinal mammary glands were transplanted with saline solution (left gland, L), or F5A1-2 cell suspension (right gland, R) at a dosage of 1×10^6 cells per gland ($N=6$ replicates). **(a)** Autopsy photograph of test subject No.97, 20 days post-surgery. The highlighted region depicts extensive tumor growth in the R gland, compared to no tumor growth in the L gland. **(b)** Autopsy photograph of test subject No.99, 31 days post-surgery. As depicted in region \textcircled{a} , tumor height (mm) was measured daily for each test organism utilizing a Vernier Calliper, and represents overall tumor size at each time point. **(c)** Calliper measurements of tumor height were recorded for living test subjects on post-surgery days 5, 19-21, 24-26, 28, and 30-31. The rate of tumor growth was determined through linear regression analysis for average tumor height (y) plotted against the number of days post-surgery (x) utilizing *Microsoft Excel*. The slope of the corresponding linear equation was utilized to determine the overall rate at which tumors develop from F5A1-2 cells: $\{y = (0.7967 \text{ mm/day})(x) - 2.8489 \text{ mm}\}$; slope = 0.7967 mm/day . Error bars indicate the standard error value for each time point. The correlation coefficient (r) was determined by calculating the square root of R^2 , a value derived through *Microsoft Excel*.

and 27-29 (Fig.22d). Linear regression analysis was utilized once again to mathematically model differences in tumor growth rate between control and Spy1A treatments of F5A1-2 transplanted cells (Fig.22d). Derived by plotting average tumor height (y) against the number of days post-surgery (x), the following linear equations were utilized to quantify the rate of tumor formation for control $\{y = (1.4 \text{ mm/day})(x) - 25.3 \text{ mm}\}$ and Spy1A $\{y = (1.3 \text{ mm/day})(x) - 22.9 \text{ mm}\}$ shRNA treated animals. Thus, tumor development in Spy1A shRNA-treated F5A1-2 cells proceeded at a slightly reduced rate of 1.3 mm per day, in comparison to control transplants estimated to expand by a rate of 1.4 mm per day (Fig. 22d). Substantiated by r values of 0.92 and 0.97 respectively, both linear relationships established between average tumor size and passage of time for control and Spy1A shRNA treated cells were sufficiently strong (Fig.22d). As calculated for the F5A1-2 tumor baseline, error bars displayed in Fig.22d represent standard error values that have been derived independently for each time point.

XI. Transient Spy1A Knockdown in F5A1-2 Cells Potentiates the Development of Ductal Outgrowths In vivo.

The natural preponderance of Spy1A mRNA and protein expression in adult virgin mammary glands was postulated to promote typical ductal morphogenesis *in vivo*, especially since Spy1A overexpression in HC11 cells gives rise to premature lobular development when transplanted into 22-day old syngeneic BALB/c mice.²² First, to resolve the effects of F5A1-2 tumorigenicity on terminal end bud development during early stages of murine pubescence, mammary glands previously injected with saline solution or control shRNA-treated F5A1-2 cells (as described above) were isolated 11 days post-surgery, followed by whole mount analysis through haematoxylin staining (Fig.23a). Although F5A1-2 transplantation did not completely abolish ductal morphogenesis, ductal side branching in the right gland was considerably reduced in relation to the left gland (Fig.23a), demonstrating the potent ability of F5A1-2 tumor cells to interfere with terminal end bud formation during post-natal mammopoiesis. Next, to determine whether RNAi-mediated Spy1A inhibition in F5A1-2 cells restores ductal side branching *in vivo*, fourth inguinal mammary fat pads were cleared in pre-pubertal FVB females, followed by transplantation of wild-type F5A1-2 cells (left gland) or shSpy1A-

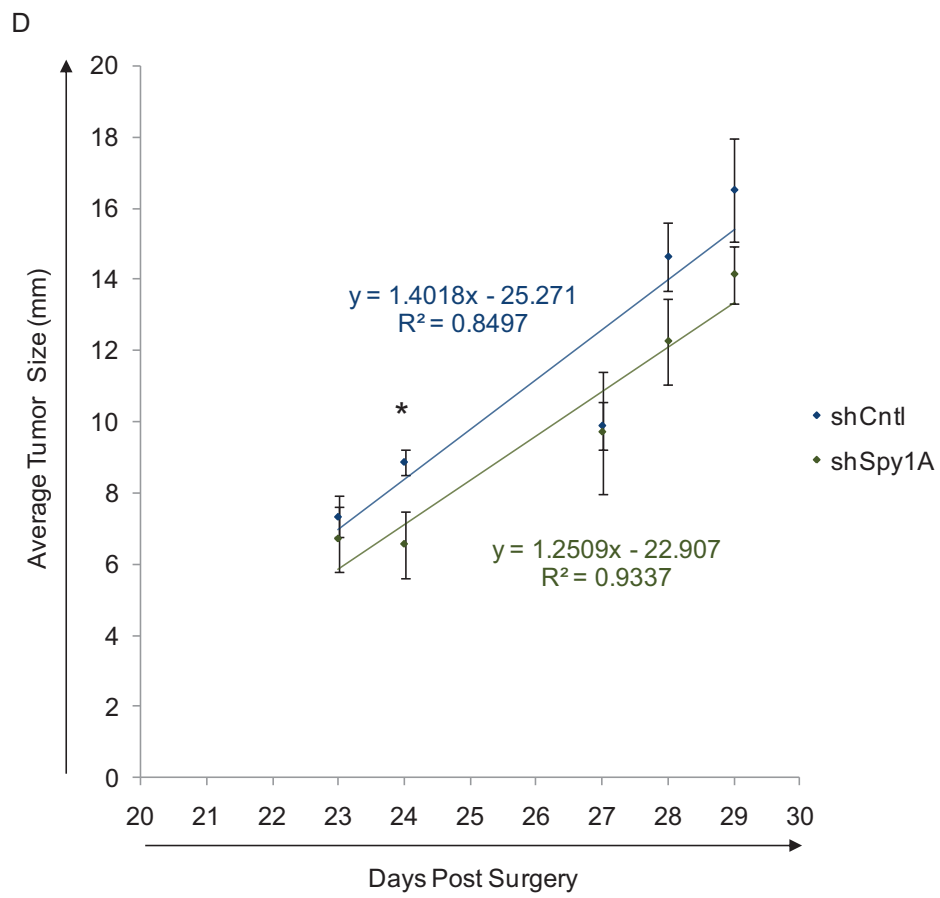
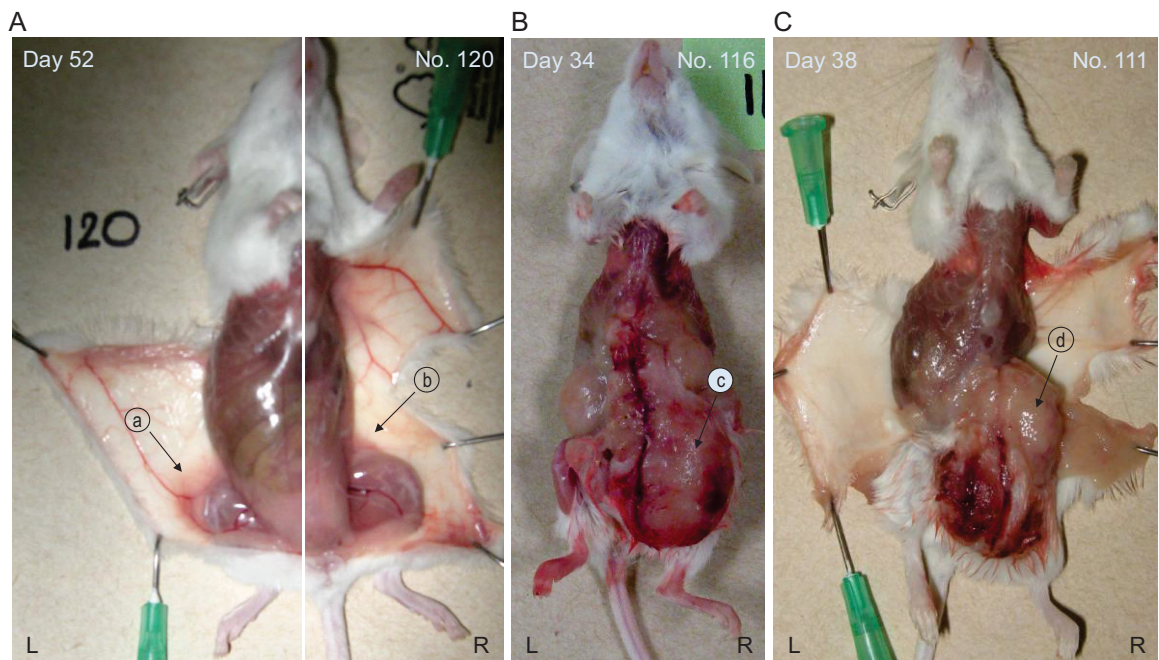


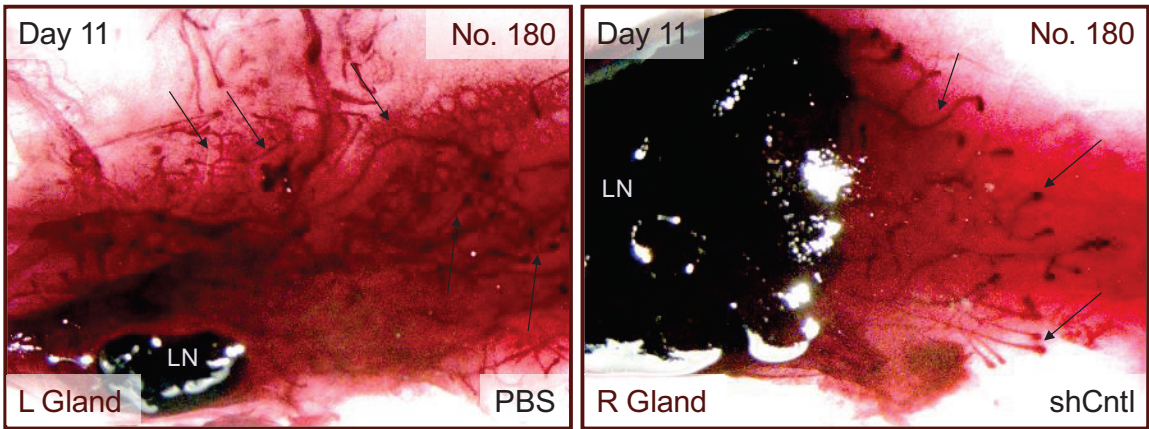
Figure 22. Transient *Spy1A* knockdown reduces F5A1-2 tumor growth rate in vivo. Cleared No. 4 inguinal mammary glands were transplanted with saline solution (left gland, L), or control shRNA-treated F5A1-2 cell suspension (right gland, R) at a dosage of 1×10^6 cells per gland ($N=15$ replicates). In parallel to the first set of surgeries, a second set was conducted via injection of saline solution (L), or *Spy1A* shRNA-treated F5A1-2 cell suspension (R) at a dosage of 1×10^6 cells per gland ($N=15$ replicates), unless otherwise stated. **(a)** Autopsy photograph of test subject No.120, 52 days post-surgery ($N=1$ replicate); No.120 was utilized as a control animal during mammary fat pad transplantation to ensure proper technique and clearing of the mammary fat pad. No. 4 inguinal mammary glands were not cleared (no treatment, L) or injected with 10 μ l saline solution (1X PBS). Region **(a)** points to an untouched fourth mammary gland. Region **(b)** demonstrates successfully clearing of the fat pad, depicted by a lack of growth in the R fourth mammary gland region; therefore, proper clearing ensured full removal of stem cell precursors residing in pre-pubertal mice (21-28 days old) prior to transplantation of treated cell types. **(b)** Autopsy photograph of test subject No.116, 34 days post-surgery. Region **(c)** points to the development of large shCntl F5A1-2 tumor masses in the R gland; F5A1-2 tumor cells have also invaded into the contralateral L gland (one replicate of 15). **(c)** Autopsy photograph of test subject No.111, 38 days post-surgery. Region **(d)** points to the development of large shSpy1A F5A1-2 tumor masses in the R gland; F5A1-2 tumor cells have once again invaded into the contralateral L gland (one replicate of 15). **(d)** Calliper measurements of tumor height were recorded for living test subjects on post-surgery days 23-24 and 27-29. The rate of shCntl tumor growth was determined through linear regression analysis for average tumor height (y) plotted against the number of days post-surgery (x) utilizing *Microsoft Excel*. The slope of the corresponding linear equation was utilized to determine the overall rate at which tumors develop from shCntl transfected F5A1-2 cells: $\{y = (1.4018 \text{ mm/day})(x) - 25.271 \text{ mm}\}$; slope = 1.4018 mm/day . Similarly, the rate of shSpy1A tumor growth was determined through linear regression analysis for average tumor height (y) plotted against the number of days post-surgery (x) utilizing *Microsoft Excel*. The slope of the corresponding linear equation was utilized to determine the overall rate at which tumors develop from shSpy1A transfected F5A1-2 cells: $\{y = (1.2509 \text{ mm/day})(x) - 22.907 \text{ mm}\}$; slope = 1.2509 mm/day . Error bars indicate the standard error value for each time point. The correlation coefficient was determined by calculating the square root of R^2 , a value derived through *Microsoft Excel*.

treated F5A1-2 cells (right gland). Test subjects were sacrificed 7 days post-surgery in preparation for whole mount analysis through haematoxylin staining (Fig.23b-c). Emanating directly from transplanted cells, the number of pronounced ductal side branches residing in right glands was markedly increased when compared to corresponding left glands (Fig.23b-c). Instead, left whole mounts were populated mostly by massive tumor structures, as evidenced by profuse purple staining dispersed throughout the tissue (Fig.23b-c). Residual cell suspensions frozen down directly after surgery were analyzed through 10% SDS-PAGE and immunoblotted for Spy1A, c-Myc, and Actin expression (data not shown). Spy1A and c-Myc levels were respectively reduced by 19% and 20% in shSpy1A-treated lysates compared to control lysates, thereby confirming Spy1A knockdown in No. SH01 (Fig.23b) and No. SH04 (Fig.23c) right glands, and further suggesting that Spy1A knockdown in F5A1-2 cells potentiates ductal morphogenesis *in vivo*. Taken together, whole mount data suggest that downregulation of Spy1A in F5A1-2 cells appears to partially restore ductal morphogenesis *in vivo*, although additional replicates are required to fully substantiate the statistical significance of whole mount data.

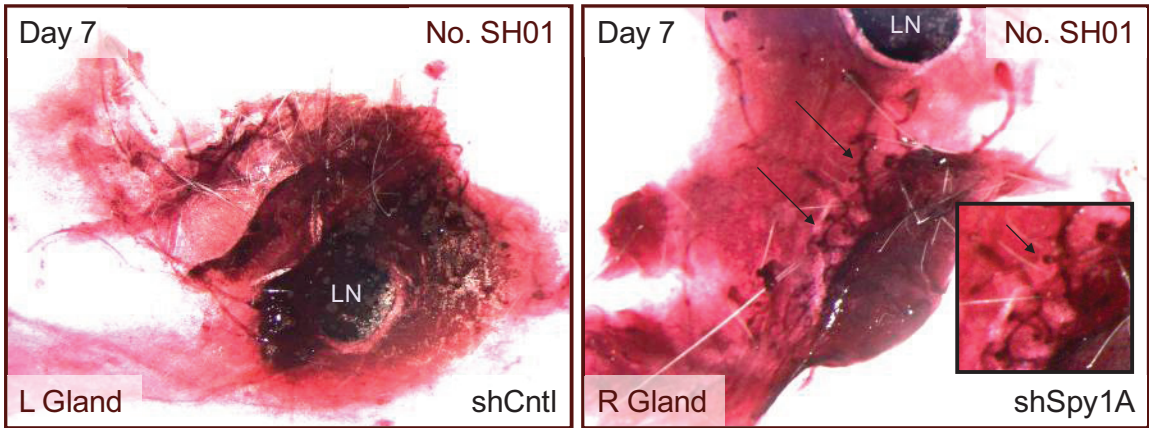
XII. Transient Abrogation of Spy1A Signaling Downregulates c-Myc and MAPK Protein Expression In vivo.

To account for biological variation in different animals and to verify that Spy1A knockdown reduces F5A1-2 tumor formation *in vivo* within the same organism, mammary fat pad transplants were repeated in 24-day old FVB females as described previously, utilizing the following schema: (a) control shRNA-treated F5A1-2 cell suspension (left gland) at a dosage of 1×10^6 cells per gland, and (b) Spy1A shRNA-treated F5A1-2 cell suspension (right gland) at a dosage of 1×10^6 cells per gland. Test subjects were sacrificed and freshly dissected 30 days post-surgery, following development of conglomerated tumor masses within the fourth inguinal mammary region. Autopsy images did not reveal significant changes in overall tumor size between control and Spy1A shRNA treatments due to F5A1-2 cell ability to invade into neighbouring tissues early on. Hence, successful separation of left and right tumors from one another was not feasible in those animals that were co-injected with control and Spy1A shRNA-

A



B



C

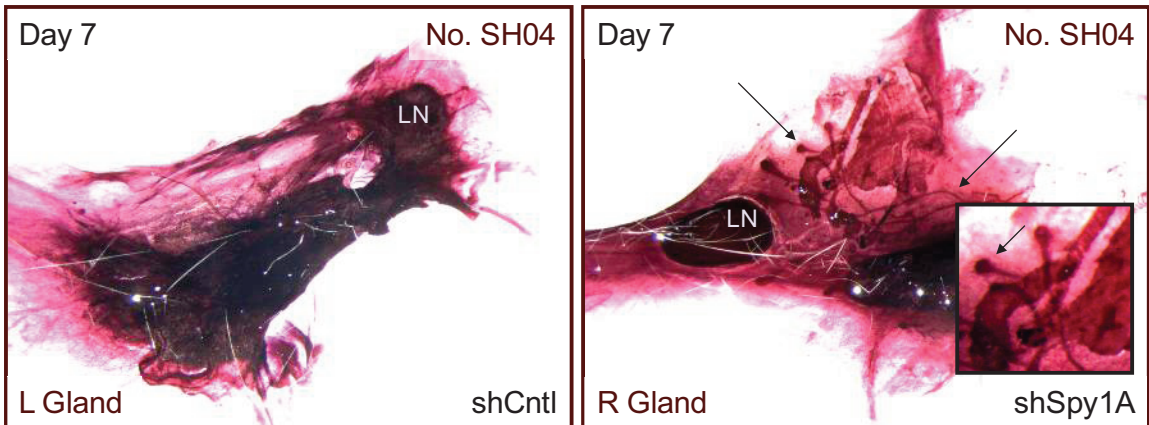
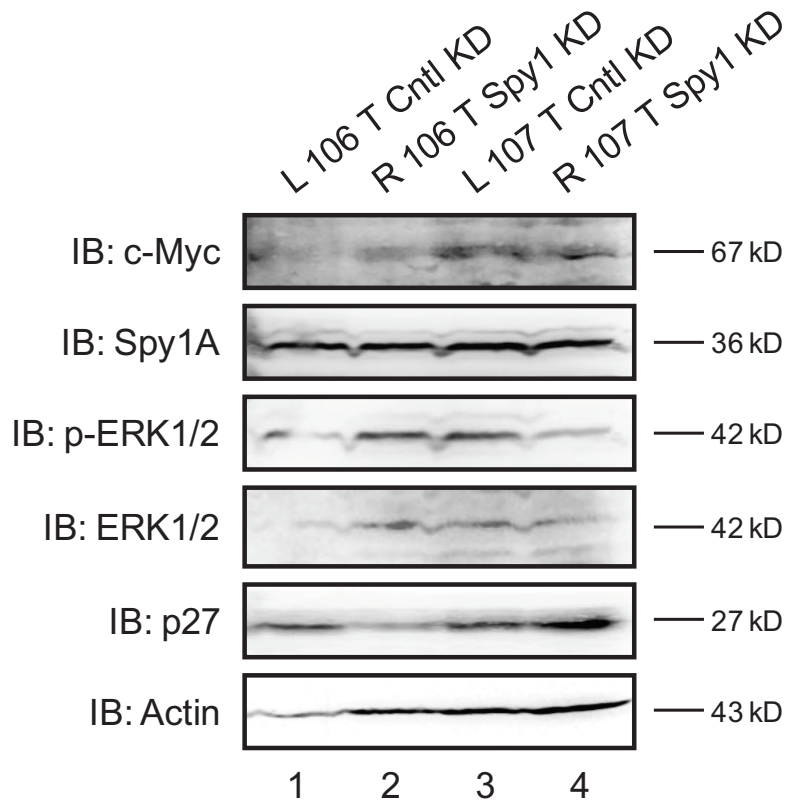


Figure 23. Transient *Spy1A* knockdown in F5A1-2 cells promotes ductal outgrowth development and ductal bifurcation in vivo. Representative regions of ductal outgrowth and bifurcation are indicated by a series of black arrows (→). The site of the lymph node (LN) has been demarcated for each whole mount, and serves as a positional frame of reference. **(a)** Mammary fat pad transplants were conducted in 28-day old FVB females. Cleared No. 4 inguinal mammary glands were transplanted with saline solution (left gland, L), or control shRNA-treated F5A1-2 cell suspension (right gland, R) at a dosage of 1×10^6 cells per gland ($N=15$ replicates) for test subject No. 180. L and R fourth glands were extracted from No.180, 11 days post-surgery, and stained with haematoxylin during the whole mount procedure. **(b-c)** Mammary fat pad transplants were performed in 23-day old FVB females. Fourth glands were cleared and transplanted with wild-type F5A1-2 cells (L) or shSpy1A-treated F5A1-2 cells (R). Test subjects SH01 and SH04 were sacrificed 7 days post-surgery in preparation for whole mount analysis through haematoxylin staining ($N=2$ replicates), and were pair-matched for age. **(b)** *L and R whole mount glands of SH01*. The boxed region represents an enlarged view of select mammary ductal outgrowths that have sprouted from the site of cell injection. **(c)** *L and R whole mount glands of SH04*. The boxed region represents an enlarged view of select mammary ductal outgrowths that have sprouted from the site of cell injection.

treated cells, due to an evident lack of tumor boundary. Although calliper measurements of tumor height were recorded regularly at various time intervals after surgery, differences in tumor growth rate could not be assessed accurately within the same organism. Taken together, these results confirm the necessity of performing individualized transplants in separate test organisms for either control or Spy1A shRNA treated F5A1-2 cells (as performed above), due to their highly proliferative and invasive nature *in vivo*.

In an effort to elucidate the *in vivo* consequences of Spy1A knockdown on MAPK, c-Myc, and CKI signaling, tumors harvested 30 days after surgery were analyzed for altered protein expression. Tissue samples were extracted from the periphery of both left and right tumor masses, since the tumor centre was speculated to contain a heterogeneous population of control and Spy1A RNAi-treated cells. Tissue homogenization and protein isolation ensued shortly thereafter for test subjects No.106 and 107, followed by 10% SDS-PAGE analysis and immunoblotting for c-Myc, Spy1A, phosphorylated and total ERK1/2, in addition to p27 (Fig.24a). Densitometric analysis (Fig.24b) was utilized to quantify changes in protein expression, during which pixel intensity of each protein band was determined and normalized to Actin, the resident loading control. Spy1A expression was effectively silenced in tumor samples excised from the right glands of test subjects No.106 and 107 by 52% and 31%, respectively, as compared to corresponding control tumor samples extracted from each left gland (Fig.24b). Spy1A knockdown resulted in c-Myc downregulation by 55% and 53%, respectively, relative to control tissue (Fig.24b). In response to Spy1A inhibition, overall phospho-ERK1/2 protein expression decreased substantially in test subject No.106, as evidenced by a 73% decrease in the ratio of p-ERK1/2 to total ERK1/2 (Fig.24b). Similarly, test subject No.107 experienced a 52% decline in overall phospho-ERK1/2 expression in tumor tissue derived from the right gland, as compared to control tissue extracted from the left (Fig.24b). Furthermore, a 52% decrease in Spy1A expression corresponded to a 71% decrease in p27 (No.106), whereas p27 expression was upregulated by 39% in response to 31% Spy1A inhibition when compared to control tissue (No.107). Results are prospectively confounded, however, by the insufficient separation of shCntl and shSpy1A tumor populations from one another in each tissue sample, and additional replicates are required to impart statistical significance.

A



B

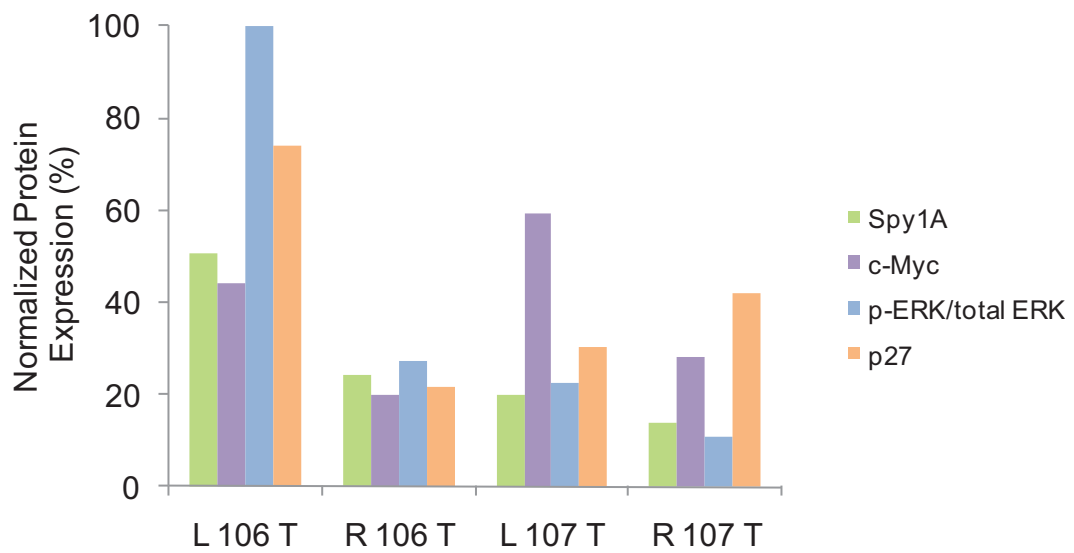


Figure 24. Transient abrogation of *Spy1A* signaling downregulates *c-Myc* expression *in vivo*. No. 4 inguinal mammary glands of 24-day old FVB females were cleared and transplanted with control shRNA-treated F5A1-2 cell suspension (left gland, L) at a dosage of 1×10^6 cells per gland, and *Spy1A* shRNA-treated F5A1-2 cell suspension (right gland, R) at a dosage of 1×10^6 cells per gland ($N=7$ replicates). Test subjects were sacrificed and freshly dissected 30 days post-surgery. Tumor growth rate could not be determined accurately in animals co-transplanted with shCntl and sh*Spy1A* F5A1-2 cells for this round of fat pad transplants. **(a)** Whole tumor protein extracts were isolated from the periphery of L and R tumor tissues to avoid the mixed tumor population located in the centre of the organism. Protein analysis was conducted through 10% SDS-PAGE for L and R tumors (T) isolated from No.106 and 107 animals ($N=2$ replicates, in total). Immunoblotting ensued for *c-Myc* (67 kD); *Spy1A* (36 kD); phosphorylated ERK1/2 (42 kD); total ERK1/2 (42 kD); p27 (27 kD); and Actin (43 kD), the resident loading control. **(b)** Densitometric analysis was completed for the immunoblot depicted in (a); all protein data were subsequently normalized to total Actin expression and converted to normalized densitometry percentages (%). *Spy1A* (green); *c-Myc* (purple); p-ERK/total ERK ratio (blue); p27 (orange).

XIII. Stable Spy1A Knockdown In Late Passage F5A1-2 Cells Confirms Reduction of c-Myc and MAPK Protein Levels In vivo.

Though PEI-mediated transfection is ideal for immediate assessment of foreign gene expression in a plethora of *in vitro* cell-based systems, its benefits are typically short-lived. Transient transfection does not stably integrate foreign DNA into the cellular genome and produces a partial or complete loss of foreign gene expression with every new mitotic cell division.⁷⁶⁻⁷⁸ Alternatively, lentiviral transduction circumvents these issues quite effectively and for this reason, F5A1-2^{shCntl} and F5A1-2^{shSpy1A} stable cell lines were transplanted into pre-pubertal No. 4 inguinal mammary glands of FVB females according to the following schema: (a) F5A1-2^{shCntl} cell suspension (left) at a dosage of 1×10^6 cells per gland, and (b) F5A1-2^{shSpy1A} cell suspension (right) at a dosage of 1×10^6 cells per gland (Fig.25a-e). Determined through GFP-fluorescence microscopy, lentiviral infection efficiencies were originally estimated to be 25-30% for F5A1-2^{shCntl} cells, and 40-50% for F5A1-2^{shSpy1A} cells (Fig.13c). Cell suspensions derived from F5A1-2^{shCntl} and F5A1-2^{shSpy1A} treatments were utilized to determine the efficacy of Spy1A knockdown in F5A1-2 stable cell lines prior to *in vivo* mammary fat pad transplantation, as determined through protein extraction and immunoblotting (Fig.13a). Results demonstrated that in relation to shCntl-1 and -2 cells respectively, Spy1A inhibition was undetectable in shSpy1A-1 cells (2.5%) and shSpy1A-2 cells (-0.5%), and further corresponded to infection efficiencies ranging from 25-50% (Fig.13b-c). GFP-fluorescence was at its highest in lentiviral-transduced stable cell lines, and thus it was speculated that the maintenance of F5A1-2 cells beyond certain passages led to the acquisition of additional mutations and modifications in signal transduction pathways in response to long-term culturing. Alternatively, Spy1A knockdown may have been selected against as a result of continued cell passaging. Nevertheless, to determine whether modest Spy1A knockdown in stable F5A1-2 cell lines sufficed to affect tumor growth rate and ductal morphogenesis *in vivo*, F5A1-2^{shCntl} and F5A1-2^{shSpy1A} cells were transplanted into the cleared fat pads of No. 4 inguinal mammary glands. Following transplantation, test subjects were sacrificed and freshly dissected 3, 6, 7, 10, or 15 days post-surgery. Representative photographs for each dissection time point are provided in Fig.25a, and showcase the anatomical changes associated with tumor development resulting from F5A1-2^{shCntl} and F5A1-2^{shSpy1A} cell

injection. Up to 7 days post-surgery, shCntl-injected glands (left) generally exhibited an increase in tumorigenic potential in comparison to shSpy1A-injected glands (right) (Fig.25a). By day 10 post-surgery, however, tumors from either side had amalgamated into a single tumor mass and thus could not be distinguished effectively or subjected to calliper measurement of tumor height (Fig.25a). Consequently, overall tumor growth rate could not be determined accurately for test subjects co-transplanted with F5A1-2^{shCntl} and F5A1-2^{shSpy1A} stable cell lines. Instead, as a more accurate measure, tumor nodule surface area was approximated per gland for the following time points: 3, 6-7, and 10 days post-surgery (Fig.25b), and also was utilized to quantify changes in overall tumor size upon Spy1A knockdown. Up to 7 days post-surgery, F5A1-2^{shSpy1A} transplants gave rise to tumor nodules that exhibited a 2-fold reduction in overall tumor size, when compared to tumor nodules derived from F5A1-2^{shCntl} transplants (Fig.25b). Although the tumor growth pattern was less clear at 10 days post-surgery, shSpy1A-derived tumor nodules occupied less total surface area, as compared to shCntl-derived tumor nodules. Taken together, *in vivo* results obtained from Fig.25b demonstrate an overall reduction in tumor nodule size despite an apparent lack of Spy1A inhibition at the protein level. The trend was confirmed up to 10 days post-surgery, however, and replicates were too few to impart statistical significance to numerical data. Therefore, results are deemed preliminary at this stage, and will require further repetition in order to assess the validity of reduced tumor nodule surface area in response to shSpy1A treatment.

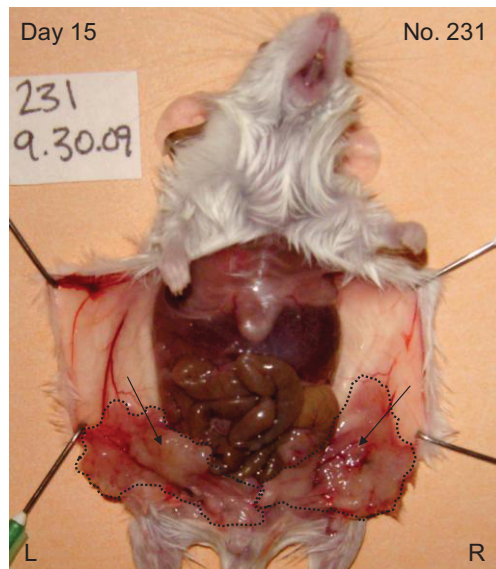
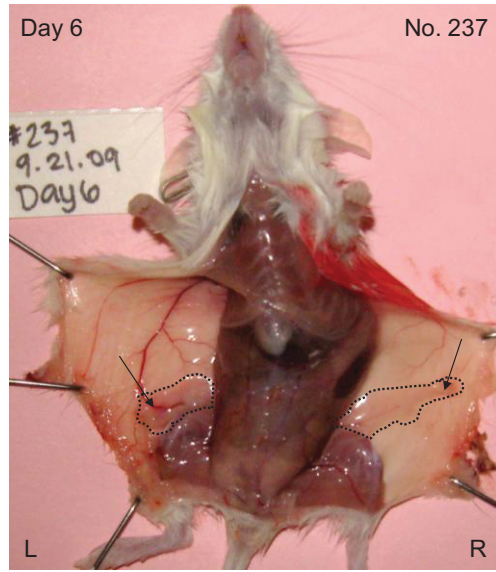
Tumor samples dissected from left and right glands on days 10 and 15 post-surgery were subjected to protein lysis and 10% SDS-PAGE analysis, coupled to immunoblotting for c-Myc, Spy1A, phosphorylated and total ERK1/2, p21, and Actin, the resident loading control (Fig.25c). Normalized to total Actin expression, all protein levels were quantified through densitometric analysis (Fig.25d). Confirmed through immunoblotting, persistent Spy1A knockdown was restricted solely to test subject No.231 (19%) and knockdown was virtually undetectable in No.235, whereas F5A1-2^{shSpy1A} tumors isolated from test subjects No.234 and 238 experienced a 10% and 3% elevation in Spy1A protein levels, respectively (Fig.25d). Thus, densitometry values indicated insignificant knockdown in three out of four shSpy1A tumor samples derived from late passage F5A1-2 cells (P63). Comparable to the expression patterns observed for Spy1A, c-Myc expression decreased

accordingly in test subjects No.231 (13%) and 235 (4%), however, increased in No.234 (10%) and 238 (1%), relative to shCntl treatment (Fig.25d). The ratio of phospho-ERK1/2 to total ERK1/2 was shown to decrease in F5A1-2^{shSpy1A} tumors derived from test subject No.231 (22%), however remained unaltered in tumors derived from No.234, 235, and 238 (Fig.25d). In addition, three out of four test subjects (No.231, 234, and 238) experienced a slight reduction in p21 protein expression ($\leq 7\%$) (Fig.25d). Alternatively, p21 levels were upregulated by 19% in F5A1-2^{shSpy1A} tumors isolated from No.235, when compared to corresponding control tumors isolated from the same animal (Fig.25d). Despite negligible changes in Spy1A, c-Myc, ERK1/2, and p21 protein, densitometry values were utilized to predict general expression profiles in response to varying degrees of Spy1A knockdown (see *Discussion*). However, further replication must ensue in order to verify predictions.

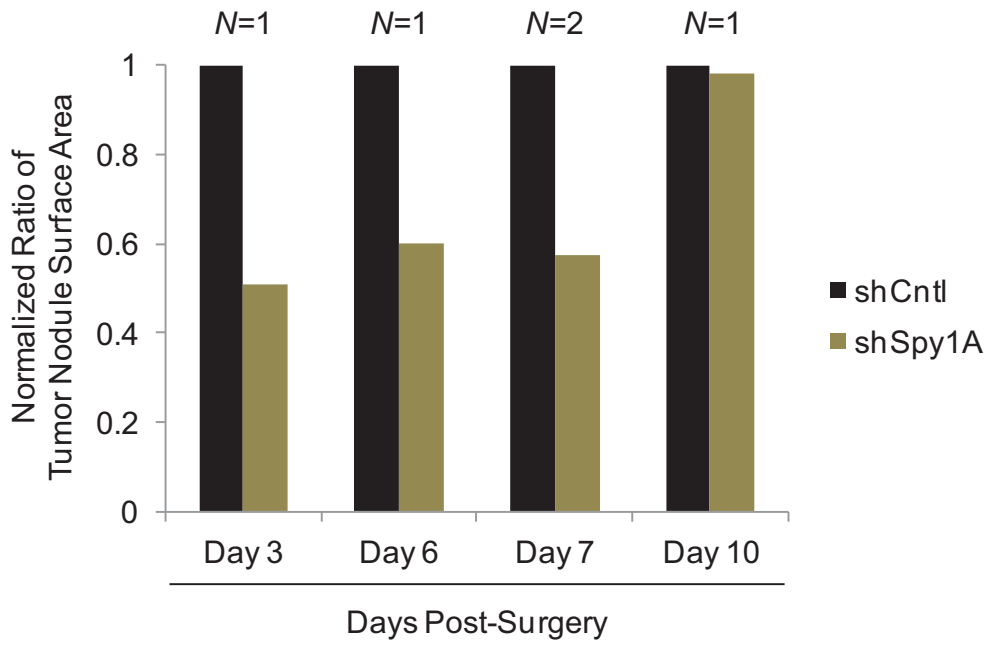
XIV. Stable Spy1A Knockdown Encourages In vivo Ductal Formation in Late Passage F5A1-2 Tumor Cells.

In vivo transplantation of stable F5A1-2 cell lines generates two distinct epithelial cell populations, namely (a) overgrown tumor masses and (b) epithelial ductal side branches, both of which are stained a dark purple colour by haematoxylin. Accordingly, it was speculated that whole mounts prepared 11 days post-surgery contained tumors too large in size to effectively observe all underlying networks of ductal side branches. Therefore, to investigate the effects of stable Spy1A knockdown on ductal morphogenesis at earlier stages of F5A1-2 tumor development, transplanted animals were sacrificed at 3, 6, and 7 days post-surgery, after which fourth inguinal mammary glands were prepared for whole mount analysis through haematoxylin staining. Resultant whole mounts were examined under GFP fluorescence microscopy, and demonstrated an increase in the number of side branches produced upon transplantation of F5A1-2^{shSpy1A} cells, when compared to control treatments. Despite ineffective Spy1A knockdown, F5A1-2^{shSpy1A} whole mounts exhibited partial restoration of ductal side branching relative to control glands, although additional replicates are required to fully substantiate the statistical significance of whole mount data. Representative GFP-fluorescence images have been provided for left (shCntl-1) and right (shSpy1A-1) whole mounts derived from test subject No.229, whose fourth glands were isolated 6 days post-surgery (Fig.25e).

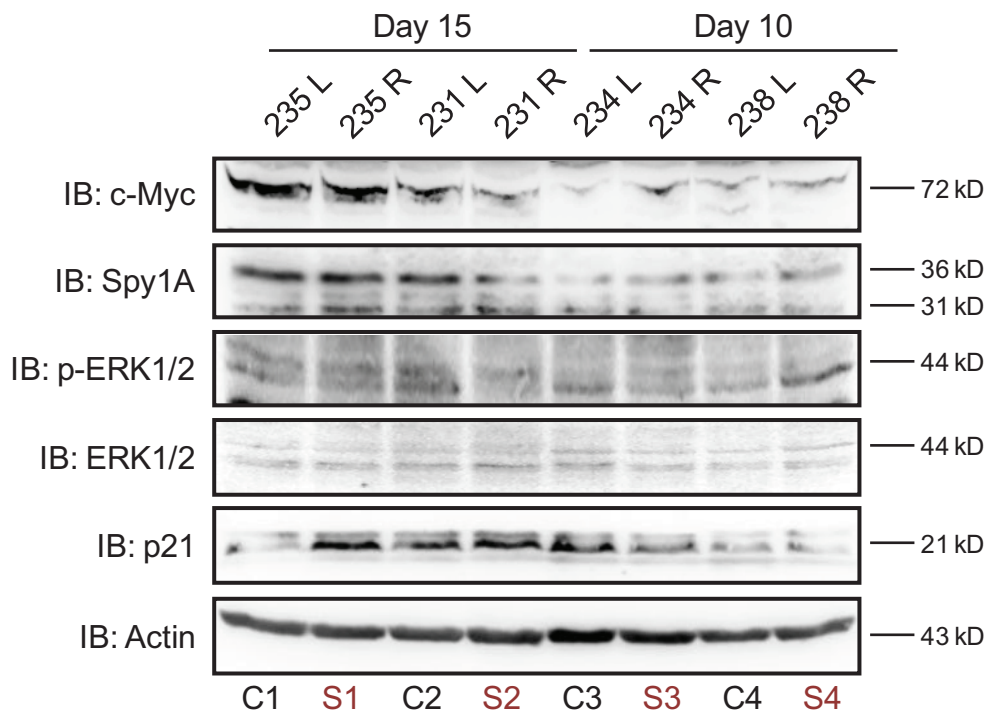
A



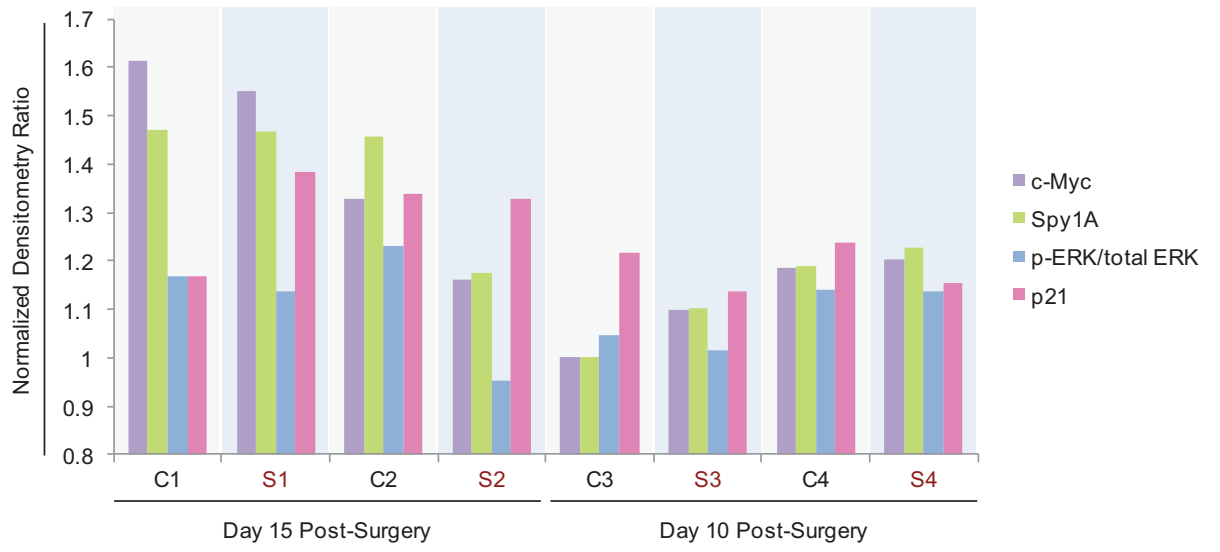
B



C



D



E

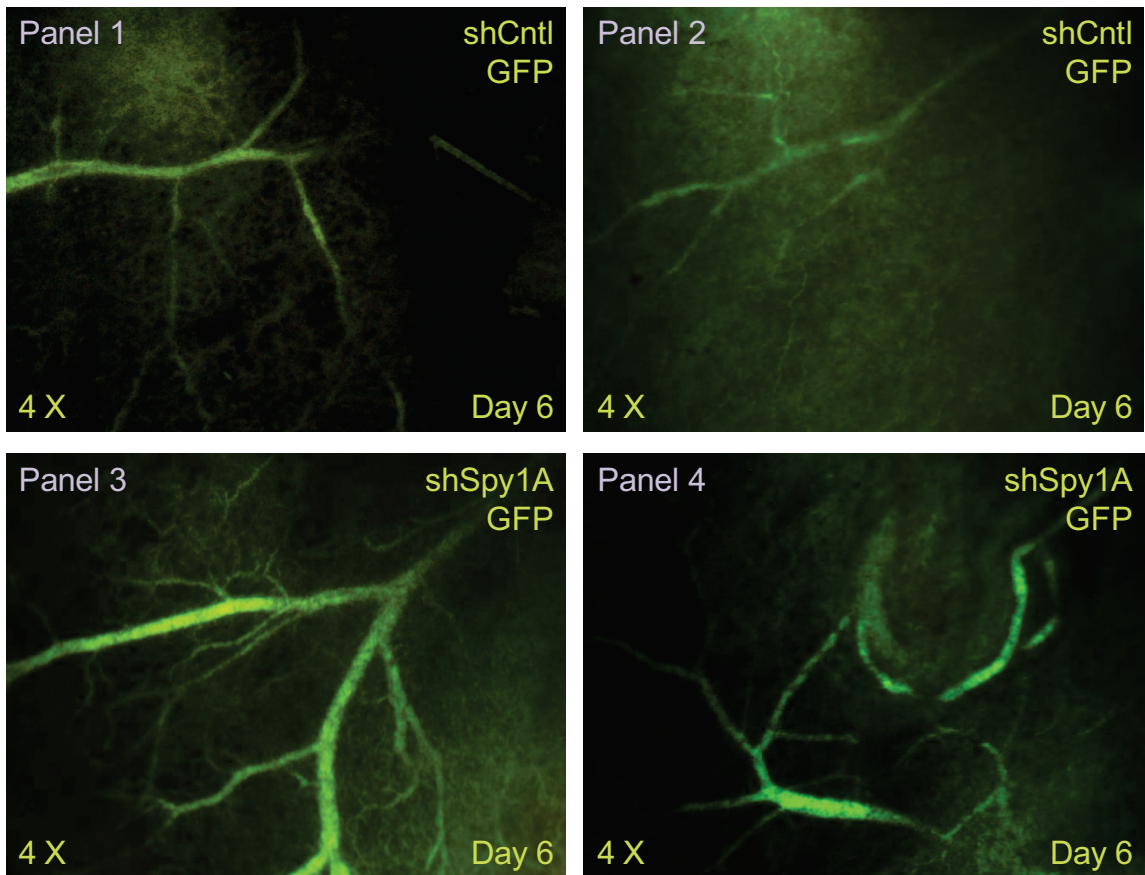


Figure 25. Stable Spy1A inhibition in late passage F5A1-2 cell lines induces MAPK Pathway and c-Myc downregulation and results in increased ductal morphogenesis *in vivo*. No. 4 inguinal mammary glands were cleared and transplanted with F5A1-2^{shCntl} cell suspension (left gland, L) at a dosage of 1×10^6 cells per gland, and F5A1-2^{shSpy1A} cell suspension (right gland, R) at a dosage of 1×10^6 cells per gland ($N=13$ replicates). Black arrows (\rightarrow) point to the tumor nodule residing in each gland. Overall No. 4 mammary glands are outlined by a dashed black line (---). **(a)** A tumor time course was established upon dissection of six representative test organisms to determine the *in vivo* effect of stable shCntl and shSpy1A cell lines on the rate of tumor formation. The time points studied did not yield tumors that could be measured with a Vernier Calliper; instead, autopsy photographs are provided for each test subject, taken on the day of animal sacrifice and dissection to assess the rate of tumor growth in late passage stable F5A1-2 cell lines: No.236 (day 3); No.237 (day 6); No.233 (day7); No.234 (day10); No.235 (day 15); No.231 (day 15). **(b)** An estimated measure of surface area (cm^2) was calculated for each tumor nodule per gland at a given time point (post-surgery). To enable comparative analysis between autopsy photographs, all surface area values were normalized to that of shCntl, and are reported as a final ratio. Black bars indicate shCntl tumor nodules (L gland); tan bars indicate shSpy1A tumor nodules (R gland). Accurate measurement of tumor nodule surface area was only feasible for select test organisms, based on autopsy photographs. Sample size per time point is provided above each set of bars. A minimum of two samples are required to calculate standard error; the standard error value at Day 7 was determined to be ± 0.01 , but could not be calculated for remaining time points. **(c)** Whole tumor protein extracts were isolated from the periphery of L and R tumor tissues on days 10 and 15 post-surgery to avoid the mixed tumor population located in the centre of the organism. Protein analysis was conducted through 10% SDS-PAGE for L and R tumors isolated from No.231 (Control knockdown (C) 2, Spy1A knockdown (S) 2), 234 (C3, S3), 235 (C1, S1), and 238 (C4, S4) animals ($N=2$ replicates, for each time point). Immunoblotting ensued for c-Myc (72 kD); Spy1A (31, 36 kD); phosphorylated ERK1/2 (44 kD); total ERK1/2 (44 kD); p21 (21 kD); and Actin (43 kD), as a loading control. **(d)** Densitometric analysis was completed for the immunoblot depicted in (c); all protein data were subsequently normalized to total Actin expression. Spy1A (green); c-Myc (purple); p-ERK/total ERK ratio (blue); p21 (fuschia). **(e)** Whole mount L and R fourth glands were isolated from test subject No.229, 6 days post-surgery, followed by GFP-detection of epithelial ductal branches derived from GFP-tagged F5A1-2 stable cells. Representative images of ductal branching networks in shCntl (*Panel 1-2*) and shSpy1A (*Panel 3-4*) glands are shown over two different panels per gland, and depict various regions of each whole mount sample (4X magnification; $N=1$ replicate).

Discussion

De novo Spy1A overexpression typically equates with more aggressive, invasive BC phenotypes; in a separate report, deregulated c-Myc upregulation correlated strongly with advanced neoplastic mammary disease as well.⁷⁹⁻⁸⁰ Additionally, Spy1A and c-Myc mitogens localize to mammary epithelial cell types,^{4,22} and evidently function within the same temporal window during post-natal mammopoiesis: that is (a) both factors positively regulate proliferative developmental events (pregnancy), and (b) both are subject to upregulation during massive mammary gland remodelling and apoptosis (involution).²² Golipour and Myers et al. (2008) further identified Spy1A as an effective tumor promoter and downstream target of c-Myc, however only briefly alluded to the possibility that Spy1A functions as a positive mediator of *de novo* c-Myc signaling during mammary tumorigenesis.²² Therefore, results reported here are the first to classify Spy1A as an effector of c-Myc-induced tumor cell proliferation *in vitro* and *in vivo*, and further demonstrate that both proliferative regulators are co-elevated in c-Myc overexpressing mammary glands and associated tumor tissue.

I also demonstrate that E2 stimulation of ER α elevates Spy1A mRNA and protein expression through prerequisite MAPK pathway activity within the MCF7 cell system. Results derived from this report also suggest that c-Myc and Spy1A may function to downregulate the CKIs p21 and p27, respectfully, in those tumors overexpressing deregulated c-Myc, according to preliminary densitometry data utilized to extrapolate and predict changes in protein expression in response to MEK or Spy1A inhibition. Additionally, I provide preliminary evidence to suggest that MAPK signal transduction may function to regulate Spy1A protein expression in a positive and negative manner, depending on cellular context, and hypothesize that MAPK function is mediated by differential regulation of the MAPK machinery on a post-translational level. Ultimately, I postulate that the phosphorylation status of MAPK effectors determines the final outcome of MAPK signaling on Spy1A in c-Myc induced mammary neoplasias, and may facilitate the development of tamoxifen resistance in human BCs initially responsive to antiestrogen drug therapy.

I. Spy1A May Alter Cellular Distribution of p27 and Downregulate its Protein Expression in MMTV-Myc Overexpressing Tumors and Related F5A1-2 Cell Lines.

Furthermore, this study is the first to demonstrate that atypical upregulation of Spy1A persists in the novel F5A1-2 primary tumor cell line, and also correlates with increased *de novo* c-Myc protein expression and p27 downregulation. Although Spy1A is accredited for its ability to promote ubiquitin-mediated p27 proteolysis,^{53,60,81} I provide preliminary evidence to suggest that p27 is paradoxically upregulated together with Spy1A in tissue samples derived from MMTV-Myc overexpressing mammary glands and corresponding tumors. Similarly, immunohistochemical analysis of p27 expression in primary human mammary tumors revealed that 44% of studied tumors exhibited high p27 staining, whereas p27 was virtually absent in the rest.⁸² In support of its uncharacteristic role during cell cycle progression, p27 has been reported to assist in cyclin D-CDK4 complex formation, complex stabilization, and subsequent nuclear import to promote movement through G₁/S.⁸³ Also, Porter et al. (2003) revealed that Spy1A requires the presence of p27 substrate to properly stimulate cell transitioning through G₁/S, and it is further postulated that a certain threshold of p27 expression is indispensable for the continued maintenance of mammary tumor cellular proliferation.^{32,53} Perhaps during augmented G₁/S in breast tumors, the tumor cell attempts to upregulate p27 in response to abnormal Spy1A elevation, and simultaneously strives to preserve the stoichiometric interaction between p27:Spy1A. Consequently, a surplus of functional p27 may be available to bind to additional molecules of nuclear localized Spy1A. Thus, enhanced association of Spy1A with its CDK2 binding partner after direct interaction with p27 may potentiate the rate of p27 phosphorylation at residue Thr-187,⁶⁰ and could possibly prime p27 for additional phosphorylation events that function to initiate cytoplasmic relocalization of p27 prior to its degradation. Rodier et al. (2001) demonstrated that *in vivo* phosphorylation of p27 on Ser10 results in its stabilization in a manner that does not impede SCF^{Skp2}-mediated proteolysis of p27.⁸⁴ Given that p27 exits the nucleus upon mitogen-activated Ser10 phosphorylation,⁸⁴⁻⁸⁵ the possibility arises that p27 in its phosphorylated form is subject to transient stabilization in the cytoplasmic fraction of tumor cells, which may account for the increased detection of p27 levels in MMTV-Myc overexpressing mammary tumors. Numerous studies have also highlighted the importance of differential phosphorylation as

a modulator of p27 function,^{84,86-89} and based on the visualization of two protein bands resulting from p27-directed immunoblotting (Fig.9), I predict that p27 exhibits multiple phosphorylation states during mammary tumorigenesis. Moreover, the argument that two protein bands signify the existence of more than one p27 isoform in MMTV-Myc glands and tumor tissue is highly refutable, since no evidence is currently available to support *in vivo* synthesis of alternate p27 splice variants.

Short-term retention of cytoplasmic p27 can precede its subsequent degradation during G₁/S, consistent with the notion that p27 regulates processes such as cell migration and possibly apoptosis, when relocated to the cytoplasm.^{85,90-91} For instance, consistent with its cell cycle role, p27 can functionally inhibit Grb2, an upstream mediator of Ras/MAPK signaling, when persistently confined to the cytoplasm.^{85,92-93} Conversely, yeast-two hybrid screening conducted by Sugiyama et al. (2001) identified the novel ability of Grb2 and Grb3-3 adaptor molecules to interact with p27 in the cytoplasm both *in vitro* and *in vivo*, and further demonstrated the essentiality of the Grb2-p27 interaction for successful proteolytic destruction of cytoplasmic p27, utilizing NIH3T3 fibroblasts.⁹⁴ In this way, the MAPK cascade is postulated to be integral for the negative regulation of p27 in c-Myc deregulated BCs. In support of this hypothesis, MEK1 inhibition in proliferating HC11 cells promoted a slight increase in p27 expression, although changes in protein expression were essentially negligible and additional replicates are required to confirm the validity of this result. Possibly confounded by the absence of functional p53, whether this outcome was an immediate by-product of Spy1A downregulation remains to be elucidated. At present, it has not been established whether MAPK signaling mediates Spy1A through a direct or indirect mechanism. Based on previous reports,⁹⁵ I postulate that MAPK signal transduction may play a role in regulating Spy1A expression by relieving the inhibitory action of p27 on CDK2, thereby permitting Spy1A/CDK2 association and consequential cell cycle movement. In support of this hypothesis, Donovan et al. (2001) demonstrated the essentiality of MAPK signaling for maintaining tamoxifen resistance in numerous BC cell lines through posttranslational mechanisms that serve to modify p27 phosphorylation, downregulate p27 protein levels, and strive to relieve p27 inhibition of CDK2 activity.⁹⁵ I also predict that c-Myc-stimulated Spy1A protein indirectly promotes the shuttling of phosphorylated p27 to the cytoplasm in mammary tumor cells that overexpress c-Myc.

More specifically, I hypothesize that upon complex formation in the nucleus, Spy1A-tethered p27 may relocate to the cytoplasm where it experiences brief stability due to its interaction with Spy1A, which ultimately permits p27 to rapidly associate with other cytosolic factors prior to inevitable CKI destruction during G₁/S.

II. Late Passage F5A1-2 Tumor Cells May Acquire Additional Mutations and/or Genetic Lesions During Long-Term Cell Culture.

Immunoblotting data accumulated from this study represent only a limited snap-shot of the dynamic signaling events required to maintain p27 downregulation and tumor promotion due to a reliance on the time of protein isolation, which is thought to explain inconsistencies in p27 expression observed across different tumor samples and cell lines. Immunoblotting was utilized to examine whole tumor changes in cell signaling and did not account for the presence of heterogeneous cell populations that typically inhabit mammary tumors. Alternatively, prolonged episodes of cell passaging often select for a single cell population, and cell culturing over extended periods is thought to promote the accumulation of genetic abnormalities or added mutations in F5A1-2 cells, accounting for discrepancies in tumor signaling that may have occurred over time. Indeed, Tainsky et al. (1984) attributed the altered tumorigenic capacity of late passage PA1 teratocarcinoma cells to spontaneous development of a guanine-to-adenine point mutation within the human ras^N oncogene, following transplantation into nude mice.⁹⁶ In addition, PA1 teratocarcinoma cells were initially isolated from a primary tumor source, analogous to the derivation of F5A1-2 cell lines.⁹⁶ Instead, live imaging of *de novo* murine mammary tumors may evade the above issues by successfully capturing all phases of fluorescently-labelled Spy1A, c-Myc, and p27 localization during tumor progression, thereby revealing the full scope of protein activity rather than focusing on one instance of time. This approach may especially benefit future analysis of c-Myc at the mRNA level, due to its hasty transcriptional activation and its nature as an immediate early gene.

III. Tamoxifen Resistance Is Thought to Arise from Constitutive c-Myc Overexpression and p21 Downregulation in Response to Persistent E2 Stimulation.

In response to estradiol exposure, ER α typically functions to promote rapid movement through G₁/S by use of a mechanism that is contingent upon transcriptional activation of c-Myc and concomitant downregulation of p27.²⁸ Additionally, MCF7 cells pre-treated with estrogen-deactivating agents like tamoxifen respond to both c-Myc upregulation and E2 stimulation by downregulating p21 mRNA and protein expression, thus demonstrating the importance of c-Myc as a critical mediator of ER α activity.²⁸ Utilizing a tamoxifen resistant version of MCF7 cells, designated as LCC9 hereafter, Mukherjee and Conrad (2005) further revealed that c-Myc and p21 are no longer altered by estrogen or tamoxifen application during antiestrogen resistance; instead c-Myc is employed as a transcriptional repressor of p21,²⁸ although its effect on SpylA in a tamoxifen resistant paradigm has never been examined. Therefore, I recommend that LCC9 cell lines be utilized in future studies to clarify the role played by SpylA in BCs that strangely circumvent antiestrogen-mediated tumor regression. Furthermore, LCC9 cell stocks have recently been obtained from the Lombardi Cancer Centre (Washington, DC, USA) for immediate analysis. Of notable interest, past reports have put forth the idea that c-Myc actively facilitates the acquisition of an antiestrogen resistance phenotype in ER α -positive breast tumors, and does so by downregulating p21 protein levels.²⁸ Although results are strictly preliminary, I provide evidence to support this conjecture by verifying p21 reduction by 20% in the presence of E2 in wild-type MCF7 cell lines (Fig.16), as previously reported.^{28,97-98} Also, c-Myc upregulation generally correlated with p21 downregulation and vice versa, and this pattern continually emerged in differentially treated mammary cell lines throughout the course of this study (HC11, MCF7, F5A1-2). Hence, in response to first-line antiestrogen drug treatment, the following mechanism may have evolved within ER α -positive BCs to counteract the inhibitory action of tamoxifen on ER α , thereby promoting persistent cell proliferation and tamoxifen insensitivity. In the presence of sustained E2 stimulation, c-Myc is thought to become rapidly upregulated by ER α and subsequently suppresses p21 promoter activity, while simultaneously activating SpylA, which ultimately functions to promote p27 inactivation. Furthermore, once SpylA has been transcriptionally stimulated by E2, it may continue to activate c-Myc through a positive feed-back loop. However, further investigation is needed to clarify the feasibility of this mechanism in mediating the

development of antiestrogen resistance.

IV. ER α Induction of Spy1A mRNA and Protein Expression May Be Mediated Preferentially Through the MAPK Cascade.

Generally speaking, E2 treatment induces Spy1A protein expression as early as 2 h post-administration in wild-type MCF7 cells, and progressively elevates Spy1A mRNA expression throughout the entire 24 h time course, thereby marking this study as the first to link ER α activation to Spy1A upregulation. In an accelerated fashion, E2 has been shown previously to stimulate ERK1/2 expression as early as 5 minutes post-treatment in various cell lines including the MCF7 cell model, and E2-directed ERK1/2 upregulation is postulated to occur via activation of plasma membrane-bound ER.⁷³ Additionally, Golipour and Myers et al. (2008) identified Spy1A as a downstream target of the MAPK pathway.²² In this study, evidence obtained from the chemical inactivation of MEK1/2 in estrogen-responsive MCF7 cells revealed the necessity of MAPK signaling for mediating E2 stimulation of Spy1A protein expression as early as 2 h post-U0126 treatment, and further identified MEK1/2 isoforms as novel upstream mediators of Spy1A, as previously predicted.²² However, ambiguity exists as to whether the MAPK pathway exerts positive or negative regulation over Spy1A, particularly since Spy1A protein levels experience persistent elevation following MAPK inhibition in late passage F5A1-2 cells. Although results are preliminary, they suggest that MAPK signaling may play an integral role in regulating Spy1A, whether through direct MAPK activation or through indirect regulation of downstream target genes. However, the mechanism through which this process occurs is currently unidentified, but is thought to rely on cellular context and tumor genotype.

V. MAPK and c-Myc Cross-talk May Not Affect Spy1A Protein Expression During c-Myc Induced Mammary Tumorigenesis.

During tumorigenesis, mutations localized to the ras oncogene bring about relentless activation of the MAPK pathway in ~30% of human malignancies and in ~5% of BCs.⁹⁶ In addition, upregulation of ERK1/2 has been reported in numerous tumor cell lines.⁹⁶ Moreover, MAPK signaling typically induces the transcription of immediate early genes

like *c-fos*, *c-jun*, and *c-myc* in response to hormonal, mitogenic, phorbol ester, or growth factor stimuli.⁹⁶ Contrary to these reports, however, MEK1/2 inhibition failed to alter c-Myc protein expression in MCF7 cells (Fig.16), as previously documented by Lobenhofer et al. (2000),⁷³ thereby suggesting that c-Myc and MAPK cross-talk may be dispensable for MAPK-mediated Spy1A regulation at the protein level. Hence, I predict that MAPK signaling mediates Spy1A function independently of c-Myc protein status. On a similar note, the ability of E2 to stimulate Spy1A (mRNA, protein) through c-Myc activation is currently unknown, and warrants further investigation. Consequently, c-Myc knockdown via transient transfection of MCF7 cell cultures with dominant negative Myc constructs or c-Myc short interfering RNA may be conducted to clarify whether ER α requires c-Myc to upregulate Spy1A. Lastly, it remains unclear whether MAPK-mediated Spy1A regulation relies on the constant synthesis of c-Myc mRNA transcripts. Resolving mRNA expression profiles of ERK1/2, Spy1A, and c-Myc under identical experimental conditions may be utilized to elucidate this aim in future studies.

VI. Spy1A May Mediate the Development of Tamoxifen Resistance in Human BCs That Initially Respond to Antiestrogens.

During the initial phases of antiestrogen drug treatment, it is speculated that tamoxifen induces conformational changes in ER α structure in order to inhibit estrogenic signaling, i.e. ER α targets that promote tumor cell proliferation and other pro-estrogenic effects.¹² Although tamoxifen effectively targets ER α when utilized to treat antiestrogen responsive breast tumors, development of tamoxifen resistance often hinders the effective treatment of unresponsive BCs.¹² Instead, antiestrogen resistant breast tumors may benefit greatly from treatment strategies that involve targeting downstream effectors of ER α in order to reduce tumor cell proliferation. Preliminary data imply that Spy1A may function as a putative downstream target of ER α (Fig.15), and upon transient inhibition, Spy1A is also able to significantly reduce cell population density *in vitro* (Fig.11). Derived from ER α -positive, ER β -negative MCF7 cells,¹² preliminary results further demonstrate the inherent ability of E2 to upregulate Spy1A mRNA and protein via preferential activation of ER α . In addition, the DNA binding activity and expression levels of ER α remain intact during

tamoxifen resistance, thereby promoting protein interaction between ER α and the c-jun component of the AP-1 transcription factor complex¹⁰¹ and maintaining ER α signaling in the presence of antiestrogens. In this way, ER α :AP-1 cross-talk may indirectly contribute to the deregulation of Spy1A expression in a manner independent of E2 stimulation.

Also, tamoxifen is able to stimulate ER α coactivators that function to maintain ER α signaling despite antiestrogen presence.⁹⁹ As a result, tumor cells may develop tamoxifen resistance.⁹⁹ For instance, tamoxifen may activate AP-1 regulated genes in the presence of E2 by upregulating AP-1 transcriptional activity, in one mechanism.⁹⁹⁻¹⁰⁰ In turn, elevated AP-1 levels may trigger a negative feedback loop that caters to tamoxifen resistance, as evidenced by the acquisition of a drug-resistant phenotype in MCF7 cells overexpressing *c-jun*.⁹⁹⁻¹⁰⁰ Furthermore, when compared to untreated ER-positive pair matched samples, tamoxifen resistant human BCs often display enhanced activity of c-Jun NH₂-terminal kinase, a potent inducer of AP-1, and exhibit increased binding of AP-1 to its respective promoter elements.^{99,101} Close examination of the putative Spy1A promoter reveals two AP-1 response elements positioned at nucleotides -715 and -630 in reference to the transcription initiation start site (position 0). However, whether Spy1A falls under AP-1 regulation during antiestrogen resistance warrants further examination. Hence, I postulate that in response to prolonged exposure, tamoxifen *indirectly* upregulates Spy1A protein, by promoting AP-1 binding to the Spy1A promoter in ER α -positive BC cells. In this way, enhanced AP-1 binding to the Spy1A promoter may exert transcriptional regulation over Spy1A. Furthermore, c-Jun overexpression¹⁰⁰ and Spy1A downregulation (Fig.14) appear to promote comparable changes in BC cell phenotype, suggesting that AP-1 responds to tamoxifen treatment by transcriptionally repressing Spy1A signaling, and in this way may disrupt the ability of Spy1A to regulate MAPK through a positive feed-back loop.

Data derived from normal mammary HC11 cells suggest a putative link omnipresent between MAPK and c-Myc signaling under controlled proliferative circumstances in the mammary organ (Fig.17), although MAPK inhibition was pronouncedly weak relative to results generated by Golipour and Myers et al. (2008).²² However, the strength of this link appears to greatly diminish during mammary tumorigenesis as evidenced by unfaltering levels of c-Myc in U0126-treated MCF7 cells partially deficient in ERK1/2 expression

(Fig.16b). Furthermore, the degree to which MAPK signaling regulates Spy1A expression during normal mammary development has not been determined, although based on data from Fig.17b, an important role may exist for functional MAPK signaling in promoting Spy1A-mediated epithelial mitogenesis in healthy mammary cells. Moreover, the protein stability of c-Myc is regulated via phosphorylation on multiple residues,⁴⁰ and ERKs that undergo constitutive phosphorylation dually phosphorylate c-Myc on Thr-58 and Ser-62 residues, and are thought to promote c-Myc self suppression.⁴⁰ Cyclin/CDK complexes phosphorylate c-Myc on Ser-62 as well.⁴⁰ Considered together, these findings imply that in the absence of functional MAPK signaling, c-Myc may no longer be suppressed and becomes subject to upregulation. Therefore, should AP-1 antagonize Spy1A expression, I predict that Spy1A may no longer exert positive regulation over MAPK signaling, leading to inactivation of the MAPK cascade. This phenomenon may encourage c-Myc to escape MAPK-mediated inhibition, thereby promoting upregulation of c-Myc and inadvertent re-activation of Spy1A expression. The resultant positive feed-back loop speculated to exist between Spy1A and c-Myc, based on results from Fig.11, may continue to promote tumor propagation in the presence of tamoxifen treatment, possibly leading to the acquisition of antiestrogen resistance.

VII. Transient Spy1A Downregulation May Participate in Early Stages of EMT in Murine and Human BCs Overexpressing Deregulated c-Myc.

In addition to promoting tamoxifen resistance *in vitro*, MCF7 cells that exogenously overexpress c-Jun closely mimic the cellular properties of the epithelial to mesenchymal transition (EMT) such as enhanced cell motility, upregulation of AP-1 regulated type IV collagenase protein (MMP-9), and marked elevation in invasive capacity.¹⁰⁰ EMT is traditionally defined as a developmental process utilized by embryonic cells of epithelial origin to gain motile properties and escape their local cellular niche to ectopic sites, in order to expand into mesoderm and other differentiated tissue.¹⁰² Epithelial cells residing in breast tumors have also been postulated to differentiate into stromal tissue.²⁶ Numerous experimental models have verified a central role for EMT during mammary tumor progression into more invasive, metastatic forms of BC, highlighted in primary tumor cells by a loss of epithelial cell fate and morphological transformation into a fibroblastic,

spindle-like cell state.^{102-105,112} In the F5A1-2 cell system, EMT-like changes were reported 24 h after Spy1A shRNA treatment. In response to ~40% knockdown of Spy1A, early passage F5A1-2 cells (<P30) appeared to undergo morphological changes in cellular phenotype, thereby yielding a higher population of spindle shaped, myoepitheliod-like cell types in relation to wild-type and control shRNA treated cells, prompting further investigation. It was speculated that a forced reduction in cell proliferation rate as a result of transient Spy1A silencing (Fig.14a) may have physically expanded the availability of unoccupied plate surface area, potentially allowing remaining live cells to monopolize the additional space by protruding outwards to neighbouring cells rather than falling victim to morphological transformation. Alternatively, variances in cellular phenotype may have resulted from changes in signal transduction and pathway networking/cross-talk, particularly since Spy1A inhibition has been shown to downregulate ERK1/2 and c-Myc protein expression. To clarify whether Spy1A inhibition influences mammary tumor cell morphology, luminal epithelial markers CK18 and CK19 were analyzed in response to RNAi treatment in both early (<P30) and late (>P60) passage F5A1-2 cells, since Spy1A expression was thought to vary with passage number. Consistent with this paradigm, transitory inhibition of Spy1A in earlier passages consistently produced changes in tumor morphology indicative of EMT, implying cell reversion to a fibroblastoid state and further supported by a 31% reduction in CK18 expression. Note that CK18 is a structural marker typically utilized in mammary gland tumor literature to detect cells of epithelial lineage.⁷⁰ Immunoblotting for CK19, yet another luminal epithelial marker,¹⁰⁶ resulted in no detection of CK19 protein in both control treated and Spy1A-abrogated F5A1-2 cells (data not shown). As a result, it could not be verified whether Spy1A attenuation promoted the acquirement of a fibroblastic or myoepithelial cellular phenotype indicative of EMT. At the very least, Spy1A downregulation may act as a potential initiator of EMT during its earliest stages, however the expression profile of Spy1A during all phases of EMT has not yet been identified. Additional insight into the molecular changes associated with epithelial to mesenchymal transitioning may be obtained from flow cytometry-mediated assessment of myoepithelial markers (smooth muscle actin, vimentin)¹⁰⁶ in F5A1-2 cell populations treated with Spy1A RNAi.

VIII. F5A1-2 Cell Lines and Associated Tumor Tissue May Alter Tumorigenic Signaling and Tumor Phenotype in Response to Spy1A Knockdown.

As stated in the *Results* section, preliminary findings from Fig.24b and Fig.25d have been utilized to predict the degree to which c-Myc and MAPK expression profiles vary when challenged with Spy1A knockdown. In combining *in vivo* expression data from test subjects No.106, 107, and 231, Spy1A protein levels were significantly reduced in tumor samples derived from shSpy1A-treated F5A1-2 cells, when compared to shCntl treatment ($p=0.035$, Student's *t*-test, 1-tail distribution, unequal variance). Likewise, ERK1/2 and c-Myc protein levels were significantly downregulated in shSpy1A tumor samples, relative to shCntl treatment ($p<0.05$, Student's *t*-test, 1-tail distribution, unequal variance). Thus, disregarding variables such as passage number of transplanted cells or post-surgery time elapsed upon tumor extraction, it is speculated that significant levels of Spy1A inhibition downregulate c-Myc and MAPK protein expression in c-Myc overexpressing BCs.

Although transient transfection assays are typically utilized to assess short-term effects of transgene expression, F5A1-2 cells transfected with shSpy1A constructs continued to exhibit Spy1A knockdown (Fig.24b) and reduced tumor growth rate (Fig.22d) up to 30 days post-surgery in select tumor samples, relative to shCntl treatment. Hence, transient Spy1A inhibition is thought to have slowed the process of cell transformation by reducing cell population size, and/or preventing cells from undergoing morphological changes that promote tumor cell proliferation.

For the purpose of examining long-term consequences of Spy1A abrogation, lentiviral transduction assays were utilized to generate stable F5A1-2 cell clones that constitutively overexpressed shCntl or shSpy1A constructs. Spy1A knockdown was initially successful in late passage (P63) stable cell lines, as evidence by a 30% reduction in Spy1A protein expression (Fig.12), however protein lysates extracted two passages later (P65) exhibited insignificant knockdown (Fig.13). It was speculated that prolonged cellular passaging led to the acquisition of a knockdown resistant phenotype due to F5A1-2 development into an advanced, aggressive form of BC. Similarly, P60 cell lines were resilient to 10 μ M U0126 and PD098059 inhibition, suggesting that MAPK inhibitors are ineffectual in treating late stage mammary neoplasias overexpressing c-Myc. Although infection efficiencies ranged

from 25-50%, Spy1A protein levels were not effectively silenced in tumor lysates derived from F5A1-2^{shSpy1A} stable cells cultured to P65, lending credence to the idea that these cells produce late stage tumors that no longer respond to conventional treatment methods. Furthermore, whole mounts transplanted with F5A1-2^{shSpy1A} cells displayed an increase in ductal side branching relative to control glands, despite insignificant Spy1A knockdown. These data suggest that partial silencing of Spy1A in only a portion of the tumor population may still be sufficient to reduce tumor growth rate, ductal epithelial side branching, and c-Myc and MAPK signal transduction, although additional replicates are needed to impart statistical significance. Furthermore, this phenomenon also suggests that *in vivo* Spy1A knockdown may restore BCs undergoing later stages of tumor progression to less aggressive neoplastic states, possibly by disrupting the necessary changes in cell phenotype responsible for cell transformation. Therefore, potential exists for Spy1A to be targeted clinically in order to reduce the severity of BCs overexpressing c-Myc.

IX. Transient and Stable Spy1A Knockdown Reduces Cell Proliferation Rate in F5A1-2 Cells and Partially Restores Ductal Epithelial Branching In vivo.

When targeted with Spy1A RNAi, F5A1-2 cell lines experience a significant reduction in tumor cell proliferation rate, as supported by *in vitro* and *in vivo* evidence. Transient Spy1A knockdown in mid-passage (P31) F5A1-2 cell lines resulted in a ~12% decrease in cell number in response to a single transfection round. Even more prominently, F5A1-2 cells that were subjected to two rounds of transfection experienced a ~50% decrease in overall cell number, thereby implicating Spy1A as a robust tumor promoter, in addition to highlighting its nature as a downstream effector of c-Myc. Moreover, as evidenced by persistent downregulation of c-Myc in response to Spy1A RNAi in early to mid-passage F5A1-2 cell lines, I predict that the mechanism by which c-Myc promotes tumor cell proliferation relies on constitutive activation of Spy1A expression, based on preliminary findings. In support of this notion, immunoblotting data obtained from *in vivo* tumor analysis closely mirrored *in vitro* results, and demonstrated that Spy1A inhibition reduces tumor growth rate, as evidenced by an 11% decline in overall tumor height. Consistent with these data, a decrease in tumor cell proliferation was evident in autopsy photographs taken during early post-surgery time points (Fig.25a). However, the relationship between

Spy1A inhibition and reduced growth rate generally diminished during later time points, and was thought to result from insufficient knockdown in late passage F5A1-2 tumor cells. Further analysis, however, will clarify the role of Spy1A during c-Myc deregulated BC across different cell passages.

Additionally, Golipour and Myers et al. (2008) previously reported that constitutive Spy1A activation in a non-tumorigenic HC11 setting leads to premature epithelial ductal development through enhanced TEB sprouting and elevated ductal side branching, *in vivo*.²² I extrapolate these data by further showing that transplantation of untreated F5A1-2 cells into cleared mammary fat pads appears to decrease the ductal side branch number. Furthermore, the emergence of rudimentary TEB structures in F5A1-2 glands appeared to be less differentiated than the mature ducts observed in the contralateral saline-injected gland (Fig.23a), suggesting that F5A1-2 transplantation may reduce the rate of ductal formation *in vivo*. However, findings are preliminary and should be replicated to confirm whole mount observations. Most intriguing was the ability of Spy1A silencing to increase epithelial ductal morphogenesis *in vivo*, as evidenced by an increase in ductal side branch number when compared to shCntl treated glands (Fig.23b-c, Fig.25e). Hence, based on whole mount observations, I hypothesize that although homeostatic levels of Spy1A may promote normal ductal formation during typical mammary development, the rate of tumor proliferation may be too advanced in F5A1-2 tumors to allow for proper establishment of the mammary ductal tree, as a result of Spy1A and c-Myc co-elevation. Ultimately, it is suggested that inhibition of Spy1A activity in human BCs overexpressing c-Myc may be therapeutically relevant, in that complete Spy1A disruption may lead to irreversible tumor regression and may even increase favourable prognosis when utilized in combination with or supplementary to antiestrogen chemo-preventative agents.

To fully understand the intracellular mechanism governing Spy1A inhibition, I report here the novel design of five shRNA constructs targeted against various regions of the Spy1A transcript. Corresponding protein regions are portrayed in Fig.6, and reveal that constructs three and four fall within the conserved Speedy/RINGO box (amino acids 66-206),¹⁸⁻¹⁹ whereas remaining constructs are positioned external to this region. Whether constructs that correspond to the Speedy/RINGO box yield the uppermost levels of Spy1A knockdown is unknown. Thus, this hypothesis may be tested through transient

transfection of F5A1-2 cell lines with each of the four remaining constructs, followed by quantification of GFP-fluorescence as an approximate measure of shRNA expression. Also, since Spy1A knockdown was derived solely through construct two, prospective experiments will benefit from utilizing all five constructs to highlight the full spectrum of effects that result upon its inhibition, since it has been established that each shRNA construct possesses a differential capacity to effectively attenuate target gene expression for reasons that are not completely understood.¹⁰⁷ Additionally, the utilization of multiple RNAi constructs to validate all outcomes of Spy1A inhibition is typically required to confirm that knockdown effects are not attributed to the vector alone. However, use of a scrambled shRNA construct that does not bind to or recognize the Spy1A transcript serves as an excellent starting point to verify the ability of each Spy1A construct to functionally repress target gene expression. In this way, if RNAi repression results in total cell lethality, other constructs exist to assess the partial inactivation of Spy1A, in order to determine its entire spectrum of effects on mammary development and tumorigenesis. In relation to post-natal mammapoiesis, I postulate that downregulating Spy1A in luminal epithelial mammary tumor cells to basal levels observed in mammary development may restore the underlying TEB developmental program that has been initially subjected to deregulation by induction of c-Myc overexpression under the MMTV-promoter.

X. Caveats Associated with Mammary Fat Pad Transplantation, Whole Mount Analysis, and Utilization of pLB to Knockdown Spy1A In vivo.

Although pLB has been documented previously to effectively silence target gene expression in diabetic mouse models under mouse U6 promoter control, pLB does not harbour a mammalian selection marker. Instead, pLB has been engineered to express GFP under control of the mammalian CMV promoter, to produce green fluorescence upon successful shRNA expression.¹⁰⁸ One method to circumvent the issues observed when co-transplanting shCntl and shSpy1A treated F5A1-2 cells within the same organism, is to replace the GFP gene – located within the control shRNA pLB vector – with another fluorescent gene such as YFP. In this way, it can be determined whether Spy1A shRNA treated F5A1-2 cells do in fact produce more invasion into the contralateral gland upon transplantation into cleared fat pads. Also, the implementation of different fluorescence

markers may be utilized to confirm that Spy1A knockdown is in actuality reducing tumor growth rate *in vivo*. Although late passage stable F5A1-2 cell lines provide us with some insight into the signaling changes invoked by Spy1A attenuation, lentiviral infection of early passage F5A1-2 cell lines (P3) with control or Spy1A shRNA constructs should be conducted. Subsequent transplantation into cleared mammary glands should also be repeated with these new stable cell lines to determine the outcome(s) of Spy1A inhibition during the earliest stages of c-Myc induced tumorigenesis. Furthermore, development of a Spy1A knockout mouse model will provide several advantages over utilizing lentiviral transduction in order to study the effects of complete Spy1A abrogation on pre-natal and post-natal mammary development, morphogenesis, and lactation. On a concluding note, carmine alum staining produces clearer visualization of epithelial ductal side branches in comparison to haematoxylin staining, as evidenced by virtually no background staining in carmine treated whole mounts depicted by Golipour and Myers et al. (2008).²² In stark contrast, whole mount glands stained with haematoxylin (Fig.23) exhibited high levels of pink background, thereby impeding proper analysis of epithelial ductal branching. Hence, it is recommended that future studies utilize carmine alum staining to assess phenotypic changes in mammary ductal morphogenesis.

XI. Assessing the Role of Spy1A in Initiating Mammary Tumor Formation is Now Feasible Due to Creation of the First MMTV-Spy1A Transgenic Murine Model.

Golipour and Myers et al. (2008) previously reported that Spy1A displays intrinsic tumor promoting activity and is able to enhance mammary tumor formation upon stable adenoviral-induced overexpression in transplanted syngeneic HC11 cell lines.²² However, whether Spy1A can actively induce tumorigenesis has not been ascertained.²² Therefore, to elucidate the role of Spy1A in tumor initiation and mammary gland development, I derived the first transgenic FVB mouse model engineered to overexpress Spy1A under control of the MMTV promoter. Chosen for its success in previous publications, the MMTV promoter has been demonstrated to specifically target transgene expression to the mammary epithelium of glands, rather than to surrounding stromal layers.^{46,48,109} The MMTV-SV40-Spy1A transgene comprises the following components in the following order: (a) MMTV-LTR promoter/enhancer, (b) c-Ha-ras 5' UTR, (c) Spy1A cDNA

sequence excised from the Spy1A-flag-pLXSN vector, as previously described in the *Materials and Methods* section of this thesis, and (d) SV40 small-t intron and poly(A) tail sequences. It is important to note that the SV40 small-t intron was previously integrated into the vector backbone due to its enhancement of transgene expression *in vivo*.¹¹⁰ Five rounds of pronuclear injection of the MMTV-SV40-Spy1A transgene have already been conducted, resulting in production of two litters, thus far. Tail clips will be excised on December 14th and 21st of the calendar year, and will further require genotypic analysis to identify MMTV-Spy1A transgenic organisms.¹¹¹ In this way, the effects of constitutively active Spy1A expression on early placode formation and mammary ductal morphogenesis may be elucidated.

XIII. Concluding Remarks and Future Directions.

Despite recognizing the importance of Spy1A signaling for c-Myc induced mammary tumorigenesis, numerous questions remain unanswered. Confirmation of Spy1A mRNA silencing in F5A1-2 cell lines may determine whether Spy1A mediates c-Myc expression on a transcriptional level, and will reveal the degree to which Spy1A is transcriptionally silenced. Thus, it is recommended that future mRNA studies be conducted by utilizing a quantitative real time PCR approach. Moreover, since it has been suggested that Spy1A, c-Myc, MAPK, p27, and p21 protein levels fluctuate between different cell passages, it will be important to determine the signaling signatures for each of these factors across P3, P31, and P60 passages of F5A1-2 cell lines. Likewise, assessing the status of ER α across cell passage will assist in determining whether F5A1-2 cells initially probe positive for ER α , but may lose expression as a result of tamoxifen resistance. Hence, F5A1-2 may represent a novel tamoxifen resistant cell model that constitutively overexpresses c-Myc. Consequently, if cells are shown to be unresponsive to tamoxifen treatment, this outcome may further imply acquisition of an antiestrogen resistance phenotype due to deregulated c-Myc expression. Instead, if F5A1-2 cells are characterized as ER α -negative and do not respond to tamoxifen, they may exhibit *de novo*/intrinsic drug resistance.

Protein localization may also be utilized to establish the tissue and cellular distribution of ER α , Spy1A, c-Myc, MAPK, p27, and p21, and may clarify their function during c-

Myc induced tumorigenesis when examined in F5A1-2 cell lines differentially treated in the following manner: (a) control or Spy1A RNAi, (b) c-Myc knockdown via transfection of dominant negative Myc constructs or c-Myc short interfering RNA, and (c) MAPK inactivation utilizing U0126 and PD098059 inhibitors. Additionally, localization studies may be expanded to other cell culture models (HC11, MCF7, LCC9). Furthermore, the putative promoter of Spy1A has been predicted to contain ER α (-900) and c-Myc (-880) response elements adjacent to one another, suggesting that both transcription factors may function to transcriptionally regulate Spy1A. Therefore, chromatin immunoprecipitation analysis may be utilized to determine the importance of ER α and c-Myc for stimulating Spy1A at the mRNA level. On a final note, resolving the role of Spy1A during tamoxifen resistance, through comparative analysis of wild-type MCF7 and LCC9 cell lines may determine whether Spy1A can be identified as a clinically relevant target for aggressive human BC forms, with particular focus on relapsing ER α -positive mammary neoplasias classified under antiestrogen resistance.

References

- (1) Canadian Cancer Society's Steering Committee: Canadian Cancer Statistics 2009. Toronto: Canadian Cancer Society 2009.
- (2) Shackleton, M. et al. (2006) Generation of a functional mammary gland from a single stem cell. *Nature*, 439: 84-88.
- (3) Sørliea, T et al. (2001) Gene expression patterns of breast carcinomas distinguish tumor subclasses with clinical implications. *Proceedings of the National Academy of Sciences U.S.A.*, 98: 10869-10874.
- (4) Blakely, C.M. et al. (2004) Developmental stage determines the effects of MYC in the mammary epithelium. *Development*, 132: 1147-1160.
- (5) McManaman, J.L., et al. (2006) Secretion and fluid transport mechanisms in the mammary gland: Comparisons with the exocrine pancreas and the salivary gland. *Journal of Mammary Gland Biology and Neoplasia*, 11: 249-268.
- (6) Hennighausen, L. and G.W. Robinson. (2005) Information networks in the mammary gland. *Nature Reviews Molecular Cell Biology*, 6: 715-25.
- (7) Kass, L. et al. (2007) Mammary epithelial cell: Influence of extracellular matrix composition and organization during development and tumorigenesis. *The International Journal of Biochemistry and Cell Biology*, 39: 1987-1994.
- (8) Fata, J.E., et al. (2000) The Osteoclast Differentiation Factor Osteoprotegerin-Ligand Is Essential for Mammary Gland Development. *Cell*, 103: 41-50.
- (9) Veltmaat, J.M., et al. (2003) Mouse embryonic mammaryogenesis as a model for the molecular regulation of pattern formation. *Differentiation*, 71: 1-17.
- (10) V. Horsley. (2009) Epigenetics, Wnt signaling, and stem cells: the Pygo2 connection. *The Journal of Cell Biology*, 185: 761-763.
- (11) Wiesen, J.F., et al. (1999) Signaling through the stromal epidermal growth factor receptor is necessary for mammary ductal development. *Development*, 126: 335-344.
- (12) Morani, A. et al. (2008) Biological functions and clinical implications of oestrogen receptors alpha and beta in epithelial tissues. *Journal of Internal Medicine*, 264: 128-142.
- (13) Prossnitz, E.R. and M. Maggiolini. (2009) Mechanisms of estrogen signaling and gene expression via GPR30. *Molecular and Cellular Endocrinology*, 308: 32-38.
- (14) Deroo, B.J. et al. (2009) Profile of Estrogen-Responsive Genes in an Estrogen-Specific Mammary Gland Outgrowth Model. *Molecular Reproduction and Development*,

76:733–750.

(15) Todorović-Raković, N. et al. (2006) Cross-talk between ER and HER2 in breast carcinoma. *Archive of Oncology*, 14: 146-150.

(16) Watson, C.J. and W.T. Khaled. (2008) Mammary development in the embryo and adult: a journey of morphogenesis and commitment. *Development*, 135: 995-1003.

(17) Gouon-Evans, V. et al. (2000) Postnatal mammary gland development requires macrophages and eosinophils. *Development*, 127: 2269-2282.

(18) Cheng, A., et al. (2005) Identification and Comparative Analysis of Multiple Mammalian Speedy/Ringo Proteins. *Cell Cycle*, 4: 155-65.

(19) Nebrada, A.R. (2006) CDK activation by non-cyclin proteins. *Current Opinion in Cell Biology*, 18: 192-198.

(20) Andrechek, E.R., et al. (2008) Patterns of cell signaling pathway activation that characterize mammary development. *Development*, 135: 2403-2413.

(21) Klein, E.A. et al. (2008) Joint requirement for Rac and ERK activities underlies the mid-G1 phase induction of cyclin D1 and S phase entry in both epithelial and mesenchymal cells. *The Journal of Biological Chemistry*, 283: 30911-30918.

(22) Golipour, A. and Myers, D. et al. (2008) The Spy1/RINGO Family Represents a Novel Mechanism Regulating Mammary Growth and Tumorigenesis. *Cancer Research*, 68: 3591-3600.

(23) Zhang, X. et al. (2005) Estrogen receptor positivity in mammary tumors of Wnt-1 transgenic mice is influenced by collaborating oncogenic mutations. *Oncogene*, 24: 4220-31.

(24) Rayala, S.K. and R. Kumar. (2007) Sliding p21-activated kinase 1 to nucleus impacts tamoxifen sensitivity. *Biomedicine and Pharmacotherapy*, 61: 408-411.

(25) Berstein, L.M. (2003) New approaches to the understanding of tamoxifen action and resistance. *Endocrine-Related Cancer*, 10: 267-277.

(26) Pontiggia, O. et al. (2009) Establishment of an in vitro estrogen-dependent mouse mammary tumor model: a new tool to understand estrogen responsiveness and development of tamoxifen resistance in the context of stromal–epithelial interactions. *Breast Cancer Research and Treatment*, 116: 247–255.

(27) Butt, A.J. et al. (2005) Downstream targets of growth factor and oestrogen signalling and endocrine resistance: the potential roles of c-Myc, cyclin D1 and cyclin E. *Endocrine-Related Cancer*, 12: S47-S59.

- (28) Mukherjee, S. and S.E. Conrad. (2005) c-Myc Suppresses p21^{WAF1/CIP1} Expression during Estrogen Signaling and Antiestrogen Resistance in Human Breast Cancer Cells. *The Journal of Biological Chemistry*, 280: 17617–17625.
- (29) Nishimoto, S. and E. Nishida. (2006) MAPK signalling: ERK5 versus ERK1/2. *EMBO Reports*, 7: 782-786.
- (30) Seger, R. and E.G. Krebs. (1995) The MAPK signaling cascade. *The FASEB Journal*, 9: 726-735.
- (31) Huber, M.A. et al. (2004) NF- κ B is essential for epithelial-mesenchymal transition and metastasis in a model of breast cancer progression. *The Journal of Clinical Investigation*, 114: 569-581.
- (32) Yuan, Y. et al. (2007) Genetic Screening Reveals an Essential Role of p27kip1 in Restriction of Breast Cancer Progression. *Cancer Research*, 67: 8032-8042.
- (33) Swanton, C. and J. Downward. (2008) Unraveling the Complexity of Endocrine Resistance in Breast Cancer by Functional Genomics. *Cancer Cell*, 13: 83-85.
- (34) Vaqué, J.P et al. (2005) Myc antagonises Ras-mediated growth arrest in leukemia cells through the inhibition of the Ras-ERK-p21^{Cip1} pathway. *The Journal of Biological Chemistry*, 280: 1112-1122.
- (35) Dougherty, M.K. et al. (2005) Regulation of Raf-1 by direct feedback phosphorylation. *Molecular Cell*, 17: 215-224.
- (36) Fukunaga, R. and T. Hunter. (1997) MNK1, a new MAP kinase-activated protein kinase, isolated by a novel expression screening method for identifying protein kinase substrates. *The EMBO Journal*, 16: 1921–1933.
- (37) Jin, Z. et al. (2004) Tobacco-specific nitrosamine 4-(methylnitrosamino)-1-(3-pyridyl)-1-butanone promotes functional cooperation of Bcl2 and c-Myc through phosphorylation in regulating cell survival and proliferation. *The Journal of Biological Chemistry*, 279: 40209-40219.
- (38) Chuang, C. and S. Ng. (1994) Functional divergence of the MAP kinase pathway: ERK1 and ERK2 activate specific transcription factors. *FEBS Letters*, 346(2-3): 229-234.
- (39) Gupta, S. and R.J. Davis. (1994) MAP kinase binds to the NH₂-terminal activation domain of c-Myc. *FEBS Letters*, 353: 281 -285.
- (40) Wang, Z. et al. (2006) Phosphorylation regulates Myc expression via prolonged activation of the mitogen-activated protein kinase pathway. *Journal of Cellular Physiology*, 208: 133-140.

- ⁽⁴¹⁾ Knoepfler, P.S. (2007) Myc Goes Global: New Tricks for an Old Oncogene. *Cancer Research*, 67: 5061-5063.
- ⁽⁴²⁾ Stone, J. et al. (1987) Definition of Regions in Human *c-myc* That Are Involved in Transformation and Nuclear Localization. *Molecular and Cellular Biology*, 7: 1697-1709.
- ⁽⁴³⁾ Boxer, L.M. and C.V. Dang. (2001) Translocations involving *c-myc* and *c-myc* function. *Oncogene*, 20: 5595-5610.
- ⁽⁴⁴⁾ Monick, M.M. et al. (1992) The immediate early genes of human cytomegalovirus upregulate expression of the cellular genes *myc* and *fos*. *American Journal of Respiratory Cell and Molecular Biology*, 7: 251-256.
- ⁽⁴⁵⁾ Zeller, K.I. et al. (2003) An integrated database of genes responsive to the Myc oncogenic transcription factor: identification of direct genomic targets. *Genome Biology*, 4: R69.
- ⁽⁴⁶⁾ Jamerson, M.H. et al. (2003) Early parity significantly elevates mammary tumor incidence in MMTV-*c-myc* transgenic mice. *Transgenic Research*, 12: 747-750.
- ⁽⁴⁷⁾ Jamerson, M.H. et al. (2004) Of mice and Myc: *c-Myc* and mammary tumorigenesis. *Journal of Mammary Gland Biology and Neoplasia*, 9: 27-37.
- ⁽⁴⁸⁾ Sinn, E. et al. (1987) Coexpression of MMTV/*v-Ha-ras* and MMTV/*c-myc* genes in transgenic mice: synergistic action of oncogenes in vivo. *Cell*, 49: 465-75.
- ⁽⁴⁹⁾ Porter, L.A. et al. (2002) Human Speedy: a novel cell cycle regulator that enhances proliferation through activation of Cdk2. *The Journal of Cell Biology*, 157: 357-366.
- ⁽⁵⁰⁾ Gastwirt, R.F. et al. (2007) Speedy/RINGO regulation of CDKs in Cell Cycle, Checkpoint Activation and Apoptosis. *Cell Cycle*, 6: 1188-1193.
- ⁽⁵¹⁾ Park, M-T. and S-J. Lee. (2003) Cell Cycle and Cancer. *Journal of Biochemistry and Molecular Biology*, 36: 60-65.
- ⁽⁵²⁾ Thornton, T.M. and M. Rincon. (2009) Non-classical P38 MAPK Functions: Cell Cycle Checkpoints and Survival. *International Journal of Biological Sciences*, 5: 44-51.
- ⁽⁵³⁾ Porter, L.A. et al. (2003) Spyl Interacts with p27^{Kip1} to Allow G₁/S Progression. *Molecular Biology of the Cell*, 14: 3664-3674.
- ⁽⁵⁴⁾ Aguda, B.D. and Y. Tang. (1999) The kinetic origins of the restriction point in the mammalian cell cycle. *Cell Proliferation*, 32: 321-35.
- ⁽⁵⁵⁾ Novák, B. and J.J. Tyson. (2004) A model for restriction point control of the mammalian cell cycle. *Journal of Theoretical Biology*, 230: 563-579.

- ⁽⁵⁶⁾ Löbrich, M. and P.A. Jeggo. (2007) The impact of a negligent G2/M checkpoint on genomic instability and cancer induction. *Nature Reviews Cancer*, 7: 861-869.
- ⁽⁵⁷⁾ Gutierrez, G.J. et al. (2006) Meiotic regulation of the CDK activator RINGO/Speedy by ubiquitin-proteasome-mediated processing and degradation. *Nature Cell Biology*, 8: 1084-94.
- ⁽⁵⁸⁾ Gastwirt, R.F., et al. (2006) Spy1 Expression Prevents Normal Cellular Responses to DNA Damage: Inhibition of Apoptosis and Checkpoint Activation. *The Journal of Biological Chemistry*, 281: 35425-35435.
- ⁽⁵⁹⁾ Cheng, A. et al. (2005) Biochemical characterization of Cdk2-Speedy/Ringo A2. *BMC Biochemistry*, 6:19.
- ⁽⁶⁰⁾ McAndrew, C.W. et al. (2007) Spy1 Enhances Phosphorylation and Degradation of the Cell Cycle Inhibitor p27. *Cell Cycle*, 6: 1937-1945.
- ⁽⁶¹⁾ Zhang, Z. and M. Gerstein. (2003) Of mice and men: Phylogenetic footprinting aids the discovery of regulatory elements. *Journal of Biology*, 2(2): II.1-II.4.
- ⁽⁶²⁾ Ohler, U. and H. Niemann. (2001) Identification and analysis of eukaryotic promoters: recent computational approaches. *Trends in Genetics*, 17: 56-60.
- ⁽⁶³⁾ R.M. Cranenburgh. (2004) An equation for calculating the volumetric ratios required in a ligation reaction. *Applied Microbiology and Biotechnology*, 65: 200-202.
- ⁽⁶⁴⁾ Florea, B.I. et al. (2002) Transfection Efficiency and Toxicity of Polyethylenimine in Differentiated Calu-3 and Nondifferentiated COS-1 Cell Cultures. *AAPS PharmSci*, 4: article 12.
- ⁽⁶⁵⁾ Welm, B.E., et al. (2008) Lentiviral Transduction of Mammary Stem Cells for Analysis of Gene Function during Development and Cancer. *Cell Stem Cell*, 2: 90-102.
- ⁽⁶⁶⁾ Moorehead, R.A. et al. (2001) Inhibition of mammary epithelial apoptosis and sustained phosphorylation of Akt/PKB in MMTV-IGF-II transgenic mice. *Cell Death and Differentiation*, 8: 16-29.
- ⁽⁶⁷⁾ Wang, S. et al. (2009) Disruption of the SRC-1 gene in mice suppresses breast cancer metastasis without affecting primary tumor formation. *Proceedings of the National Academy of Sciences U.S.A.*, 106: 151-156.
- ⁽⁶⁸⁾ Andrecheka, E.R. et al. (2009) Genetic heterogeneity of Myc-induced mammary tumors reflecting diverse phenotypes including metastatic potential. *Proceedings of the National Academy of Sciences U.S.A.*, 106: 16387-16392.
- ⁽⁶⁹⁾ Leder, P. (2009, December). *Available Strain Details: 01XG2* . Retrieved 2007-2009,

from Mouse Repository: Mouse Models of Human Cancers Consortium:
http://mouse.ncifcrf.gov/available_details.asp?ID=01XG2

- ⁽⁷⁰⁾ Dontu, G. et al. (2004) Role of Notch signaling in cell-fate determination of human mammary stem/progenitor cells. *Breast Cancer Research*, 6: R605-R615.
- ⁽⁷¹⁾ Heldring, N. et al. (2007) Estrogen Receptors: How Do They Signal and What Are Their Targets. *Physiological Reviews*, 87: 905-931.
- ⁽⁷²⁾ Lenormand, J.-L. et al. (1999) Speedy: A novel cell cycle regulator of the G2/M transition. *The EMBO Journal*, 18: 1869-1877.
- ⁽⁷³⁾ Lobenhofer, E.K. et al. (2000) Inhibition of Mitogen-activated Protein Kinase and Phosphatidylinositol 3-Kinase Activity in MCF-7 Cells Prevents Estrogen-induced Mitogenesis. *Cell Growth and Differentiation*, 11: 99-110.
- ⁽⁷⁴⁾ Chammas, R. et al. (1994) Laminin and tenascin assembly and expression regulate HC11 mouse mammary cell differentiation. *Journal of Cell Science*, 107: 1031-1040.
- ⁽⁷⁵⁾ Merlo, G.R. et al. (1995) p53-dependent and p53-independent activation of apoptosis in mammary epithelial cells reveals a survival function of EGF and insulin. *The Journal of Cell Biology*, 128: 1185-1196.
- ⁽⁷⁶⁾ Kircheis, R. et al. (2001) Design and gene delivery activity of modified polyethylenimines. *Advanced Drug Delivery Reviews*, 53: 341-358.
- ⁽⁷⁷⁾ Brunner, S. et al. (2000) Cell cycle dependence of gene transfer by lipoplex, polyplex and recombinant adenovirus. *Gene Therapy*, 7: 401-407.
- ⁽⁷⁸⁾ Grimm, S. (2004) The art and design of genetic screens: Mammalian culture cells. *Nature Reviews Genetics*, 5: 179-189.
- ⁽⁷⁹⁾ Zucchi, I., et al. (2004) Gene expression profiles of epithelial cells microscopically isolated from a breast-invasive ductal carcinoma and a nodal metastasis. *Proceedings of the National Academy of Sciences U.S.A.*, 101: 18147-18152.
- ⁽⁸⁰⁾ Pavelic, Z.P. et al. (1992) c-myc, c-erbB-2, and Ki-67 Expression in Normal Breast Tissue and in Invasive and Noninvasive Breast Carcinoma. *Cancer Research*, 52: 2597-2602.
- ⁽⁸¹⁾ Al Sorkhy, M. et al. (2009) The Cyclin-dependent Kinase Activator, Spy1A, Is Targeted for Degradation by the Ubiquitin Ligase NEDD4. *The Journal of Biological Chemistry*, 284: 2617-2627.
- ⁽⁸²⁾ Sgambato, A. et al. (1997) Deregulated expression of p27^{Kip1} in human breast cancers. *Clinical Cancer Research*, 3: 1879-1887.

- ⁽⁸³⁾ Cheng, M. et al. (1999) The p21^{Cip1} and p27^{Kip1} CDK ‘inhibitors’ are essential activators of cyclin D-dependent kinases in murine fibroblasts. *The EMBO Journal*, 18: 1571–1583.
- ⁽⁸⁴⁾ Rodier, G. et al. (2001) p27 cytoplasmic localization is regulated by phosphorylation on Ser10 and is not a prerequisite of its proteolysis. *The EMBO Journal*, 20: 6672-6682.
- ⁽⁸⁵⁾ Abukhdeir, A.M. and B.H. Park (2008) p21 and p27: roles in carcinogenesis and drug resistance. *Expert Reviews in Molecular Medicine*, 10: e19.
- ⁽⁸⁶⁾ Vlach, J. et al. (1997) Phosphorylation-dependent degradation of the cyclin-dependent kinase inhibitor p27. *The EMBO Journal*, 16: 5334–5344.
- ⁽⁸⁷⁾ Carrano, A.C. et al. (1999) SKP2 is required for ubiquitin-mediated degradation of the CDK inhibitor p27. *Nature Cell Biology*, 1: 193-199.
- ⁽⁸⁸⁾ Chu, I. et al. (2007) p27 Phosphorylation by Src Regulates Inhibition of Cyclin E-Cdk2. *Cell*, 128: 281-294.
- ⁽⁸⁹⁾ Tomoda, K. et al. (2002) The Cytoplasmic Shuttling and Subsequent Degradation of p27^{Kip1} Mediated by Jab1/CSN5 and the COP9 Signalosome Complex. *The Journal of Biological Chemistry*, 277: 2302–2310.
- ⁽⁹⁰⁾ Connor, M.K. et al. (2003) CRM1/Ran-mediated nuclear export of p27^(Kip1) involves a nuclear export signal and links p27 to export and proteolysis. *Molecular Biology of the Cell*, 14: 201-213.
- ⁽⁹¹⁾ Coqueret, O. (2003) New roles for p21 and p27 cell-cycle inhibitors: a function for each cell compartment? *Trends in Cell Biology*, 13: 65-70.
- ⁽⁹²⁾ Moeller, S.J. et al. (2003) p27^{Kip1} inhibition of GRB2-SOS formation can regulate Ras activation. *Molecular and Cellular Biology*, 23: 3735-3752.
- ⁽⁹³⁾ McAllister, S.S. et al. (2003) Novel p27^(kip1) C-terminal scatter domain mediates Rac-dependent cell migration independent of cell cycle arrest functions. *Molecular and Cellular Biology*, 23: 216-228.
- ⁽⁹⁴⁾ Sugiyama, Y. et al. (2001) Direct Binding of the Signal-transducing Adaptor Grb2 Facilitates Down-regulation of the Cyclin-dependent Kinase Inhibitor p27^{Kip1}. *The Journal of Biological Chemistry*, 276: 12084–12090.
- ⁽⁹⁵⁾ Donovan, J.C.H. et al. (2001) Constitutive MEK/MAPK Activation Leads to p27^{Kip1} Deregulation and Antiestrogen Resistance in Human Breast Cancer Cells. *The Journal of Biological Chemistry*, 276: 40888-40895.
- ⁽⁹⁶⁾ Dunn, K.L. et al. (2005) The Ras-MAPK signal transduction pathway, cancer and

chromatin remodeling. *Biochemistry and Cell Biology*, 83: 1-14.

⁽⁹⁷⁾ Foster, J.S. et al. (2001) Multifaceted Regulation of Cell Cycle Progression by Estrogen: Regulation of Cdk Inhibitors and Cdc25A Independent of Cyclin D1-Cdk4 Function. *Molecular and Cellular Biology*, 21: 794-810.

⁽⁹⁸⁾ Cariou, S. et al. (2000) Down-regulation of p21^{WAF1/CIP1} or p27^{Kip1} abrogates antiestrogen-mediated cell cycle arrest in human breast cancer cells. *Proceedings of the National Academy of Sciences U.S.A.*, 97: 9042-9046.

⁽⁹⁹⁾ Altundag, K. et al. (2004) Possible interaction between activator protein-1 and proto-oncogene B-cell lymphoma gene 6 in breast cancer patients resistant to tamoxifen. *Medical Hypotheses*, 63: 823-826.

⁽¹⁰⁰⁾ Smith, L.M. (1999) cJun overexpression in MCF-7 breast cancer cells produces a tumorigenic, invasive and hormone resistant phenotype. *Oncogene*, 18: 6063-6070.

⁽¹⁰¹⁾ Johnston, S.R.D. et al. (1999) Increased activator protein-1 DNA binding and c-Jun NH2-terminal kinase activity in human breast tumors with acquired tamoxifen resistance. *Clinical Cancer Research*, 5: 251-256.

⁽¹⁰²⁾ Vincent-Salomon, A. and J.P. Thiery. (2003) Host microenvironment in breast cancer development: Epithelial–mesenchymal transition in breast cancer development. *Breast Cancer Research*, 5: 101-106.

⁽¹⁰³⁾ Cowling, V.H. and M.D. Cole. (2007) E-cadherin repression contributes to c-Myc-induced epithelial cell transformation. *Oncogene*, 26: 3582-3586.

⁽¹⁰⁴⁾ Wang, X. et al. (2007) Krüppel-Like Factor 8 Induces Epithelial to Mesenchymal Transition and Epithelial Cell Invasion. *Cancer Research*, 67: 7184–7193.

⁽¹⁰⁵⁾ Yang, J. et al. (2004) Twist, a Master Regulator of Morphogenesis, Plays an Essential Role in Tumor Metastasis. *Cell*, 117: 927-939.

⁽¹⁰⁶⁾ Péchoux, C. et al. (1999) Human Mammary Luminal Epithelial Cells Contain Progenitors to Myoepithelial Cells. *Developmental Biology*, 206: 88–99.

⁽¹⁰⁷⁾ Paddison, P.J. et al. (2002) Short hairpin RNAs (shRNAs) induce sequence-specific silencing in mammalian cells. *Genes and Development*, 16: 948-958.

⁽¹⁰⁸⁾ Kissler, S. et al. (2006) *In vivo* RNA interference demonstrates a role for Nramp1 in modifying susceptibility to type 1 diabetes. *Nature Genetics*, 38: 479-483.

⁽¹⁰⁹⁾ Guy, C.T. et al. (1992) Expression of the neu protooncogene in the mammary epithelium of transgenic mice induces metastatic disease. *Proceedings of the National Academy of Sciences U.S.A.*, 89: 10578-10582.

⁽¹¹⁰⁾ DiMattia, G. E. (2009, March 11). Re: MMTV questions. (L. A. Porter, Email Communication).

⁽¹¹¹⁾ Drysdale, L.E. ES Cell Technician, London Regional Transgenic and Gene Targeting Facility. (2009, November 26). Transgenic update. (L. A. Porter, Email Communication)

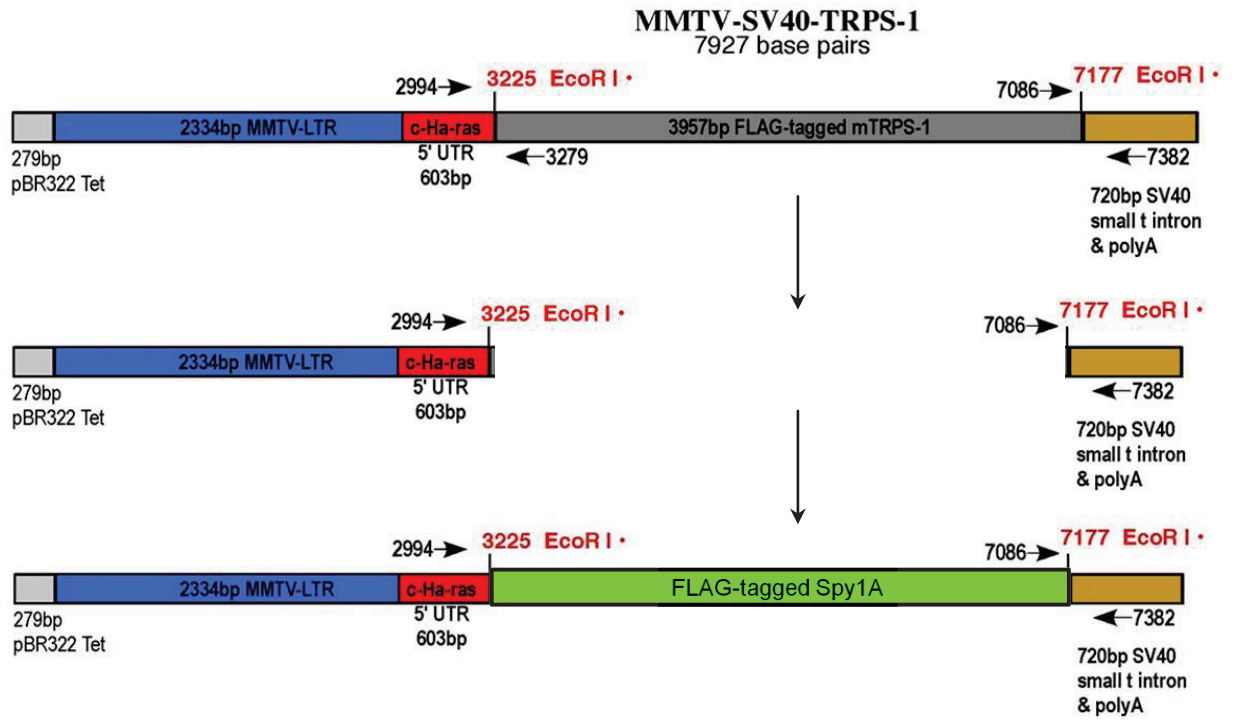
⁽¹¹²⁾ Yu, M. et al. (2009) A developmentally regulated inducer of EMT, LBX1, contributes to breast cancer progression. *Genes and Development*, 23: 1737-1742.

Appendix

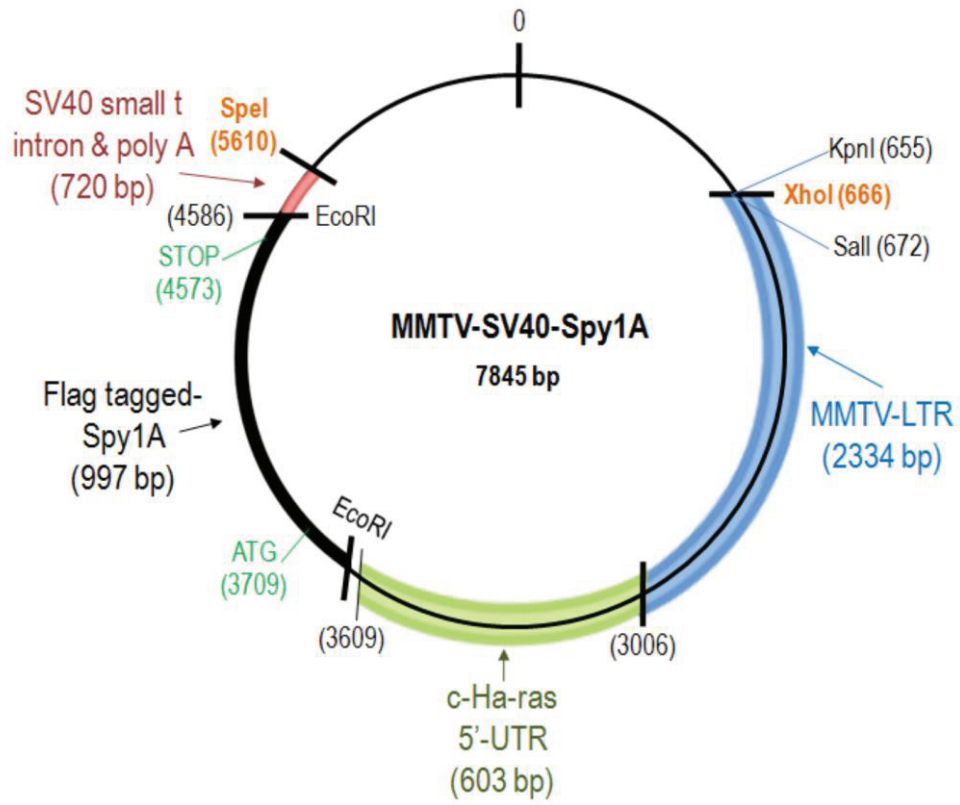
Appendix Table of Contents

<i>Diagrammatical Representation of the Cloning Strategy for the MMTV-SV40-Spy1A Transgenic Vector</i>	124
<i>Vector Map for MMTV-SV40-Spy1A</i>	125
<i>Anaesthetizing a Mouse</i>	126
<i>Mammary Fat Pad Transplantation</i>	127
<i>Mammary Gland Whole Mount Protocol</i>	129
<i>Overview of Lentiviral Production – PEI-Mediated Protocol</i>	131
<i>Lentivirus: Titering Your Lentiviral Stocks</i>	133
<i>Lentiviral Transduction</i>	135
A. Preparation.....	135
B. Methods.....	135
C. Additional Notes.....	137
D. Solutions.....	138
<i>Appendix References</i>	139

Diagrammatical Representation of the Cloning Strategy for the MMTV-SV40-Spy1A Transgenic Vector



Vector Map for MMTV-SV40-Spy1A



Anaesthetizing a Mouse

(Protocol obtained and adapted from L.A. Porter)

Note: A mouse should not be under for more than 20 minutes; after this time, it becomes more difficult to bring them back.

- fill up isoflurane machinery
- open oxygen tank
- turn on isoflurane machinery
 - move nozzle until the red bulb sits at level "3"
- check hoses and make sure they connect from the oxygen input to the isoflurane
- place mouse in anaesthetizing chamber
 - make sure gas hose is connected to the chamber
- turn on isoflurane to level 0.5 for 30 seconds.
 - slowly increase in increments of 0.5 until you reach 2.5
- when mouse is fully under, perform the following steps:
 - remove mouse from chamber and put on the mouthpiece
 - switch the isoflurane hose from the chamber to the mouthpiece, also
- give mouse eye drops to prevent drying out during surgery
- when surgery is complete:
 - remove mouse from mouthpiece and return to chamber
 - switch hoses from mouthpiece back to chamber
 - turn isoflurane from 2.5 to 0 and switch hoses so they bypass the isoflurane

Mammary Fat Pad Transplantation
(Protocol obtained and adapted from L.A. Porter)

1) Cells:

- cells form tumours within 3 weeks
- to prepare cells:
 - wash with 1X PBS
 - trypsinize
 - resuspend in 1X PBS ~ 5ml
 - count (inject 500 000 to 1 million cells/10 μ l)
 - spin 1250xg for 2-5min at 4°C
 - resuspend in appropriate amount of 1X PBS
 - 10 μ l per gland
 - 2 glands per mouse
 - + extra 10 μ l
 - keep cells on ice, bring to surgery room
- cells should be proliferating, not confluent

2) Mice:

- retrieve mice from holding room; bring 2 cages for (1) holding and (2) recovery
- place recovery cage on heating pad, and arrange the following items nearby:
 - surgical drapes
 - forceps (curved and straight)
 - scissors
 - syringe (25mL-Hamilton Cat. No. 1481318 and 1mL)
 - back-up syringe
 - stapler
 - 70% EtOH
 - gauze
 - eye drops (human eye drops work fine = "gel" kind is best)
 - kimwipes
- female mice can be kept 8/cage
- male mice: 2/cage is best, 3/cage usually causes fights
- keep males separate from females
- we inject 4th pair of mammary glands
- puberty starts in mice at ~ 4 weeks, so we want to clear the fat pad before then
- pups are weaned at 21 days
- fat pad clearing and injections are best performed at 21-24 days (up to 28 days)

3) Injections

- place warming pad (already heated via microwaving) on surgical table; place surgical drape over warming pad

To put mice under:

- mouse should not be under for more than 20 min - after this time it may become more difficult to bring the animal back
- 1 min O₂
- isoflurane gas utilized as the anaesthetic of choice: flow rate established at 0.5 intervals for 30 seconds; increase 0.5 intervals every 20 seconds up to marking 2.5
- move back down to 2.25 for surgery

Injection:

- when mouse is fully anaesthetized, move animal from cone to mouthpiece
- inject 100 µL pain medication (buprenorphine-0.1 mg/mL) with 1mL needle, 253/8 guage, under skin on back
- give mouse eye drops (prevents drying out during surgery)
- turn mouse over and wash abdomen with 70% EtOH
- using forceps to pinch skin, make a vertical incision (should be less than 0.5 cm long)
- pull back the skin on one side, using thumb to keep abdominal cavity in place
 - may need to use forceps to pull abdominal cavity away from skin to expose mammary gland
- cut mammary gland horizontally under lymph node
- use curved forceps to pull out bottom half of the fourth mammary gland
- inject 10 µl of previously prepared cells into fat pad above lymph node
 - use 25 mL 263/8 gauge needle (30 is too small)
 - insert needle; pull up, slowly inject cells, while ensuring that no liquid leaks out, and remove needle gently
- use forceps to pull skin back
- staple by holding skin together with forceps (should require at least 3 staples)

To bring mice back:

- remove mouthpiece, and put mouse back under cone (be careful not to clip the tail!)
- decrease anaesthetic every minute by 0.5 intervals
- keep mouse under 100% O₂ until awake (may need to be nudged to wake up)
- put mouse into recovery cage
 - keep something in recovery cage for mouse to hide under (i.e., egg carton, paper towel)

Recovery:

- no solid foods recommended on the day of surgery (Rob gives solid food anyway)
 - can make a paste with mouse food and water to feed to them
- no pain medication given after surgery
- check mice a few hours after surgery to be sure wound has been closed completely
- check mice again 24 h later
 - look for holes, blood in cage, signs of illness, etc.
- tumors may appear 7-21 days later, depending on cell type and concentration used

Mammary Gland Whole Mount Protocol

(Protocol obtained and adapted from J. Rosen)¹

⁽¹⁾ Rosen, J. (2005, August 30). *Mammary Gland Whole Mount Protocol*. Retrieved 2009, from Rosen Lab Website: <http://www.bcm.edu.rosenlab>

1. (a) *Optional*: Inject animals with BrdU 2 hours harvesting tissue
(b) Fix tissue for 2 hours in fresh, cold 4% paramormaldehyde on ice.
2. Rinse tissue in 70% ethanol until ready to stain (up to 2 weeks).

All of the following steps are conducted by submerging tissue-cassettes containing glands into the solution. Thus, many glands can be processed in one jar at once.

Defat

Acetone 3 x 30 min

Note: This prohibits later immunohistochemical analysis by creating high background. If you want to try to do immunohistochemical on these glands, skip this step (or use the carmine alum protocol instead).

Rehydrate

100% EtOH 1 x 30 min
95% EtOH 1 x 30 min

Stain

Haematoxylin stain:

0.13 g FeCl₃•6H₂O

13.5 ml distilled water

Dissolve, and add 1.74 mL stock (10%) Harris hematoxylin

Add 200 ml 95% ethanol

Adjust pH to 1.25 with concentrated (12N) HCl (pH is critical)

Note: Make stain fresh each time, and check that stain turns blue by putting tiny amount in a weigh boat and running under crude tap water. Stain should turn bright light blue. If not, throw out and try again.

Place glands in haematoxylin stain for 1.5 hours until whole gland looks purple. If you did not defat in acetone (for future immunohistochemistry), stain overnight to allow haematoxylin to permeate through fat. Monitor stain by holding gland to the light.

Rinse in Crude tap H₂O until water is clear.

Destain

Acid ethanol 2 x 30 min
(200 ml 50% EtOH + 416 ul 12N HCl)

Note: Monitor destaining by holding gland up to the light. You should be able to clearly see blue epithelium with a fairly clear background.

Dehydrate

70% EtOH 2 x 30 min
95% EtOH 2 x 30 min
100% EtOH 2 x 30 min

Complete dehydration of glands is critical for complete clearing.
Incomplete dehydration will result in brown background in the fat.
Use fresh 95% and 100% EtOH and do not take shortcuts.

Clear

Xylene 2 x 1 hour (or can go overnight)

Note: An alternate method of clearing the glands is to use BABB for 1-2 hours

BA = benzylalcohol

BB = benzylbenzoate

Mix chemicals in a 1:2 ratio (BA:BB)

Note: leaving glands in BABB for extended time periods results in the lightening of the haematoxylin stain.

For imaging, remove gland from tissue-cassette and press between two glass slides and flatten. Secure with mini binder clips and view under a dissecting microscope.

For long-term storage, transfer to methyl salicylate in glass scintillation vials and KEEP DARK. (If exposed to light, the blue will fade to brown)

Stock Haematoxylin (10%)

- Harris haematoxylin (Fisher, powder)

- Add 10g of powder to 100 ml of 95% ethanol, leave overnight stirring and it will go into solution. Keep covered in foil. Let sit at least 3 weeks to 1 month for best stain.

Overview of Lentiviral Production – PEI-Mediated Protocol


(Protocol obtained and adapted from Maimaiti, J. and L.A. Porter)

J. Maimaiti. July 2009.

Adapted from Segura, M.M. et al. (2007);¹ Shore, A. and H.L. LaMarca (2008).²

⁽¹⁾ Segura, M.M. et al. (2007) Production of lentiviral vectors by large-scale transient transfection of suspension cultures and affinity chromatography purification. *Biotechnology and Bioengineering*, 98: 789-799.

⁽²⁾ Shore, A. and H.L. LaMarca (2008, March). *Lentiviral Propagation*. Retrieved 2009, from <http://www.bcm.edu/rosenlab/protocols/Lentivirus%20Protocol.pdf>

 ***Lentiviral particles should be treated as Risk Group Level 2 (RGL-2) organisms.*** Follow all published RGL-2 guidelines for handling and waste decontamination. Pipettes and media should be decontaminated in 10% bleach for at least 20 minutes before disposal. Please contact Jiamila prior to beginning this work to ensure all safety measures have been put into place.

Aim of Procedure: To produce a concentrated lentiviral stock.

Time scale.

Day 1	Seed HEK293 Lenti-X Cells.
Day 2	Co-transfect with pLB construct and lentiviral packaging vectors.
Day 3	Change media on transfected cells.
Day 4	Virus collection.
Day 5	Virus collection.
Day 6	Virus collection, viral concentration, and storage.

Routine Subculture of HEK293 Lenti-X Cells.

Maintain HEK293 Lenti-X cells in DMEM (DMEM, 10% FBS, 1% pen/strep). Cell cultures should be passaged three times a week between ratios of 1:4 and 1:6. Frequent passaging, in addition to maintenance of cell cultures at fewer than 80% confluence should be implemented to maintain a high transfection efficiency. Therefore do not allow cells to reach greater than 80% confluency.

Day 1 – Seeding HEK293 Lenti-X Cells.

Seed HEK293 Lenti-X cells at a density of 3.5×10^6 cells per 100mm dish in 8 ml DMEM + 10% FBS (no antibiotics). Cells should be seeded approximately 24 hours before transfection and incubated at 37°C, 5% CO₂. Please note that cells should exhibit ~60-70% confluency at the time of transfection. (recommended: split 1 plate of cells at 60% confluency into 2 plates).

Day 2 – Transfection.

Use 1µg DNA/ml media.

DNA: PEI ratio = 1:3 (i.e., if you need 8 µg DNA, you need 24 µg PEI)

1. Prepare 10 µg DNA in 800µl DMEM (no FBS, no antibiotics).

Transfer vector (pLB): pMDG (VSVG expressor): pMDL2 (gag-pol expressor): pRSV Rev = 2:1:1:1

- 4µg of Transfer vector (PEIZ) (1mg/ml) 4 µl
 - 2µg pMDG (VSVG expressor) (1mg/ml) 2 µl
 - 2µg pMDL2 (gag-pol expressor) (1mg/ml) 2 µl
 - 2µg pRSV Rev (1mg/ml) 2 µl
2. Add 30 µg PEI transfection reagent (10mg/ml) into DNA+DMEM mix, vortex 10 sec.
 3. Incubate DNA+DMEM+PEI mix at RT for 10 minutes.
 4. Add DNA+DMEM+PEI mix drop-wise onto overnight cell culture(s).
 5. Incubate cultures for 4-5 hours at 37°C, 5% CO₂.
 6. After the 4 hour incubation period, replace the media with fresh DMEM+FBS (10%) and incubate overnight at 37°C, 5% CO₂.

Day 3, Day 4 and Day 5 – Virus Collection.

- Harvest lentiviral-containing supernatant after 24, 48, 72 hours of growing in a 50 ml tube. After each collection, gently add fresh media to the cell culture(s), i.e., 8 ml DMEM+10% FBS. Store the virus at 4°C overnight.

Virus Concentration and Storage Notes

- Syringe filter-sterilize each of the collected viral suspensions using a 30 ml syringe and a 0.45 µl syringe filter.
- Transfer filtered viral suspension into ultrasound centrifuge tube (at most, 33 ml).
- Spin virus at 25,000 rpm for 3 hours at 4°C (use Beckman ultrasound centrifuge).
- Decant the supernatant and allow the centrifugation tubes to rest upside down on a paper towel to remove as much liquid as possible. Kim wipes/tissue may also be used to wipe around the tube. Make sure to remove as much supernatant as feasible.
- Turn centrifugation tubes right-side up, immediately. Resuspend viral pellet in 300 µl 1X PBS that has been filter sterilized into the tube without pipetting.
- Allow the tubes to incubate on ice for 30 minutes or overnight.
- Following the incubation period, carefully pipette up and down several times. From this point on, the virus must be treated very gently, so as not to damage the viral membrane.
- Remove the viral supernatant, aliquot into the necessary number of cryovials (25 µl aliquot for each vial) and store at -80°C for future utilization.

Lentivirus: Titering Your Lentiviral Stocks
(Protocol obtained and adapted from Maimaiti, J. and L.A. Porter)

DAY 0:
Plate 293T cells.

Plate 7.0×10^4 cells/well (24-well plate) in a final volume of 500 μ l/well in 10% FBS/DMEM media per well, and designate the following:

- a) 1 well \rightarrow count cells prior to transduction
- b) 1 well \rightarrow untransduced control
- c) 4 wells for each virus \rightarrow serial dilutions

Incubate at 37°C overnight.

DAY 1:
Transduce 293T cells.

Cells should be ~60% confluent at the time of transduction.

1. Count the number of cells present in 1 well (usually 3×10^5 cells immediately prior to transduction).
2. Prepare 10-fold serial dilutions ranging from 10^{-2} to 10^{-4} . Depending on the concentration of your virus, you may need to expand this range (i.e., 10^{-2} to 10^{-12}). Dilute the virus in DMEM (no FBS and no antibiotics):
 - 2.5 μ l stock virus + 247.5 μ l media $\rightarrow 10^{-2}$
 - 25 μ l 10^{-2} virus + 225 μ l media $\rightarrow 10^{-3}$
 - 25 μ l 10^{-3} virus + 225 μ l media $\rightarrow 10^{-4}$
 - 25 μ l 10^{-4} virus + 225 μ l media $\rightarrow 10^{-5}$
3. Aspirate media from 293T cells.
Add 200 μ l of diluted virus to each designated well, as previously outlined. Be sure to include 1 untransduced well.
Incubate cells at 37°C, 5%CO₂ overnight

Note: You may supplement your virus dilution media with polybrene at 8 μ g/ml (our stock is 1mg/ml). I add 0.2 μ l polybrene into each well or prepare 1 ml media with 8 μ l of polybrene to be utilized for viral dilution.

DAY 2: 24 hours post-transduction.

4. Aspirate media containing virus and replace with 500 μ l of fresh 10% FBS/DMEM.
Incubate cells at 37°C for an additional 48 hours at 5% CO₂.

DAY 4: 72 hours post-transduction.

5. Visualize the percentage of GFP expression utilizing GFP-fluorescence microscopy. GFP expression should range between 100% and 0%. Pick the wells that have about 5-20% GFP+ cells in order to titre the virus by flow cytometry.
 - Collect the cells in 1ml 1X PBS and centrifuge at 3000 rpm for 5 minutes.
 - Resuspend cell pellet in 400 µl 1X PBS and place into flow cytometry tubes for subsequent analysis and viral titration.

Calculate titre: use numbers from samples that were between 5-20% GFP+ to ensure that you are within the acceptable linear range.

$$T = \frac{(P \times N)}{(D \times V)}$$

T = titre (TU/ml)

P = % GFP+ cells (e.g., N = 0.2 for 20% GFP+ cells)

N = number of cells at the time of transduction

D = dilution factor (e.g., $10^{-3} = 0.001$)

V = volume of viral inoculum (0.2 ml)

Note: Formula for virus titer calculation:

$$\text{titre} = \{(F \times Cn) / V\} \times DF$$

F the frequency of GFP-positive cells determined by flow cytometry

Cn the total number of target cells infected

V the volume of the inoculum

DF the virus dilution factor

Example: Dilution	0	10^{-1}	10^{-2}	10^{-3}	10^{-4}
DF	0	10	100	1000	10000
F	0 (0%)	0.12 (12%)	0.01 (1%)	0.003 (0.2%)	0.0004 (0.05%)
Cn	2×10^5	2×10^5	2×10^5	2×10^5	2×10^5
V (ml)	1	1	1	1	1
Titre (TU/ml)	0	2.4×10^5	2×10^5	6×10^5	8×10^5

Thus, the titre of the lentiviral stock is 2.2×10^5 TU/ml (*i.e.* .average of 2.4×10^5 and 2×10^5).

Lentiviral Transduction

(Protocol obtained and adapted from Maimaiti, J. and L.A. Porter)

A. Preparation

- a. Prepare mammalian cells so that they are growing exponentially and are no more than 70-80% confluent before transduction.
- b. Prepare a stock solution of polybrene at 1 mg/ml in water.
- c. 96-well plate.

B. Methods

Day 1.

Add 1.6×10^4 cells in fresh media to the number of wells needed for each construct in a 96-well plate. Duplicate or triplicate wells should be used for each lentiviral construct. Incubate 18-20 hours at 37°C in a humidified incubator in an atmosphere of 5% CO₂.

Note: Growth rates of cells vary greatly. Adjust the number of cells plated to accommodate a confluency of 70% upon transduction. Also, account for the length of time the cells will be growing for before downstream analysis, when determining the plating density.

Day 2.

Remove media from wells. Add 110 µl media and polybrene (final concentration of 8 µg/ml) to each well. Gently swirl the plate to mix. Add 2-15 µl of lentiviral particles to appropriate wells. Gently swirl the plate to mix. Incubate 18-20 hours at 37°C in a humidified incubator, in an atmosphere of 5% CO₂.

Note: When transducing a lentiviral construct into a cell line for the first time, a range of volumes or MOIs should be tested. 2, 5, 10, and 15 µl of lentiviral particles per 1.6×10^4 cells or MOIs of 0.5, 1, and 5 should be used to determine the optimal transduction efficiency and knockdown for each cell line (see *Additional Notes*).

Note: Cells may be incubated for as little as 4 hours before changing the media containing lentiviral particles. Overnight incubation may be avoided when toxicity of the lentiviral particles are of a concern.

Day 3.

Remove the media containing lentiviral particles from wells. Add fresh media to a volume of 120 µl to each well.

Note: For cell types that do not strongly adhere to the plate, 100 µl of media may be removed and replaced with 100 µl fresh media.

Day 4.

Remove media from wells. Add fresh media containing puromycin. The appropriate concentration of puromycin for each cell type is different. If the concentration for the desired cell type is unknown, a titration experiment must be performed. Typically, 2-10 $\mu\text{g/ml}$ are sufficient to kill most untransduced mammalian cell types.

Day 5 and on.

Replace media with fresh media every 3-4 days until colonies can be identified under GFP-fluorescence microscopy. Pick a minimum of 5 colonies and expand each clone to assay for knockdown of the target gene.

A puromycin titration (kill curve) should be performed when working with a new cell type.

DAY 1

- Plate target cells in a 12-well plate 24 hours prior to viral infection.
- Add 1 ml of complete optimal medium (with serum and antibiotics) and incubate cells overnight. The cells should be approximately 50% confluent on the day of infection (Day 2).

NOTE: It is possible to use other plate formats for transduction, as well. In this case, the amount of cells should be adjusted depending on the growth area of the well or plate.

DAY 2

- Prepare a mixture of complete medium with Polybrene® (sc-134220) at a final concentration of 5 $\mu\text{g/ml}$.
- Remove media from plate wells and replace with 1 ml of Polybrene-media mixture per well (for 12-well plate).

NOTE: Polybrene is a polycation that neutralizes charge interactions to increase binding between the pseudoviral capsid and the cellular membrane. The optimal concentration of Polybrene depends on cell type and may need to be empirically determined (usually in the range of 2-10 $\mu\text{g/ml}$). Excessive exposure to Polybrene (>12 hr) can be toxic to some cells.

- Thaw lentiviral particles at room temperature and mix gently before use.
- Infect cells by adding the shRNA Lentiviral Particles to the culture.
- Swirl the plate gently to mix and incubate overnight. The amount of viral particles to use varies greatly depending on the characteristics of the cell line used.

NOTE: Keep thawed shRNA lentiviral particles on ice. Repeated freeze-thaw cycles and prolonged exposure of the particles to ambient temperatures may result in decreased viral titres.

NOTE: When transducing an shRNA lentiviral construct into a cell for the first time, we suggest using several volumes of shRNA lentiviral particle stock. In addition, we recommend to include one well with cells transduced with Control shRNA Lentiviral Particles (sc-108080).

NOTE: Use co-GFP Control Lentiviral Particles (sc-108084) to measure the transduction efficiency.

DAY 3

- Remove the culture medium and replace with 1 ml of complete medium (without Polybrene). Incubate cells overnight.

DAY 4

- To select stable clones expressing the shRNA, split cells 1:3 to 1:5, depending on the cell type, and continue incubating for 24-48 hours in complete medium.

DAY 5-6 and forward

- Select stable clones expressing the shRNA via GFP expression.
- Replace media with fresh media every 3-4 days, until fluorescent colonies can be identified. Pick several colonies, expand them, and assay them for stable shRNA expression.

NOTE: For shRNA expression analysis by 10% SDS-PAGE, prepare cell lysates as follows:

- Wash cells once with 1X PBS.
- Lyse cells in 100 µl of a 1:1 mixture of 2x Electrophoresis Sample Buffer (sc-24945) and RIPA Lysis Buffer (sc-24948) by gently rocking the 12-well plate or by pipetting up and down.
- Sonicate the lysate on ice if necessary.

C. Additional Notes

Calculation of MOI Value

Multiplicity of Infection (MOI): Multiplicity of Infection is the number of transducing lentiviral particles per cell. It is highly recommended that for each new cell type to be transduced, a range of MOIs should be tested. This will determine the optimal amount of lentiviral supernatant needed for efficient transduction of each cell line used.

To calculate:

$(\text{Total number of cells per well}) \times (\text{Desired MOI}) = \text{Total transducing units needed (TU)}$

(Total TU needed) / (TU/ml reported on C of A) = Total ml of lentiviral particles to add to each well

Determining the Optimal Puromycin Concentration

Each cell line responds differently to puromycin selection. Addgene recommends that you determine the optimal puromycin concentration for your cell line before initiating your experiment.

Day 1

- a. Plate target cells (2×10^5 cells/well) in 6 well plates and grow at 37° C, 5% CO₂ overnight.

Day 2

- b. The target cells should be approximately 80-90% confluent.
- c. Dilute puromycin in the preferred culture media for your target cells. The final concentration of puromycin should be from 1-10 µg/mL, in 1 µg/mL increments.
- d. Label plates from 1-10 and add appropriate puromycin-containing media to cells.

Days 3 +

- e. Examine cells each day and change to fresh puromycin-containing media every other day.
- f. The minimum concentration of puromycin that results in complete cell death after 3-5 days is the concentration that should be used for selection in your experiments. (You may wish to repeat this titration with finer increments of puromycin to determine a more precise optimal puromycin concentration.)

D. Solutions

Hexadimethrine Bromide (Polybrene). Prepare a 1mg/mL solution of polybrene (Sigma-Aldrich catalog #H9268) in 0.9% NaCl. Autoclave to sterilize. Stock solution is stable at 4°C for up to one year. The powder form of polybrene is stable at 4°C for several years.

Protamine Sulfate. Store protamine sulfate (MP Biomedicals catalog #194729) at 4°C. Freely soluble in hot water and slightly soluble in cold water.

Puromycin. Prepare a 50mg/mL stock solution of puromycin (Sigma-Aldrich catalog #P8833) in distilled water. Sterilize by passing through a 0.22 µm filter. Store aliquots at -20°C.

Appendix References

Bainbridge, J. W., et al. (2001) *Gene Therapy*, 8: 1665-8.

Besnier, C., Takeuchi, Y. & Towers, G. (2002) *Proceedings of the National Academy of Sciences USA*, **99**: 11920-11925.

Demaison, C. et al. (2002) *Human Gene Therapy* 13, 803-813.

Naldini, L., et al. (1996) *Science*, 272: 263-267.

Salmon, P. and D. Trono. (2007) *Current Protocols in Human Genetics*, Chapter 12:Unit 12.10.

Segura, M.M. et al. (2007) *Biotechnology and Bioengineering*, 98: 789-799.

Vita Auctoris

Evangelia Kirou was born in the year of 1985 in Thessaloniki, Greece. She graduated from Sandwich Secondary School in 2003. From there she went on to the University of Windsor where she obtained an Honours B.Sc. in Biological Sciences with Thesis in 2007. She is currently a candidate for the Master's degree in Biological Sciences at the University of Windsor and hopes to graduate in Winter 2010.